



Dissertation Thesis

Carbon-based Functional structures from Pyrolysis of Kevlar Fabric Wastes

Study programme: P3106 Textile Engineering
Study branch: Textile Technics and Materials Engineering

Author: **Daniel Karthik, M.Tech.**
Thesis Supervisor: prof. Ing. Jiří Militký, CSc.
Department of material engineering

Liberec 2023

Declaration

I hereby certify, I, myself, have written my dissertation as an original and primary work using the literature listed below and consulting it with my thesis supervisor and my thesis counsellor.

I acknowledge that my dissertation is fully governed by Act No. 121/2000 Coll., the Copyright Act, in particular Article 60 – School Work.

I acknowledge that the Technical University of Liberec does not infringe my copyrights by using my dissertation for internal purposes of the Technical University of Liberec.

I am aware of my obligation to inform the Technical University of Liberec on having used or granted license to use the results of my dissertation; in such a case the Technical University of Liberec may require reimbursement of the costs incurred for creating the result up to their actual amount.

At the same time, I honestly declare that the text of the printed version of my dissertation is identical with the text of the electronic version uploaded into the IS/STAG.

I acknowledge that the Technical University of Liberec will make my dissertation public in accordance with paragraph 47b of Act No. 111/1998 Coll., on Higher Education Institutions and on Amendment to Other Acts (the Higher Education Act), as amended.

I am aware of the consequences which may under the Higher Education Act result from a breach of this declaration.

May 28, 2023

Daniel Karthik, M.Tech.

Acknowledgments

Having handed in this dissertation, I owe an immense amount of gratitude to a large number of individuals for their invaluable assistance. I would like to begin by expressing my utmost gratitude and appreciation to my supervisor, Prof. Ing. Jiří Militký, CSc. EURING, for being extremely supportive and helpful during the entire process of my research and study programme. Having him as my mentor has played a vital role in shaping me as a researcher and accomplishing my objectives at every stage of my tenure at the Technical University of Liberec. My sincere thanks to the supervisor specialist, Dr. Vijaykumar Narayandas Baheti for his invaluable support towards my research work. I truly thank them both for their encouragement, cooperation, and concentrated discussions throughout this work. They have helped me realize the significance of condensing and presenting my ideas in a coherent and approachable fashion.

I would also like to sincerely appreciate Dr. Blanka Tomková (Head of Department, KMI), prof. Dr. Jakub Wiener, Dr. Veronika Tunáková, Dr. Miroslava Pechočiaková, and Dr. Mohanapriya Venkataraman for their insightful comments throughout the course of my research. I would also like to thank Doc. Ing. Vladimír Bajzík, Ph.D. (Dean of the Faculty of Textile Engineering), Dr. Iva Mertová (Vice-Dean for Development and Ph.D. Studies), and Dr. Jana Drašarová (Vice Dean for Science and Research) for their crucial guidance. I would also like to thank from the bottom of my heart the laboratory personnel in the Department of material engineering, who were always available to assist me. It will be incomplete, without my special thanks to Ing. Hana Musilová and Mrs. Bohumila Keilová, for their relentless support every step of the way, since my very first day at the Technical University of Liberec. I am especially grateful to Dr. Karel Kupka (TriloByte Statistical Software s.r.o., Pardubice) for granting me the exceptional opportunity to work in his laboratory, under his expert supervision and guidance.

Finally, I would like to express my heartfelt gratitude to my family and friends for their unconditional love and encouragement. I am indebted to my father, Mr. Philemon Gandhi, for his unending support in myriad ways, and for this, I will be forever grateful. I owe an enormous debt of gratitude to the people who have been my closest friends and trusted associates over the years, for their ongoing support and inspiration.

Abstract

This dissertation is dealing with the use of fibrous aromatic polyamide (Kevlar) waste for the development of microporous and electrically conductive materials based on activated carbon. A method of controlled, one-stage carbonation is used.

The waste Kevlar fabric was obtained from a regional manufacturing plant in the Czech Republic. Activated carbon structures were prepared by pyrolysis under different conditions, i.e. several types of inert atmosphere, optimized time-temperature mode of heat stress, and final carbonization temperature (in the range of 500 °C to 1200 °C) so as to create porous and electrically conductive structures.

The thermal degradation of Kevlar and the composition of volatile products of its pyrolysis were investigated.

The geometric, physical, morphological, electrical, and thermoelectric properties of the prepared activated carbon structures were studied with respect to different thermal modes and different types of inert atmospheres. The electromagnetic interference (EMI) shielding capability in the high frequency (i.e. at 2.45 GHz) and low frequency (i.e. below 1.5 GHz) regions was investigated using the waveguide method and the coaxial line transmission method.

Furthermore, the ohmic heating behavior of activated carbon structures was studied as a function of the applied electric power and time.

Progressive changes in concentrations of gaseous products of thermal decomposition of Kevlar depending on the pyrolysis temperature and their differences in volatility were evaluated using an algorithm for the separation of mixed spectra obtained by UV spectroscopy.

Keywords: Kevlar, pyrolysis, activated carbon, carbonization, graphitization, organic volatile compounds, spectral matrix decomposition, joule heating, electromagnetic shielding.

Abstrakt

Tato disertační práce se zabývá využitím vlákněných aromatických polyamidových (Kevlarových) odpadů pro vývoj mikroporézních a elektricky vodivých materiálů na bázi aktivovaného uhlíku. Je použita metoda řízené, jednostupňové karbonizace.

Odpadní Kevlarové textilie byl získány z regionálního výrobního závodu v České republice. Aktivované uhlíkové struktury byly připraveny pyrolýzou za různých podmínek, tj. několika typů inertní atmosféry, optimalizovaného časově teplotního režimu tepelného namáhání a finální teploty karbonizace (v rozmezí 500 °C až 1200 °C) tak, aby vznikly porézní a elektricky vodivé struktury. Byla zkoumána tepelná degradace Kevlaru, a složení těkavých produktů jeho pyrolýzy.

Geometrické, fyzikální, morfologické, elektrické a termoelektrické vlastnosti připravených aktivovaných uhlíkových struktur byly studovány s ohledem na různé tepelné režimy a různé typy inertní atmosféry. Schopnost stínění proti elektromagnetickému rušení (EMI) ve vysokofrekvenčních oblastech (tj. na 2,45 GHz) a nízkofrekvenčních oblastech (tj. pod 1,5 GHz) byla zkoumána pomocí metody vlnovodu a metody koaxiálního přenosu. Dále bylo studováno chování ohmického ohřevu aktivovaných uhlíkových struktur jako funkce použitého elektrického výkonu a času.

Progresivní změny koncentrací plynných produktů tepelného rozkladu Kevlaru v závislosti na teplotě pyrolýzy a jejich rozdíly v těkavosti jsou vyhodnoceny pomocí algoritmu pro separaci směsných spekter získaných UV spektroskopii.

Klíčová slova: Kevlar, pyrolýza, aktivovaný uhlík, karbonizace, grafitizace, těkavé produkty pyrolýzy, rozklad matice UV spekter, ohmický ohřev, elektromagnetické stínění.

Table of Contents

1. Introduction.....	9
2. Upcycling of Polymeric wastes to Carbon-based functional materials.....	10
3. Carbon-based functional materials	12
4. Theory of Pyrolysis and Carbonization	15
5. State of the Art in Kevlar Pyrolysis.....	21
6. Thermal degradation of Kevlar and its volatile compounds	22
7. Development of porous and electrically conductive activated carbon fabric from Kevlar wastes.....	30
8. Electromagnetic Shielding Effectiveness of Kevlar-derived activated carbon	42
9. Joule heating behavior of Kevlar-derived activated carbon fabrics	51
10. Conclusion	50
11. Appendix – Full texts.....	52
12. Future prospects.....	96
13. References.....	96
14. List of Publications.....	103

List of Figures

Fig. 2. Upcycling of Fibrous wastes to Carbon-based functional materials. Recreated from. ..9	9
Fig. 3. Classification of carbon-based materials and potential applications..... 10	10
Fig. 4. Pore of ACF and granular activated carbon 12	12
Fig. 5. Main stages involved in the production of ACFs. 13	13
Fig. 1. Structure of Kevlar 14	14
Fig. 6. Two-step thermal processing of PAN into carbon: oxidative stabilization and formation of a ladder structure, followed by carbonization..... 20	20
Fig. 7. Single step thermal processing of Kevlar into carbon: direct carbonization. 18	18
Fig. 8. Speculated thermal decomposition mechanism of Kevlar 19	19
Fig. 9. Thermal degradation of Kevlar fabric by TGA. 20	20
Fig. 10. Schematic illustration of the continuous process of pyrolysis, condensation of volatiles, and subsequent UV-VIS Spectroscopy analysis 25	25
Fig. 11. Reconstructed UV-VIS spectra (a) of the two assumed components, and (b) of the two identified components at temperatures 500 – 1100°C 29	29
Fig. 12. Schematic of activated carbon fabric preparation from Kevlar fibrous wastes. 31	31
Fig. 13. Visual observation of Flexibility Kevlar-derived activated carbon fabric in comparison to some commercial fabrics..... 33	33
Fig. 14. Microstructure of Kevlar fibers and corresponding carbon fibers under elevated pyrolysis temperatures (a) Kevlar without pyrolysis (b) activated carbon at 800 °C; (c) and activated carbon fabric at 1200 °C..... 34	34
Fig. 15. Porous structure of ACF by fractal simulation. 35	35
Fig. 16. Adsorption-desorption isotherm of Kevlar-derived activated carbon fabrics 37	37
Fig. 17. Parallel electrode measurement setup..... 39	39
Fig. 18. (a) The direct current, room temperature conductivity versus pyrolysis temperature; and (b) Electrical resistivity of activated carbon fabrics from methods 1, 2, and 3 41	41
Fig. 19. Schematic representation of the EMI shielding mechanisms (a) Wave impedance and propagation of electric and magnetic fields, (b) electromagnetic transverse oscillating wave, and (c) electromagnetic wave propagation model in EMI shielding materials 44	44
Fig. 20. Measurement setup of waveguide method and its schematic mechanism (bottom)... 45	45

Fig. 21. Measurement set up of coaxial transition line method	45
Fig. 22. Electromagnetic shielding effectiveness (a) Effect of carbonization temperature at 2.45 GHz, and (b) Effect of frequency in low-frequency region.....	46
Fig. 23. Schematic diagram of Joule heating phenomenon.	48
Fig. 24. Temperature-voltage relation. (a) Maximum temperature difference (ΔT_{\max}) estimated for electrically conductive fibers at varying input electrical current and voltage, (b) Kevlar-derived activated carbon fabrics	49
Fig. 25. Temperature – time relation of (a) Kevlar-derived activated carbon fabrics, (b) composites with carbon black.....	50

List of Tables

Table 1. Temperature-dependent pyrolysis products of Kevlar 49.....	19
Table 2. Major products identified by Py-GC/MS of Kevlar at 600 °C in an inert atmosphere	24
Table 3. Effect of pyrolysis conditions on the elemental composition of Kevlar and carbonized Kevlar.	26
Table 4. Yield of Kevlar-derived activated carbon.....	32
Table 5. Effect of carbonization temperature on physical and mechanical properties of activated carbon fabric produced from Kevlar.	33
Table 6. Effect of carbonization temperature on the electrical conductivity of activated carbon fabric	41

1. Introduction

The dire consequences of climate change and ecological problems continue to have an impact on society's growing understanding of the value of sustainability, circular economy, and recyclable/reusable goods [1]–[3]. Due to the expanding demand for textiles, the amount of waste produced during the production and end-of-life of textile materials has substantially increased, adding to the issues associated with its disposal. It is projected that 92 million tons of textile waste are generated every year around the world, and in addition to the enormous amount of clothing abandoned each year, only 15% of it is recycled, with the remaining 85% ending up in landfills or incinerated [4], [5]. The European Union discards an estimated 5.8 million tonnes of textiles annually, with a mere 25% of this amount being subjected to recycling processes [6]. Within Europe, the per capita generation of textile waste exceeds 15 kilograms, whilst it is projected that the consumption of clothing and footwear will face a 63% increase by the year 2030 [7].

The advantages of polymeric fibers for the world's rapidly expanding population have led to an increase in their consumption for versatile areas of application. However, regardless of how polymeric fibrous materials have improved the standard of our living, it is tough to manage fibrous wastes. Existing approaches to lowering discarded polymers are not enough to address the build-up of polymeric wastes [8]. Recycling, landfills (including discarded ones), and incineration are all options for managing polymeric fibrous wastes. However, toxic gases are produced when polymers are burned. Additionally, conventional recycling has drawbacks because the recycled polymer has diminished durability and flexibility.

In contrast to the conventional recycling mechanism, the most innovative and cutting-edge approach to managing fibrous wastes is 'upcycling' into solid carbonaceous materials. One of the primary approaches of upcycling is pyrolysis (at temperatures >250), followed by carbonization (>800 °C), in an inert environment and at a variable heating rate, to produce carbon-rich materials. The carbonized materials created by upcycling polymeric fibrous wastes are used as adsorbents for waste purification, energy and the environment, and electrical energy storage (EES) devices. The goal of the upcycling process is to create carbon-rich solid residues instead of oils or volatile compounds. The significant combination of favorable chemical and physical properties found in carbon-based functional materials, including their excellent electrical conductivity, excellent heat conductivity, high mechanical strength, front-line optical properties, and, chemical stability, has drawn much attention [9].

Activated carbon fibers are products with tunable porosity and electrical conductivity due to carbonizing conditions, physico-chemical activation, and adding of doping agents. They are usually derived from semi-crystalline precursors such as viscose rayon, phenolic resins, polyacrylonitrile, or isotropic coal tar pitches, by a number of lengthy and multistep processes [10]–[13]. In particular, oxidative stabilization, as a common step in the production process, is considered a limiting factor for the economic conversion of low crystalline precursor fibers into carbon fibers. More recently, the utilization of highly ordered polymer precursors (i.e., Aramids) which do not require oxidative stabilization, have been studied for activated carbon fiber production [14]–[16].

This dissertation represents a set of published scientific papers accompanied by a detailed discussion of the current state of knowledge about Kevlar carbonization and related topics.

The full texts of the 4 selected papers are in the appendix. The remaining articles are in the references of this dissertation.

The principal objectives discussed here are:

- Development of porous and electrically conductive activated carbon by single-stage carbonization and physical activation of Kevlar fabric under varying conditions of temperature, rate of heating, and pyrolysis atmosphere, without any intermediate stabilization step and holding time.
- Investigation of the carbonization of Kevlar fabric by three different methods.
- Characterization of morphology, physical, chemical, electrical, and thermoelectric properties of activated carbon fabrics.
- Description of progressive changes in concentrations of decomposition products as a function of pyrolysis temperature and their difference in volatility, by using an algorithm for separation of mixture spectra obtained by UV spectroscopy.
- Evaluation of surface and volume electrical resistivity, EMI shielding effectiveness of activated carbon fabrics, and the Joule heating behavior of the activated carbon fabrics.

2. Upcycling of Polymeric wastes to Carbon-based functional materials

Upcycling polymeric waste entails using advanced and refined processes to treat the material. Innovative strategies for turning wastes into valuable materials include investigating novel paths and applications for the end goods. Consolidating and evaluating current operational procedures and conditions is critical for developing an efficient and cost-effective upcycling process for plastic wastes [9]. Carbonized materials derived from upcycling of polymeric fiber

wastes are consumed for versatile applications such as adsorbents in waste purification, energy and the environment, and electrical energy storage (EES) systems. The purpose of the upcycling process, as indicated in Fig. 2, is to produce carbon-rich solid wastes rather than oils or volatile chemicals.



Fig. 1. Upcycling of Fibrous wastes to Carbon-based functional materials. Recreated from [9].

The process of upcycling through pyrolysis entails the thermal degradation of waste polymeric substances, with the aim of retrieving the desirable material that can serve as an initial product for the creation of novel materials. This strategy of thermal recycling has been extensively researched in the discipline of fiber recovery [17].

The development of carbonaceous materials is influenced by factors such as the nature of the precursor used, the application of activating agent, and emphatically the process conditions of pyrolysis. In fact, the operational parameters in the pyrolysis process have a discernable effect on the resulting manner of decomposition and on the final characteristics of the product [18]–[20]. Upcycling waste polymers using pyrolysis provides several advantages over traditional recycling techniques. It may, for example, handle a wide range of polymer waste materials, such as mixed or contaminated materials that are usually difficult or impossible to recycle using other methods.

The sustainability and environmental impact of the pyrolysis technologies used to upcycle waste polymers are still being investigated. Here are a few recent developments in this subject matter:

- i. The use of catalysts increases the effectiveness of the pyrolysis process and reduces the quantity of energy used [21].
- ii. Microwave-assisted pyrolysis has been shown to save time and energy by heating the polymer wastes with microwaves [22].

- iii. Co-pyrolysis involves pyrolyzing polymer wastes along with biomass, such as wood or agricultural waste. Biomass serves as a catalyst, lowering the amount of energy needed for the process and enhancing the quality of the end products [23].
- iv. Recycling the products of pyrolysis to further upcycling, as this can necessitate utilizing them as raw materials for the creation of new materials [24].
- v. Performing a life cycle assessment to help better understand how pyrolysis operations affect the environment and point up opportunities for improvement [25].

3. Carbon-based functional materials

Carbon-based materials have multiple hybridization states (sp^1 , sp^2 , sp^3) and allotropic structures. Carbon atoms may make strong covalent bonds with other carbon atoms or a wide range of metallic and non-metallic elements, creating a huge number of compounds from small molecules to long-chained structures. Bonding (hybridization of carbon atom orbitals) and dimensionality (non-nanoscale dimensions) classify the most frequent carbon materials. Fig. 3 shows carbonaceous minerals in all dimensions, from 0D (fullerenes) to 3D (amorphous carbon, graphite, diamond). Nanoscale carbons such as fullerenes and fullerites, carbon onions (multi-shell fullerenes), nanotubes, whiskers, nanofibers, cones, horns, rings, and nanodiamonds are being researched for potential applications. Graphite, carbon fibers, glassy carbon, activated carbons, carbon black, and diamond are already widely used in industry [26].

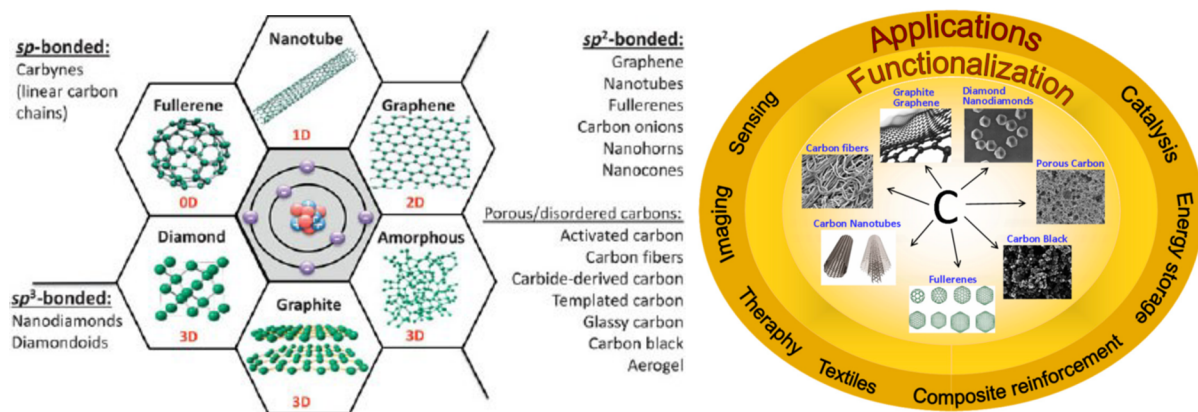


Fig. 2. Classification of carbon-based materials and potential applications [27], [28].

Activated carbon fibers, mesoporous carbon, graphite, graphene, CNTs, fullerenes, and carbon quantum dots are a selection of carbon-based materials derived from fibrous sources [29]–[31].

Activated carbon fiber (ACF) has a fiber shape and a clearly defined porosity structure, making it a viable microporous material. High packing density, outstanding volumetric capacity, rapid adsorption/desorption, and low handling effort are just a few of ACF's unique properties. Because of their exceptional structural (physical and chemical), thermal (heat transfer), and electric qualities, carbon-based materials may be useful in a broad spectrum of applications [32].

Numerous research endeavors have effectively transformed waste into functional materials that are carbon-based. These materials possess engineered micro-/nanostructures and surface chemistry that can be adjusted through diverse techniques. The carbon-based functional materials derived from waste have exhibited encouraging outcomes in various potential applications, particularly in the domains of water remediation and energy storage. The waste materials that have been employed as economical feedstocks for the synthesis of carbon-based functional materials can be broadly categorized into two groups. The initial classification pertains to biowastes, consisting of carbohydrates that are capable of undergoing natural decomposition via the carbon cycle. This category of waste typically exhibits a minimal effect on the surrounding ecosystem. Several instances of organic waste materials that can be utilized for various purposes include natural deceased plant components, agricultural residuals such as husks and coir shells, and other household waste such as paper waste. The second classification pertains to non-biodegradable waste, which undergoes slow decomposition through natural means. The detrimental effects on ecosystems are caused by a particular category of waste materials, which encompasses a range of synthetic materials produced by humans, such as plastic bags and bottles, textiles, rubber tires, as well as intricate industrial sludge, and municipal waste [27].

3.1. Activated carbon fibers

Activated carbon derived from fibrous sources, also known as activated carbon fiber (ACF), has been demonstrated to have a higher specific surface area, adsorption rate, and adsorption efficiency than granular activated carbon obtained from petroleum pitch or coal, which is traditionally used as precursors [33], [34]. Processing ACFs from carbon-rich precursors comprises the same stages as typical carbon fiber synthesis, with the addition of an activation phase to further enhance pore distribution. Additionally, the costs associated with producing fibrous structures specifically for the manufacturing of ACFs are avoided. [35].

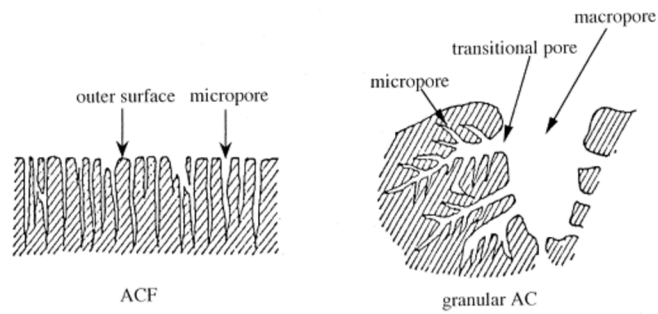


Fig. 3. Pore of ACF and granular activated carbon [36].

In addition to their porous nature, ACFs offer various other benefits because of their fibrous shape with high surface area, trivial mesoporosity, and almost no microporosity (shown in Fig. 4), high accessible porosity, and improved contact efficiencies with media, allowing them to have potential applications in popular research fields like natural gas storage, the adsorbent in the heavy metal industry, treatment, and purification of water. ACFs can also be used in the textile sector for a variety of purposes, including filtration, catalytic support, household fabrics, medical masks, and personal protective equipment, to name a few. The availability of resources, ease of activation, inorganic content, and carbon yield, as well as the associated costs, constitute some of the variables that affect the precursor utilized to produce ACF. [35].

With an internal surface area of roughly 500–2000 m²/g, activated carbon has a very high porosity structure. The study of potential, less expensive sources as well as techniques for making activated carbon compounds has garnered much interest lately. Activated carbon is a superior adsorbent for removing colors, heavy metals, dangerous smoke, unwanted odor, taste, and organic compounds from the environment [37], [38]. Large surface area, well-developed internal structure, and the presence of different surface functional groups rely on the type of raw material utilized, the type of activating agent, and the circumstances of the pyrolysis and activation processes [15], [39].

3.2. Manufacturing process of ACF's

The prevailing steps involved in the production of ACF's mainly include the following stages (as shown in Fig .5): stabilization, pre-treatment for-instance, acid impregnation (prior to carbonization), carbonization/pyrolysis, and in some cases activation (physical or chemical activation). However, it must be mentioned that pre-treatment and stabilization steps depend on the type of precursor and are not necessarily included in the preparation of ACF.

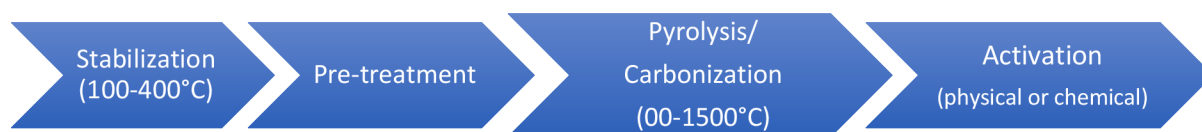


Fig. 4. Main stages involved in the production of ACFs.

In the stabilization phase, controlled low-temperature heating in air at a temperature between 200 and 300 °C stabilizes the precursor. This procedure, which is essential for producing high-quality carbon fibers, may take several hours, depending on the temperature, precursor diameter, and precursor fiber properties. By thermal decomposition at high temperatures and under the direct flow of inert gas, carbonization (or pyrolysis) converts the initial component into a carbonized substance. Fibers that have been thermally stabilized are carbonized in an inert environment that contains gases like nitrogen (N₂) or argon (Ar). In most cases, the type of application for the produced carbon fibers determines the carbonization temperature. ACFs may also require activation using either physical or chemical methods. Physical activation entails activating the resulting char at a high temperature in the presence of suitable gases, such as carbon dioxide, steam, or their mixtures. Chemical activation entails activating the resulting char through the reaction of potent chemicals, such as ZnCl₂, H₃PO₄, and alkali-metal hydroxides (NaOH and KOH) [40], [41].

3.2.1. Types of precursors

The ideal features of precursors required to manufacture carbon fibers are easy conversion to carbon fiber, high carbon yield, and cost-effective processing [42]. The usual preference as precursors for activated carbon materials is low-crystallinity feed-stocks like polyacrylonitrile, phenolic resins, coal tar pitch, etc. The precursor materials of the carbon fibers are important because the combination of various properties and behaviors (mechanical, physical, and chemical) potentially required [43], [44]

Following are some of the prevalent and widely used choices of precursors for carbon production:

- i. Polyacrylonitrile (PAN) precursors: More than 80% of the worldwide carbon fiber market is accounted for by goods based on polyacrylonitrile (PAN). Following PAN-based carbon fiber are pitch-based carbon fiber, rayon-based carbon fiber, and

polyolefin-based carbon fiber. Most industrial firms have been successfully preparing carbon fiber with PAN precursors for many years now [45], [46].

- ii. Cellulosic precursors: The utilization of cellulose precursors has been discovered to be advantageous in the production of carbon fibers due to the thermal decomposition of cellulose without undergoing a melting process and the existence of a highly organized crystalline configuration. They contain 44.4% carbon, although in reality, the reaction is more involved than simple dehydration, thus the yield of carbon is only about 25–30% [30].
- iii. Pitch-based precursors: Pitch-based precursors are complex mixtures of polyaromatic molecules and heterocyclic compounds that have a high yield (85%), and the resulting carbon fibers have a high modulus due to their graphitic nature. Pitch-based carbon fibers, on the other hand, exhibit inferior compression and transverse properties than PAN-based carbon fibers [47].
- iv. High-performance fibrous wastes precursors: These precursors are beneficial mainly due to well ordered oriented structure with a higher portion of carbon. One of the most useful representants is aromatic polyamides (aramids).

Aramids are full aromatic polyamides, which are long-chain aromatic polyamides where the amide connections are connected to two aromatic rings to the extent of at least 85% [12]. As a polyamide synthesized by condensation, poly(p-phenylene terephthalamide) (PPTA), prevalently known as Kevlar[®] (hereafter referred to as Kevlar), are fully crystalline with a small fraction of randomly oriented material and Fig. 1 depicts the chemical structure.

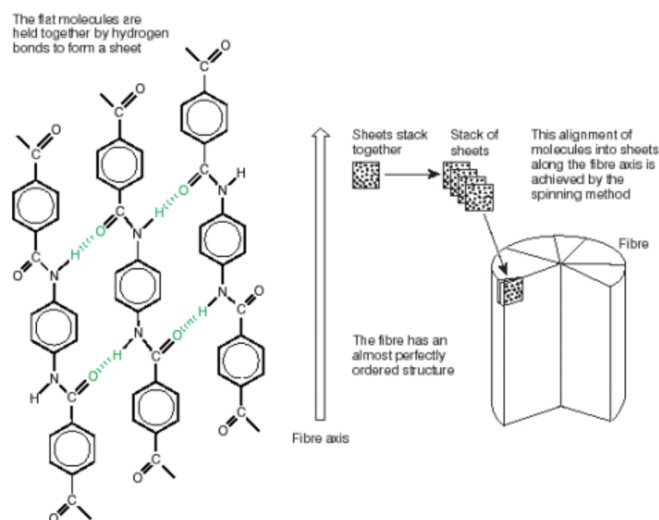


Fig. 5. Structure of Kevlar [48].

Freeman et al. [49] first used Kevlar fibers as precursor materials to obtain carbons with high surface areas, narrow pore size distributions, and acceptable yields and mentioned homogeneous pore size distributions of obtained activated carbon fibers [10], [16]. Later, a number of studies focused on the preparation of activated carbon fibers from Kevlar and Nomex fibers were proposed [11], [50]–[53]. More substantially, the oxidative stabilization phase that is frequently necessary for the carbonization of low melting precursors can be avoided by taking advantage of Kevlar fibers' excellent thermal stability. Additionally, as Kevlar flocks are leftovers from the manufacture of the material, their lower price may be a benefit if they are used as the precursor [54].

Alternatively, over the years, a trend has emerged for the production of low-cost, useful carbonaceous materials from various types of precursors such as regenerated cellulose [30], [44], [55], Polyethylene terephthalate (PET) [33], [56], Polyethylene (PE) [57]–[59], Polypropylene (PP) [60], polyamides [52], polyaramids [15], polybenzobisoxazole (PBO) [61], polyvinylidene fluoride (PVDF) [62], poly(vinylacetylene) [63], polyvinyl alcohol [64], and phenolic resins [65] have been investigated for manufacturing carbon fibers.

4. Theory of Pyrolysis and Carbonization

The term "Pyrolysis" is frequently limited to high-temperature reactions that only produce gases and char, but it also refers to the thermolysis of organic macromolecules at temperatures between 250 and 800 °C (in the absence of oxygen) that produces gaseous, liquid, and solid byproducts. The carbonization phase, following pyrolysis, is realized at 800°C and is characterized by fundamental variations in the physical and chemical properties of the organic material and is irreversible [3]. In general, most hydrocarbons undergo covalent bond rupture and rearrangement during pyrolysis, and depending on the nature of the precursor, the pyrolysis mechanism can be simple or quite complex. Methane, for example, can produce some carbon species as well as hydrogen just above the temperature at which its formation energy becomes positive. A long-chain branched polymer, on the other hand, might exhibit intricate fragmentation patterns with concurrent secondary and tertiary reactions, as well as the release of volatile products [66], [67].

The first stage of the pyrolysis process involves an intramolecular endothermic chemical reaction that either involves the rearrangement of chemical bonds followed by the elimination

of small molecules, or the cleavage of chemical bonds followed by the stabilization of the unstable fragments (the former reactions take place at around 300 °C, and the latter above 500 °C [49], [68], [69]. Under the influence of heat, hetero atoms (oxygen and hydrogen) are removed, and the substance becomes richer in carbon. The remaining carbon atoms form aromatic sheets with a certain planar structure. These sheets are then placed in a random manner, creating spaces between them, resulting in the pyrolyzed product's principal porosity [70].

In general, polymers breakdown to a primary char and water below 550°C. Further heating above 550°C gradually converts the primary char to a conglomerate of loosely linked small graphitic regions that is virtually independent of the structure of the original polymers [71]. According to one study, polymer char creation includes the following steps: cross-linking, aromatization, aromatic fusion, turbostratic char formation (an incomplete phase of graphitization), and graphitization. The char's structure is thus thought to be made of polynuclear aromatic compounds containing heteroatoms (O, N, P, S), with crystalline and amorphous parts [72].

It can be challenging to execute an experimental analysis of the precise behavior of a particular polymeric material that has been subjected to thermal degradation due to its great complexity. Numerous parameters affecting the structure and properties of carbonizates influence the mechanism of carbonization of macromolecular compounds and the qualities of the final carbon products. These include the initial polymer preparation approach, heat treatment conditions, the presence of additional chemical substances in the environment of thermochemical reactions, and, in general, specific attributes of the carbon material preparation process [73], [74].

The characteristic nature and quantity of the products of pyrolysis at various phases of thermal decomposition are governed by several variables. Different chemical compounds are released depending on the temperature at which the degradation advances. Typically, the primary fragments of the polymeric molecules are chemically active, and they initiate a secondary reaction right away. In general, the final products are less toxic, the more complete the combustion process takes place. The following factors could potentially have an impact on the volatile products in any particular thermal degradation scenario:

- i. type and quantity of the precursor material;

- ii. type of combustion,
- iii. size of the pyrolyzing enclosure,
- iv. rate of ventilation (oxygen content),
- v. temperature and rate of heating,
- vi. source of heat,
- vii. the physical form of the material (sheet, foam, powder, etc.)

When the temperature is varied, analysis of the decomposition products has also shown that the nature of the products from condensation, recombination, or cross-reactions significantly varies. The products of pyrolysis that are created by heat in an inert atmosphere are different from those that are obtained in an oxygen-rich environment [74].

The process of thermal decomposition of materials is of major significance to their structural and thermal properties. Furthermore, the products of the decomposition of a material may play a vital role with regard to great temperatures or fire exposure [68], [69], [75]–[77]. Therefore, it is of prime importance to investigate the thermal decomposition process of a polymeric material. Early investigations on the pyrolysis of Kevlar were based on chemical analysis and the study of volatile degradation products, which revealed that carbon was acquired through non-isotropic and non-graphitizable structures [78]–[81].

5. State of the Art in Kevlar Pyrolysis

Carbon-based materials are typically produced using a range of complex and multistep procedures from semi-crystalline precursors such as viscose rayon, phenolic resins, polyacrylonitrile (PAN), or isotropic coal tar pitches. This results in a higher production cost due to the requirement for thermal stabilization (in air at temperatures ranging from 200 to 300 °C). Dehydrogenation, oxidation, and nitrile cyclization reactions occur during this process (as shown in Fig .6.), which is followed by carbonization in an inert environment at temperatures ranging above 400 °C. However, due to the rigid-rod structure and high degree of aromaticity, direct carbonization is applicable in the case of Kevlar in order to obtain carbon (shown in Fig .7.) [82], [83]. Progressive decomposition of amide groups occurs at temperatures between 550 and 575 °C, resulting in the formation of intermediate aryl nitrile species. Kevlar appears to be chemically stable up to about 545 °C; Above 500 °C a significant weight loss takes place with no significant structural destruction until ca. 550 °C; However, the main chemical

transformation occurs over a narrow temperature range, from 550 to 575 °C, where the maximum rate of weight loss due to depolymerization occurs at 575 °C. Further decomposition causes the cleavage of C=O and C-N bonds, which eventually results in polyaromatic compounds above 600 °C [15].

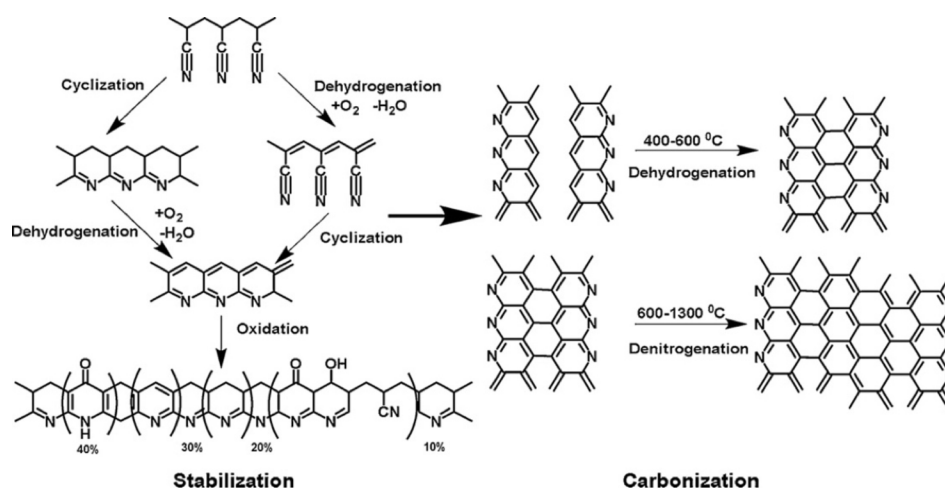


Fig. 6. Two-step thermal processing of PAN into carbon: oxidative stabilization and formation of a ladder structure, followed by carbonization [82].

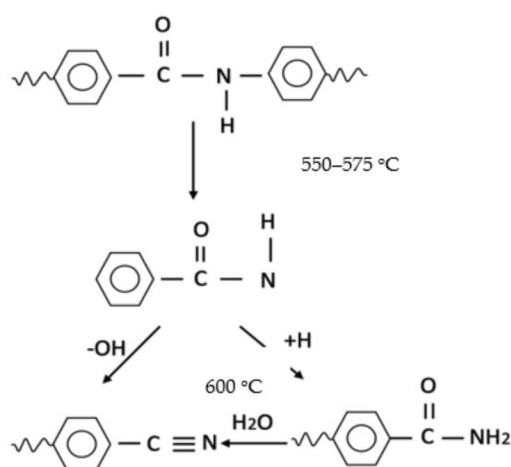


Fig. 7. Single step thermal processing of Kevlar into carbon: direct carbonization [15], [83].

A pyrogram of evolved gasses during thermal degradation (at 20 °C/min heating rate) of Kevlar shows that most of the degradation products are released from 550 °C – 650 °C [81], [84]. The volatiles evolving from Kevlar pyrolysis is constituted of various aromatic products with one, two, or three rings. These compounds were frequently formed from Ph-CO and HN-Ph (phenyl group: Ph) bonds cleavage and mainly contained amino and nitrile substituents. Both

homolytic and heterolytic reactions are involved in the formation of the thermal degradation products of aromatic polyamides. At 400 °C, Kevlar pyrolysis mostly produces H₂O and CO₂, according to Krasnov et al. [15], who similarly came to the conclusion that the thermal degradation mechanism involves hydrolysis of the NH-CO bonds and subsequent decarboxylation of carboxyl end groups. a tentative degradation pathway accounting for the formation of radicals in the polymer is shown in Fig .8 [69].

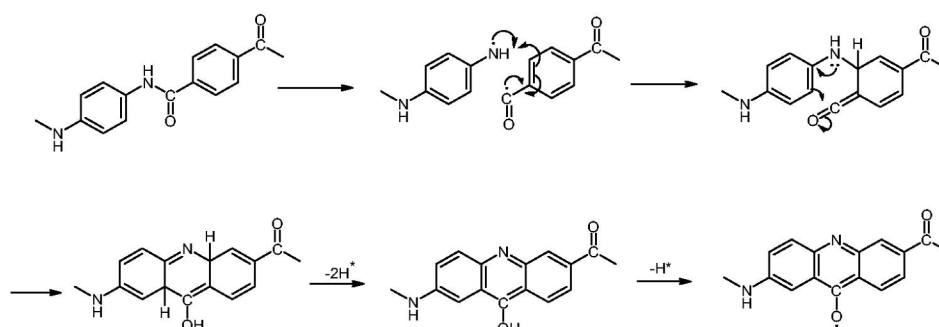


Fig. 8. Speculated thermal decomposition mechanism of Kevlar [69].

Water molecule for the hydrolysis reaction was expected to come from the dehydration of ammonium end groups generated by the interaction of terminal amino groups. Homolytic bond cleavage was more common at high temperatures, and heterolytic bond cleavage was more common at lower temperatures [85], [86]. However, the homolytic cleavage of the HN-CO bonds and aromatic -NH bonds are considered to be the initial reaction of the degradation process [87]. These are followed by -NH protonation, dehydration of intermediate end groups, and heterolytic cleavage of the NH-CO bond, all of which have been validated by other studies. [11], [83], [85].

Table 1. Temperature-dependent pyrolysis products of Kevlar 49 [85].

Temperature (°C)	Products	Comments
300–500	CO ₂ (trace amount), H ₂ O	Steady increase in yield of water with increasing temperature.
520	1,4-phenylenediamine	A significant increase in CO ₂ evolution occurs.
540	Benzonitrile, aniline, benzanilide, N-(4-aminophenyl)benzamide	
550	Benzoic acid, terephthalonitrile, 4-cyanoaniline	1,4-phenylenediamine is the most prominent product. H ₂ O and CO ₂ evolution increases.
560	Benzene	Major products are CO ₂ , 1,4-phenylenediamine, benzonitrile, aniline, benzanilide and N-(4-aminophenyl)benzamide.
580	—	Increase in evolution of all products.
590–600	H ₂ , CO, HCN, toluene, 4-tolunitrile, biphenyl, 4-aminobiphenyl, 4-cyanobiphenyl	
600–700	CH ₄ , C ₂ H ₄ , C ₂ H ₆ , CH ₃ CN	All secondary species increase markedly in this temperature range.

As shown in Table 1, below 500 °C only water and trace amounts of carbon dioxide were detected. At 520°C, 1,4-phenylenediamine was the initial structurally related product evolved. Thereafter, the formation of hydrolysis products, followed by nitriles and compounds containing phenyl end groups, followed by the formation of biphenyl derivatives, was observed for Kevlar, in the temperature range from 300 to 700 °C and many degradation products such as benzene, benzanilide, amino-benzanilides, cyano-benzanilides, and cyano-amino-benzanilides are commonly observed [85], [88]. The evidence of nitrogen oxides being formed during the thermal decomposition of Kevlar was also observed [89].

5.1. Investigation of Kevlar thermal stability

To study the thermal stability, the evolution of the weight with respect to heating rate, the degradation temperature, and the behaviour at specific temperatures, Thermogravimetric analysis performed on Kevlar at a heating rate of 10 °C/min under nitrogen showed that about 55 wt% of the material is lost from 550 °C to 650 °C and further slower degradation from 560 °C onwards [90]. The initial phase of the decomposition started at 526 °C [69] at a heating rate of 10 °C/min in air, and at 20 °C/min initial decomposition occurred at 548.1°C [91]. Also, at a heating rate of 10 °C/min, in argon, maximum mass loss initiates lower than 570 °C.

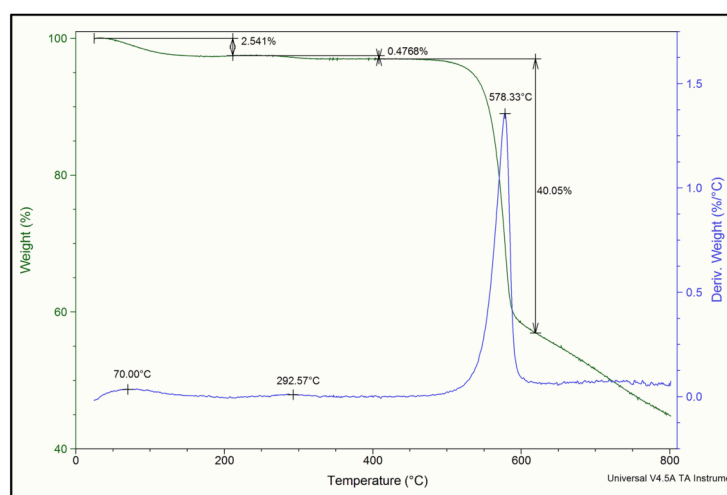


Fig. 9. Thermal degradation of Kevlar fabric by TGA. (Reevaluated based on [81], [90], [91])

The TGA curve (shown in Fig. 8) indicates the thermal decomposition of Kevlar at a heating rate of 20°C/min, under N₂ flow, by demonstrating the weight loss (%) as a function of temperature increase; when the temperature rises, weight percentage drops as a result of various

reactions that occur. When the weight percentage changes, the first stage of decomposition in the TGA curve begins at a lower temperature and continues all the way to a high temperature. The final segment of the curve denotes the material crystallization, and the temperature at which crystallization begins varies depending on the composition of the material.

Loss of water reduces the weight by about 3% near 100 °C, after which no further loss occurs up to ~300 °C. A small weight loss (0.3-0.5% of initial weight) occurred in the range 300 °C - 400 °C, possibly because of concurrent oxidation [85]. In general, no significant weight loss took place below 500 °C, and above 550 °C rapid weight loss occurred up to ~600 °C. The total weight loss at 600 °C is about 40% and above 600 °C ensuing weight loss is relatively slower, reaching a weight loss of about 55% approaching 800 °C. Nonetheless, TGA alone does not give any information about the thermal decomposition products that are released as volatiles. For this reason, TGA is often coupled with other analytical techniques such as mass spectrometry (MS) or Fourier-transform infrared spectrometry (FTIR) [92].

5.2. Heating and Atmospheric conditions

When exposed to argon, Kevlar thermally degrades in a single step, with a mass loss peak occurring at 579 °C and a corresponding mass loss of 39.74%. When the temperature reaches 1000 °C, there is a 59.73% mass loss. In air, a high mass loss peak is seen for Kevlar at 570.2 °C and a lesser one at 694.2 °C, which equates to mass losses of 39.4% and 92.72%, respectively. At 1000 °C, Kevlar has a mass loss of 98.42%, in air [89]. Contrary to air, under N₂ atmosphere, in the temperature range of 300 to 400 °C, there was a slight weight loss (0.3-0.5% of starting weight), which may have been caused by concurrent oxidation. Above 500°C, the (exothermic) weight loss in air grew quickly, reaching a residual weight of approximately 5% at 590 °C. In an environment containing N₂, no appreciable weight loss occurred below 500 °C, and up to 590 °C, rapid weight loss occurred. The subsequent weight loss is gradual; depending on the heating rate, the total nitrogen weight loss at 700°C is between 40 and 50% [81].

5.2.1. Influence of natural gas (biomass generated)

Recent developments have shown that the utilization of biomass in the pyrolysis process serves as an additional source of heat, lowering the amount of energy needed for the process and enhancing the quality of the end products. Biomass is regarded as carbon neutral when transformed into a variety of goods due to its relatively quick rate of production and

carbonaceous nature. The term "biomass resources" refers to a broad category of sources, including agricultural, wood (including solid briquette), or forest remains [23]. Charcoal is a type of solid biomass fuel that is derived from the process of carbonization, also known as pyrolysis, of wood. It is claimed that charcoal generates a more efficient and sustained fire, with higher temperatures and longer burning times, compared to coal. Although carbon monoxide can be produced during the incomplete combustion of coal, it is generated at high levels when charcoal is burned [93]. Karthik et.al, utilized charcoal, being inexpensive and readily available, as a source of CO₂, as well as heat to facilitate the pyrolysis process of Kevlar wastes, which contributes to lower production costs [15].

5.2.2. Influence of CO₂ gas (from salts)

CO₂ has been used as a reaction medium in pyrolysis in order to increase efficiency. The use of CO₂ in the pyrolysis of biomass feedstocks has been experimentally proven effective in increasing pyrolysis thermal efficiency [94]–[96]. It improves the efficiency of thermal cracking of volatile species generated during pyrolysis and may alter product yield (i.e., the composition of the gas, liquid, and solid phases in the pyrolytic product) and product characteristics [97]–[99]. CO₂ can increase pyrolysis of biomass and volatile condensation, while also encouraging tar cracking and inhibiting tar polymerization [100], [101]. When biomass is pyrolyzed in CO₂, it decomposes more deeply than when it is pyrolyzed in N₂ [102].

In order to prevent any oxidation in the pyrolyzing atmosphere, it has recently been revealed that ammonium bicarbonate can be used as a cheaper substitute and a source of CO₂ production during the pyrolysis of Kevlar [103]. Ammonium bicarbonate ((NH₄)HCO₃), an inorganic compound, decomposes above 36°C, releasing gases such as ammonia and carbon dioxide; it can also be broken down into these gases by strong acids and bases described as follows [104]: NH₄HCO₃ → NH₃ + H₂O + CO₂. Ammonium bicarbonate does not produce an alkaline sodium carbonate residue when it is heated to decomposition, in contrast to sodium bicarbonate. Therefore, it doesn't affect the pH of the decomposed product [105].

6. Thermal degradation of Kevlar and its volatile compounds

Understanding the thermal decomposition of materials holds significant importance in relation to their structural and thermal characteristics. Additionally, it has been observed that the resultant product from the breakdown of a material can have significant implications in the

context of high-temperature scenarios, as evidenced by various studies [68], [69], [82]–[84]. Consequently, it is crucial to examine the thermal decomposition mechanism of a polymer material. The production of carbonaceous materials is subject to various factors, including the type of precursor utilized, the utilization of activating agents, and notably, the pyrolysis process conditions [11], [19], [20].

Thermal degradation of polymers involves both chemical and physical processes, which work in tandem. Chemical processes are responsible for the formation of flammable volatiles, while physical changes, such as shrinkage and charring, can modify the breakdown characteristics of a material. Thermal decomposition can produce carbonaceous (char) or inorganic residues (originating from heteroatoms included in the original polymer, either within the structure or as a result of additive inclusion), or a combination of the two [72]. According to previous research, a process of fiber dehydration is conducted to remove moisture and volatile components from the raw material. Subsequently, pyrolysis and carbonization are employed in an inert atmosphere to generate heat, which facilitates the disintegration of molecular bonds and the formation of carbon structures, through non-isotropic and non-graphitizable structures [51], [78]–[81], [106]. There are different commercially available techniques often selected to identify degradation products of materials. However, the pyrolysis of polymeric waste materials, as a scheme of upcycling, and subsequently acquiring significant information on its thermal degradation process and volatiles thereof, demands simple, unsophisticated, and economic approaches.

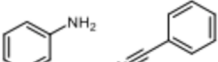
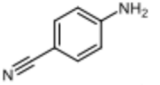
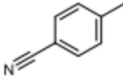
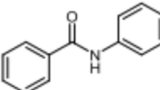
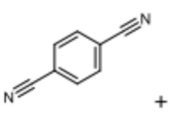
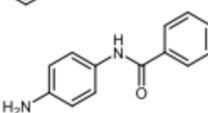
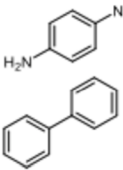
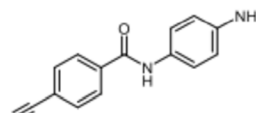
6.1. Analysis of volatile products of Kevlar pyrolysis

Indirect information has usually come from the characterization of the pyrolyzate, and thus numerous studies on the pyrolysis of Kevlar and other aramid polymers have dealt with the analysis of compounds that evolved during pyrolysis. There are several analytical techniques that have been explored, in order to gain more information on the thermal degradation of Kevlar and the volatile products exposed therefrom. The different techniques that are often chosen to identify degradation products majorly include mass spectrometry, Fourier-transform infrared spectrometry [69]; Infrared spectroscopy [18], [83]; pyrolysis-gas-chromatography/mass spectrometry (Py-GC/MS) [69], [84]; pyrolysis-field ionization mass spectrometry (Py-FIMS)

and pyrolysis-gas chromatography (Py-GC) [88]; Electron paramagnetic resonance (EPR) [89];

Py-GC/MS, being one of the most sought-after techniques in this respect, was performed on Kevlar at 600 °C in order to identify its different decomposition products. Evolved gas analysis at a heating rate of 20 °C/min was reported showing that most of the degradation products are released from 550 °C – 650 °C [84]. The identified products of the pyrolytic decomposition of Kevlar at 600 °C in an inert atmosphere are reported in Table 2 [69].

Table 2. Major products identified by Py-GC/MS of Kevlar at 600 °C in an inert atmosphere [69].

Product	Name	Product	Name
	aniline + cyanobenzene		p-cyanoaniline
	p-tolunitrile		benzanilide
	p-dicyanobenzene + p-phenylenediamin		4'-aminobenzanilide
	phenylbenzene		4-cyano-4'-aminobenzanilide

Although there are several commercial techniques of analysis as mentioned, there are some drawbacks, such as high costs (prohibitively expensive to purchase and maintain) and complex sample preparation (including extraction and clean-up procedures), which can be labour-intensive and expensive and calls for alternative tools of undemanding access, cost, and utilization. In the present work, we attempted to suggest a relatively simpler and cost-effective approach, that one could make use of, to gather initial information on volatile compounds. Furthermore, with the support of this estimated information the choice of utilizing a more sophisticated program or a more suitable technique (like Py-GC-MC or TGA-FTIR), for precise identification of the constituent compounds, could be essentially employed, if required.

The experimental procedure in the present work allows for volatile products of pyrolysis to be collected by condensing the fumes on a cold surface (in our case, a glass slide), which is then dissolved in isopropanol (IUPAC name: Propan-2-ol). For 24 hours, the dissolved solutions are

kept in a cool, dry environment to guarantee that all of the condensed pyrolysis volatiles have completely dissolved. Utilizing an Ultraviolet–visible (UV-Vis) Spectrophotometer and a StellarNet diode array (resolution 2nm), the UV-Vis absorption spectra of the samples in isopropanol, is analyzed, as shown in Fig. 9. This is followed by the potential identification of volatile compounds, by means of a spectral matrix decomposition algorithm to decompose measured spectra into possible spectra of individual components [103].

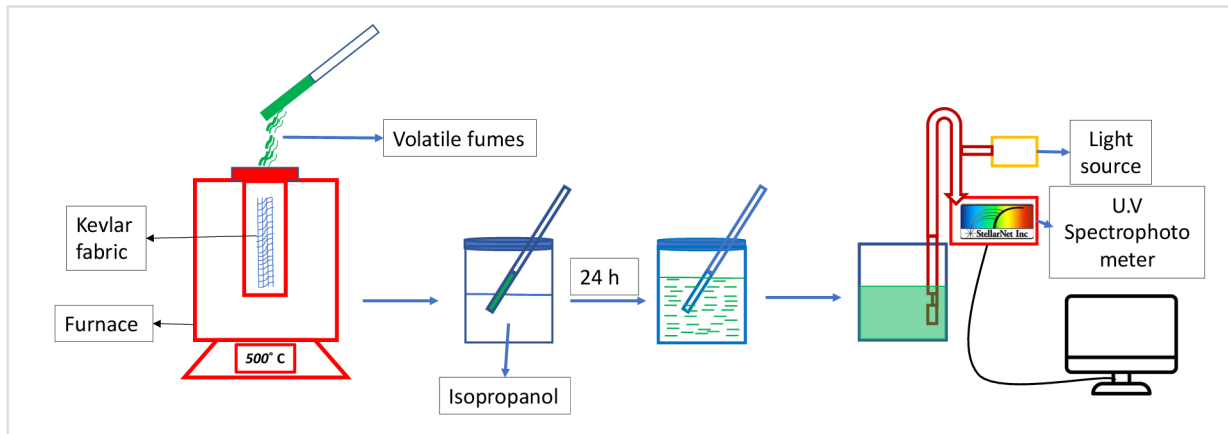


Fig. 10. Schematic illustration of the continuous process of pyrolysis, condensation of volatiles, and subsequent UV-VIS Spectroscopy analysis [107].

6.2. Elemental composition of carbonized Kevlar

The significant elemental composition (C, N, O) of the pyrolyzed materials obtained from Kevlar, at various conditions of temperature and atmosphere are shown in Table 3. The experimental evidence reveals that an increase in temperature from 600 °C to 1000 °C resulted in a corresponding increase in the proportion of carbon. The carbon content that was measured exhibits a high level of concurrence with the values that have been previously documented in the literature [83], [108]. A reduction in the content of oxygen and nitrogen has been observed. The observation made suggests that Kevlar macromolecules undergo decomposition at elevated temperatures, leading to the elimination of various constituent elements. The composition of the pyrolyzed material comprises hydrogen and sulfur in low amounts, and a small quantity of other impurities, including S, Na, Cu, Cl, and Ca, which constitute the remaining percentage.

Table 3. Effect of pyrolysis conditions on the elemental composition of Kevlar and carbonized Kevlar.

Treatment conditions	T (°C)	C (wt %)	N (wt %)	O (wt %)
Untreated [109], [110]	20	69.07	11.44	14.35
Air [110]	600	68.67	11.58	15.27
N ₂ gas [110]	600	69.86	11.71	13.61
	700	68.62	11.47	14.25
Argon [83]	~600	73.2	10.1	11.7
	~1000	75.4	5.5	17.0
CO ₂ from charcoal [15]	800	69.17	8.66	13.19
	1000	89.26	2.56	5.87
Mixed gasses from ammonium bicarbonate salt [107]	600	76.1	8.3	12.0
	1000	88.5	1.4	8.3

6.3. Ultraviolet-visible (UV-Vis) spectra of volatiles

UV-Vis spectroscopy, applicable to any type of suspension, is one of the most robust and straightforward techniques for quantifying the portion of light lost as it travels through a sample, relative to its blank counterpart [111]. Although UV-Vis spectra are generally insufficient for identifying compounds precisely as compared to Py-GC/MS, It has recently been reported that UV-Vis spectra of a suspension, along with the assistance of an algorithm for the separation of mixture spectra using spectral matrix decomposition, such as singular value decomposition, to decompose measured spectra into potential spectra of individual components, can be used to identify compounds. Following this, the constituent class of volatile chemicals created at the required wavelengths of the two components was retrieved from a database, This offers us an estimated idea of the types or classes of volatiles that are produced throughout the pyrolysis process [103]

In the present work, UV-Vis spectroscopy is used to quantitatively determine elemental concentrations of volatiles collected (as described in section) during the pyrolysis of Kevlar, on the basis of Beer-Lambert law which states that the absorbance of a suspension is directly proportional to the concentration of the absorbent present in the solution and the path length. According to the Beer-Lambert Law, the type and concentration of molecules are significant in the process of radiation absorption [112]. The Beer-Lambert Law is a useful tool for calculating the outcomes of spectroscopic tests (for example, the concentration of an absorbent, the extinction coefficient of the absorbing material, and so on), as in the case of a single compound, which is usually written as:

$$\log_{10} \frac{I_0}{I} = \epsilon c l \text{ or } A = \epsilon c l \quad (1)$$

where: I_0 – intensity of incident beam; I – intensity if transmitted beam; A – absorbance; ϵ - molar decadic extinction constant; c – concentration of absorbing species; and l – path length [112].

However, for multiple dimensions, it can be expressed as [113]:

$$\mathbf{A} = \mathbf{S} \mathbf{C} + \mathbf{E} \quad (2)$$

$$\mathbf{A} = \begin{bmatrix} a_{11} & \dots & a_{1j} & \dots & a_{1s} \\ \vdots & & \vdots & & \vdots \\ a_{i1} & \dots & a_{ij} & \dots & a_{is} \\ \vdots & & \vdots & & \vdots \\ a_{n1} & \dots & a_{nj} & \dots & a_{ns} \end{bmatrix} \quad (3)$$

where $\mathbf{A}(n \times s)$ is the matrix of measured absorbances, a_{ij} is the absorbance in j -th sample (spectra) at i -th wavelength, $\mathbf{S}(n \times m)$ is the matrix of absorption coefficients, $\mathbf{C}(m \times s)$ is the concentration matrix, $\mathbf{E}(n \times s)$ is the matrix of errors, n is the number of wavelengths (corresponding to wavelength resolution of the spectrophotometer), s is number of samples (spectra) and m is number of different absorbing compounds present in the samples. Each column of matrix \mathbf{A} is in fact one discrete UV -VIS spectrum corresponding to a given sample.

It is considered, $\mathbf{A} = \mathbf{U} \mathbf{D} \mathbf{V}^{-1}$ be a singular value decomposition of the spectral absorbance matrix \mathbf{A} with $\mathbf{U}(n \times s)$, diagonal $\mathbf{D}(s \times s)$, $\mathbf{V}(s \times s)$ with columns of \mathbf{U} and rows of \mathbf{V}^{-1} sorted

in decreasing order of diagonal elements of \mathbf{D} . (containing on diagonal singular values expressing relative importance of individual components of mixture spectrum). Assume that number of real compounds (individual components) is smaller than number of samples and individual concentrations are not in the same ratios. Then the dimensionality can be reduced to assumed k compounds (individual components in mixture spectrum) by decreasing the size of the matrices (cutting off rows/columns) to $\mathbf{U}_k (n \times k)$, diagonal $\mathbf{D}_k (k \times k)$, and $\mathbf{V}_k (s \times k)$, then $\mathbf{A} = \mathbf{UDV}^{-1}$ becomes

$$\mathbf{A} = \mathbf{U}_k \mathbf{D}_k \mathbf{V}_k^{-1} + \hat{\mathbf{E}} \quad (4)$$

Where $\hat{\mathbf{E}} (n \times s)$ can be interpreted as the matrix of estimated errors. By introducing a rotation matrix \mathbf{R} of an appropriate size [114], [115], (4) can be re-written as

$$\mathbf{A} = (\mathbf{U}_k \mathbf{D}_k \mathbf{R}) (\mathbf{R}^{-1} \mathbf{V}_k^{-1}) + \hat{\mathbf{E}} \quad (5)$$

It can be seen that (2) is a special case of (5) implying that the factors in brackets are reconstructed spectra of the assumed individual compounds and their concentrations in samples for a particular \mathbf{R} .

$$\begin{aligned} (\mathbf{U}_k \mathbf{D}_k \mathbf{R}) &= \mathbf{S}^* \approx \mathbf{S} \\ (\mathbf{R}^{-1} \mathbf{V}_k^{-1}) &= \mathbf{C}^* \approx \mathbf{C} \end{aligned} \quad (6)$$

Since both concentrations and absorption coefficients are non-negative numbers, the rotation matrix should ensure that all elements of the two matrices be non-negative. There exist many strategies how to find optimal \mathbf{R} .

As a criterion the roots for a minimum of selected column of \mathbf{S} , $\arg \min_{\mathbf{R}} \left\{ (S_{\cdot j}^*)^2 \right\}$ is used. This algorithm is general based on the Beer-Lambert law validity; this algorithm is oriented to decompose spectra into m components according to criterion the roots for a minimum of selected column of matrix \mathbf{S} (eqn. 5). Other programs are obviously decomposing arbitrary spectrum without use the information about their origin (Beer-Lambert law) and number of components is not optimized [84], [116]. Two components were here identified automatically

as optimal by program. For two assumed components the reconstructed individual spectra and concentrations according to eqn. (5) are shown in Fig. 10 (a) and (b).

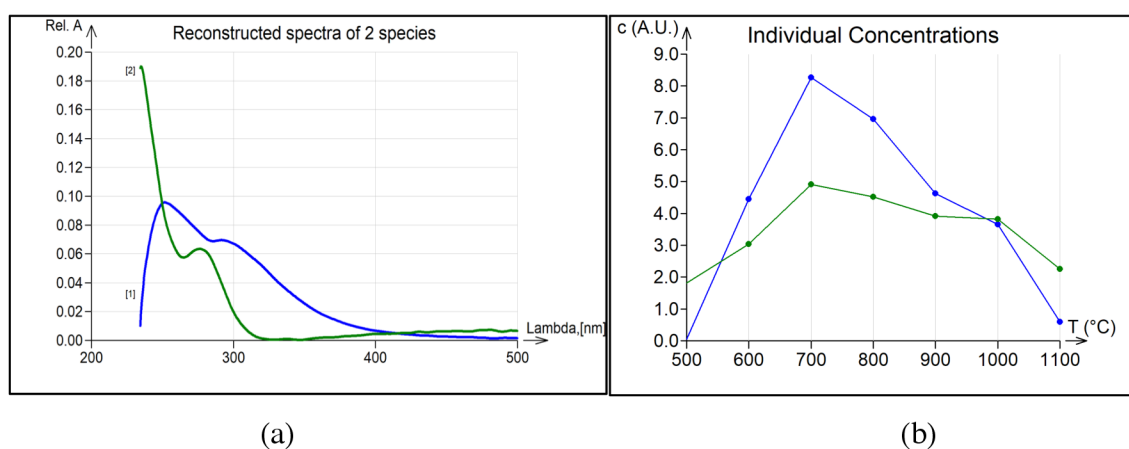


Fig. 11. Reconstructed UV-VIS spectra (a) of the two assumed components, and (b) of the two identified components at temperatures 500 – 1100 °C [103].

Typically, the reconstructed spectra of the assumed components (in the present work, two components) may potentially comprise a mixture of compounds. The chemical identification of pyrolysis products has been previously documented through a variety of methods [1, 6, 7, 9, 10, 12, 15] (also illustrated extensively in section,). Czégény and Blazsó [117] reported that the decomposition pyrograms of Kevlar, as analyzed by Py-GC-MS, yielded benzonitrile, aniline, benzeneamine, and benzoic acid as the primary products in the temperature range of 600 - 800 °C. The formation of benzonitrile was attributed to the homolytic cleavage of the aromatic -NH bond, followed by protonation and dehydration. At 600 °C, benzene, and benzonitrile were identified as the predominant fragments, with near attainment of 80% at 750 °C, according to a separate investigation. In addition, a multitude of compounds including benzaldehyde, benzoic acid, benzoate, and aniline were synthesized as reported in reference [12]. This study utilized an 'Organic Compounds Database' to identify the constituent class/types of compounds present at the specified wavelength maxima of the two components. It is noteworthy that certain volatile compounds identified in prior research, fall under one of the categories of volatile compounds obtained in the current study [103]. It was found that one of the components identifies aniline (n,n-dimethylaniline, n-ethylaniline, 3,5-dichloroaniline, p-iodoaniline); and the other component identifies benzonitrile (tolunitrile, chlorobenzonitrile, bromobenzonitrile) which has been confirmed previously [12], [117].

7. Development of porous and electrically conductive activated carbon fabric from Kevlar wastes

The majority of textile waste treatment methods do not fully maximize the potential of textile materials and lack economic viability. The conversion of specific textile residues into carbon or partially carbonized structures presents notable economic benefits. The control and optimization of carbonization processes are crucial in the production of carbon materials that exhibit specific characteristics such as tuned porosity, sorption capacity, thermal resistance, and electrical conductivity. These properties are greatly dependent on the precursor utilized [43], [44]. The utilization of Aramid fibers, which are highly ordered polymer precursors, has been studied for the production of activated carbon fiber, and it is noteworthy that these precursors do not require oxidative stabilization, unlike PAN-based precursors [49]. The rigid-rod structure and high degree of aromaticity exhibited by Kevlar make direct carbonization a viable method for obtaining carbon. The fibrous wastes of Kevlar have demonstrated their suitability in the production of porous activated carbon due to their exceptional inherent structure and minimal ash content. This material offers several benefits over other carbon sources, including its cost-effectiveness, high density, superior purity, and lack of contaminants [15]. The conversion of Kevlar woven fabric wastes into activated carbon can be achieved through physical activation by means of a straightforward and regulated thermal treatment process. Optimization of the variables involved in the carbonization process can lead to the attainment of a greater specific surface area and enhanced electrical conductivity of the resulting product. Such carbonized products have the potential to serve as highly effective materials for electromagnetic shielding purposes [15].

7.1.Preparation of carbon structures from Kevlar fabric wastes

From the pyrolysis-based upcycling of various polymeric fiber wastes, there are numerous possibilities for the preparation of improved carbon structures, based on the mode of heating and type of heating equipment, heating rate, and internal atmospheric conditions. Carbonized materials obtained from upcycling involve the thermal decomposition of waste polymeric materials in order to recover carbon-rich products. This method has been the subject of substantial research in the field of fiber recovery.

There are various carbonization procedures that can be used, including microwave heating [22], cyclic oxidation [118], and hydrothermal processes [119]. To prepare carbon structures, however, we describe straightforward, cost-effective direct carbonization procedures in the current work. Distinct from our previous work on the development of carbon functional materials from acrylic fibrous wastes, we here demonstrate a novel and direct process of carbonization to produce carbon functional materials from Kevlar woven fabric wastes, without the need for an intermediate stabilization step. This is done at carbonization temperatures varying from 500 – 1200 °C and without any holding time. Fig. 11. shows the different stages of the production of activated carbon fabric from Kevlar fibrous wastes [15].

The effectiveness of the pyrolysis process, as well as the yield at the end of it, can be improved by using one of several different carbonization atmospheres. Ar₂ (94), N₂ (88), and CO₂ (101-103), are some examples of these. It has been demonstrated through experimentation that including CO₂ increases the thermal efficiency of the pyrolysis process (), and deeper decomposition relative to N₂ (109). In the present work, we utilize charcoal [15] and ammonium bicarbonate salt [107] (in separate methods) as sources of producing CO₂ and mixed gasses, respectively, which are inexpensive and commonly available in comparison to N₂ gas. This is done in order to potentially avoid the presence of oxygen inside the furnace during the carbonization process.

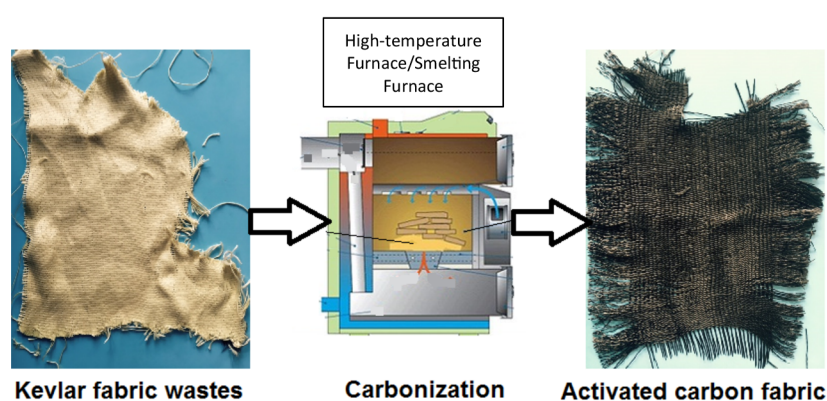


Fig. 12. Schematic of activated carbon fabric preparation from Kevlar fibrous wastes [15].

7.2. Yield of carbonized product from Kevlar

The carbon-rich products obtained by various methods are listed in Table 5, with details of their yields in percentages. In all cases, the yield of activated carbon is reduced with an increase

in carbonization temperature. The present work involved the implementation of three distinct methods based on atmospheric conditions inside the furnace. Specifically, the present methods utilized the CO₂ produced from charcoal, a combination of gases derived from ammonium bicarbonate salt (NH₄HCO₃), and Nitrogen gas (N₂), respectively. It can be observed that the use of charcoal contributes to higher yield at higher carbonization temperatures, which makes it a remarkable and cost-effective substitute in comparison to yield from other atmospheres. In the presence of charcoal, the yield is about 31% at 1200 °C, which still is substantial, relative to other atmospheres.

Table 4. Yield of Kevlar-derived activated carbon.

Atmospheres	Heating rate (min/°C)	Carbonization temperatures (°C)	Yield (wt%)
Air	10, 10	600, 650	32 [120], 10 [121]
Argon	10, 20	650, 800	65 [120], 41 [122]
Nitrogen	2, 10	650, 650	61 [109], 45 [121]
Charcoal (CO ₂)*	5	800, 1000	58, 36
Ammonium bicarbonate salt (CO ₂)*	~55	800, 1000	30, 23
Nitrogen*	20	800, 1000	46, 34

* reported in the present work [15], [103], [107]

7.3. Physical and morphological characteristics of Kevlar-derived activated carbon

Along with the change in chemical composition, the physical properties undergo modification during the carbonization process, to eventually produce highly porous and light-weight activated carbon structures [16]. The physical features of activated carbon fabrics produced from Kevlar are altered by the carbonization temperature, as shown in Table 6. After carbonization at 1200 °C, it was discovered that the areal density and thickness of Kevlar fabrics decreased by more than 50%. Due to increased porosity, decreased inter-fiber/yarn friction, and abrasion at fiber/yarn cross-over locations brought on by the decomposition of organic materials from Kevlar fabric during the carbonization, it was determined that stiffness decreased with an increase in carbonization temperature. Unlike our prior experience with acrylic fibers [123], the carbonization of the Kevlar fabrics resulted in a small change in their

dimensions, which suggested that Kevlar fabrics have superior thermal stability because of the highly ordered arrangement of macromolecules.

It is interesting to note that carbonized Kevlar has been proven to be more flexible than conventional carbon and Kevlar fabric (see Fig. 12). This suggested that the activated carbon textiles being created had better drape qualities, which would increase comfort when used as personal protective structures. In general, although lacking in mechanical strength, the carbonaceous products produced at higher carbonization temperatures preserved their fabric shape and possessed structural integrity, making them appropriate for handling for potential application and additional analysis.

Table 5. Effect of carbonization temperature on physical and mechanical properties of activated carbon fabric produced from Kevlar [15].

Sample	Areal density (g/m ²)	Thickness (mm)	Shrinkage	Flexibility	Dusting	Stiffness (N.m)	Breaking force (N)	Breaking elongation (%)
Kevlar	217.6	1.16	-	-	-	40.92±8.13	126.74±9.07	1.79±0.23
800 °C	124.8	0.61	Good	Average	Good	8.48±1.17	2.7±1.30	1.15±0.49
1000 °C	101.3	0.54	Good	Good	Average	5.38±1.01	2.25±1.06	1.67±0.49
1200 °C	90.7	0.46	Average	Excellent	Poor	4.16±0.93	2.09±1.01	0.94±0.27

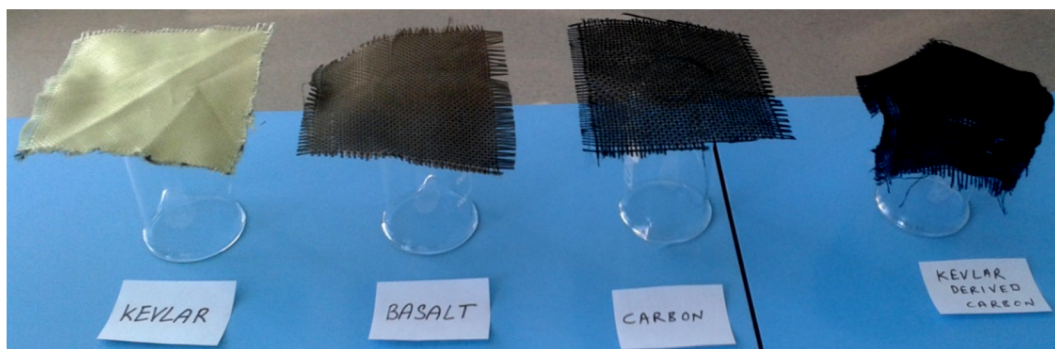


Fig. 13. Visual observation of Flexibility Kevlar-derived activated carbon fabric in comparison to some commercial fabrics [15].

Furthermore, it can be observed that the carbon fibers and activated carbon fibers exhibited a significantly rougher surface in comparison to the unheated Kevlar fibers. This phenomenon

was attributed to the generation of additional pores on the Kevlar fibers during the carbonization process [122]. As illustrated in Fig. 3, the surface of the fibers acquired under elevated temperatures exhibited a markedly uneven texture and displayed prominent ridges. Fig. 3(b) depicts the corrugation of carbonized fiber surfaces resulting from the disruption of hydrogen bonds and π - π interactions within Kevlar macromolecules at a temperature of 800 °C. It is observed that the surface roughness exhibited an upward trend in tandem with the rise in the carbonization temperature [50]. This trend was indicative of the emergence of more added pores or rough surfaces subsequent to the physical activation of Kevlar fabric wastes. The emergence of discrete micropores on the surface of Kevlar fibers can additionally be observed upon exposure to a temperature of 1000 °C, as depicted in Fig. 13(c) [123].

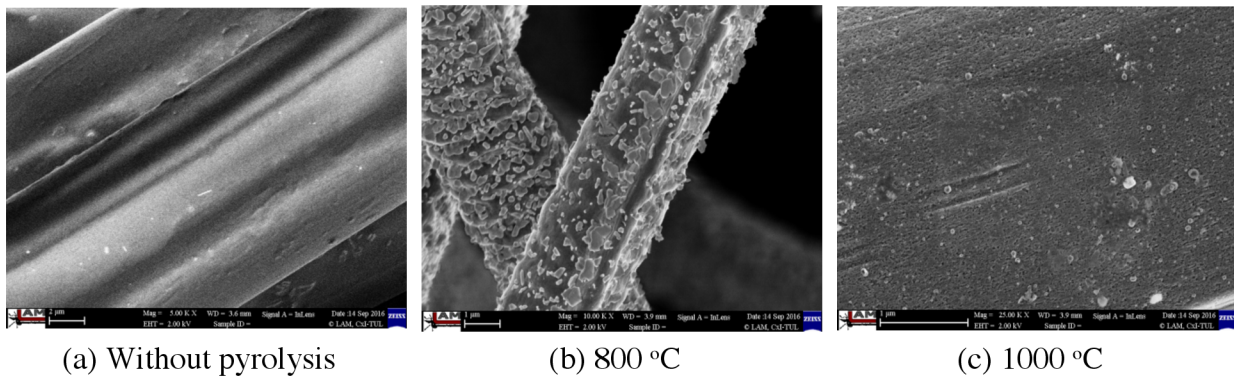


Fig. 14. Microstructure of Kevlar fibers and corresponding carbon fibers under elevated pyrolysis temperatures (a) Kevlar without pyrolysis (b) activated carbon at 800 °C; (c) and activated carbon fabric at 1200 °C [15].

7.4. Specific Surface Area of Kevlar-derived activated carbon

Compared to conventional carbon fibers, activated carbon fiber (ACF) has a number of important advantages. High specific surface area, high adsorption capacity, and extremely high rates of gas or liquid phase adsorption are a few of these. It is well-known that due to its highly porous in nature and large pore volume of activated carbon fibers, it has widely been utilized for gas separation, solvent recovery, pollutant removal from water, wastewater treatment, and as a catalyst or catalytic support for various energy storage and conversion processes. Numerous types of materials (both natural and synthetic) have been investigated as precursors since the pore characteristics of activated carbon are mainly dependent on the precursor materials and the synthesis method. Coal, coconut shells, wood, agricultural wastes, or

industrial wastes are some of the most often used precursors in the synthesis of activated carbon. For the use of the resulting product, precise structural and surface qualities are crucial, and these features can be described by a variety of physicochemical methods, such as BET (Brunauer-Emmett-Teller) surface area, XRD (X-ray powder diffraction), and SEM (scanning electron microscopy) [124]–[126]. Fig. 9 shows the models for pore structure on the basis of the fractal simulation and the displayed model of pores existing in the porous material is expressed using a simulation device consistent with the results obtained from Transmission electron microscope (TEM) observation of a section sample of an ACF [127].

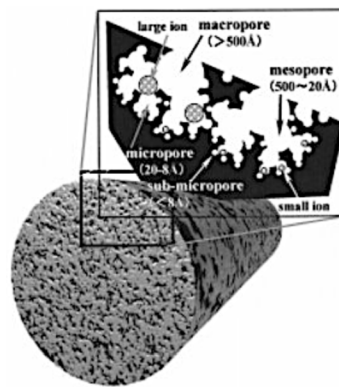


Fig. 15. Porous structure of ACF by fractal simulation.

Two alternative processes, namely physical (or thermal) activation, and chemical activation can be used to create the porous texture of carbon compounds. When creating porous carbons through chemical activation, the precursor is heated up while being exposed to a chemical agent in a single process. ACFs obtained from Kevlar by physical activation, either with steam or CO_2 , or chemical activation with Phosphoric acid yielded N_2 adsorption isotherms of type I with a small contribution of type IV, as well as a small type H4 hysteresis loop that becomes more evident as the burnoff (BO) increases [51].

ACFs with BET surface areas are about $1000 \text{ m}^2/\text{g}$ are produced when Kevlar is physically activated with CO_2 , according to earlier studies in the literature, even at significant burn-offs. Pre-impregnating Kevlar with small amounts of phosphoric acid has a strong effect on pyrolysis and subsequent CO_2 physical activation of the char results in ACFs with surface areas close to $1700 \text{ m}^2/\text{g}$ and pore volumes that are more than double the values corresponding to ACFs prepared by CO_2 physical activation from non-impregnated Kevlar [11], [16]. It is to be mentioned that similar porous textural characteristics have been obtained with different varieties of Kevlar i.e., either Kevlar pulp or the more crystalline conventional Kevlar [49].

The gasification of non-graphitic carbon and heteroatoms, the reaction with graphitic carbon, and the restructuring of layers of pseudo-graphitic planes are all responsible for the loss of small molecules (CO and CO₂) and the creation of improved porosity and surface area during physical activation. An increase in the thickness of the layers of graphitic planes after carbonization and the selective gasification of the less organized carbonaceous material may also be related to the formation of microporosity [38], [105].

In a previous study, by carbonizing Kevlar fibers at 900 °C in an argon atmosphere and then activating them with CO₂ at 800 °C, Martinez-Alonso et al. produced activated carbon fibers with BET-specific surface areas of 986 m²/g, total pore volumes of 0.50 cm³/g, micropore volumes of 0.43 cm³/g, and ultra micropore volumes of 0.28 cm³/g. Giraldo et al. also synthesized ACFs from Kevlar, but they first carbonized the fibers at temperatures of 800, 900, and 1000 °C under flowing nitrogen before activating them with water vapor at 750 °C for one or two hours. The best material has a micropore volume of 0.24 cm³/g and a specific surface area of 460 m²/g. N₂, and CO₂, adsorption data indicate that the resulting ACFs are essentially microporous, with a narrow pore size distribution closely associated with the crystalline character of the precursor [90].

The specific surface area of activated carbon fibers plays a crucial role in influencing the electrical properties and electromagnetic shielding behavior through the absorption of the radiations [123]. The porosity and surface area created during the carbonization process is due to the loss of non-graphitic molecules as volatiles and selective gasification of the less ordered fractions of the carbonaceous material, and the reorganization of layers of pseudo-graphitic planes [79]. The specific surface area of carbonized Kevlar fabrics can be obtained by Nitrogen adsorption–desorption isotherm measurements at 77.35 K, using BET (Brunauer-Emmett-Teller) surface area analysis [124]–[126].

The Kevlar chars investigated in earlier studies [49] show a tendency to attain a limit in pore development not previously observed with comparable rayon-based chars [128]. In the latter case, the pore volume per unit mass continues to increase beyond 90% burn-off. An explanation for this behavior can be advanced in terms of the gasification-induced densification effect [49], whereby significant shrinkage of the carbon structure is observed at all stages of burn-off. In the case of carbon dioxide-activated rayon chars, it has been shown that at higher levels of burn-off, both pore widening and pore narrowing can occur [128]. Further, with subsequent

activation (physical or chemical) of the carbonized material, the surface area immensely increases with higher micropore volume ($\geq 1000 \text{ m}^2/\text{g}$ at $\sim 800^\circ\text{C}$) [50], [83].

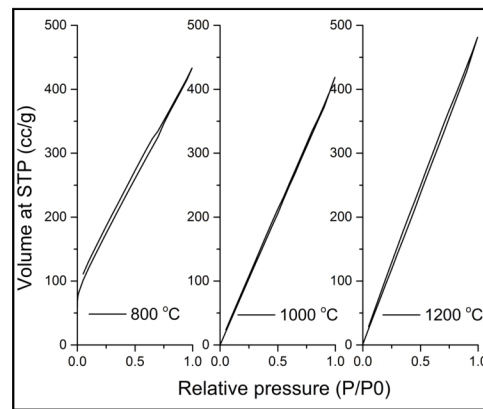


Fig. 16. Adsorption-desorption isotherm of Kevlar-derived activated carbon fabrics [15].

The present work examined the BET analysis of Kevlar-derived carbon fabric structures after carbonization at 800°C , 1000°C , and 1200°C without additional activation. The results showed a type I isotherm from the nitrogen adsorption/desorption isotherm, indicating uniform micropores in the materials (shown in Fig.14.). This classification is consistent with the subdivision proposed by Rouquerol et al [129] and the International Union of Pure and Applied Chemistry (IUPAC) classification [16], [50] [117]. Furthermore, the study revealed the presence of a type IV contribution featuring a type H4 hysteresis loop, a characteristic commonly observed in materials containing slit-shaped pores as described by Gregg et al [130]. Additionally, an increase in carbonization temperature was found to result in a narrower type H4 hysteresis loop, indicating a minimal impact of carbonization temperature on the formation of mesoporosity within the structure [39]. It can be seen that there is a small rise in the specific surface area as the carbonization temperature increases. Specifically, the activated carbon fabric that was produced at a temperature of 1200°C exhibited a specific surface area of $248 \text{ m}^2/\text{g}$. The observed specific surface areas, which are relatively lower, and the limited pore development at higher carbonization temperatures, as compared to prior research, may be attributed to the potential pore collapse or closure due to gasification-induced densification, as reported in previous studies [45], [76], [116][38], [131]. Upon a more thorough analysis of the isotherms, it is apparent that the desorption branch exhibits a near-parallel trend in every instance, indicating that the adsorbate has been confined within the highly restricted pore network. At increased levels of burn-off, the low-pressure hysteresis demonstrates a decrease,

which suggests that the pore system is becoming increasingly accessible. As a result, a reduced proportion of the adsorbate is confined at low relative pressures [49].

7.5. Electrical conductivity of Kevlar-derived activated carbon

Depending on the intended application, the electrical conductivity of activated carbon fibers is a crucial defining property in addition to high porosity. The electrical characteristics of activated carbon fibers are highly variable and mostly dependent on the fiber structure. Higher levels of crystallinity in carbon fibers lead to higher levels of thermal and electrical conductivity. The porous structure is dramatically developed when the carbonized fibers are further activated, which significantly lowers the thermal and electrical characteristics. Additionally, it was discovered that higher degrees of activation remove material from ACF, increasing porosity but decreasing conductivity in the process. The available cross-section for current to travel through the activated carbon fiber diminishes as the surface area increases. Therefore, a decrease in the graphitic organization and the cross-section area accessible for an electric charge to travel through a fiber resulted in a decrease in electrical conductivity. For electrical applications and joule heating, the electrical conductivity of activated carbon fiber is a critical concern [132].

According to one study, the electrical resistivity of activated carbon fibers follows Mott's law with an exponent of 1/2 as illustrated in the equation below [97].

$$\sigma(T) = \sigma_0 \exp \left[-\sqrt{\left(\frac{T_0}{T}\right)} \right] \quad (7)$$

Here, σ_0 is the conductivity constant, T is the temperature being measured, and T_0 is the fitting parameter that is sensitive to the energy needed for hopping. Exponent 1/3 is preferable to exponent 1/2, according to a different study [133]. By increasing the carbonization temperature, electrical conductivity increases. When ACF is created at higher temperatures, turbostratic structure is more likely to form in the core sections of the fiber, increasing electrical conductivity at higher temperatures. By aligning non-graphitic compounds during the carbonization process, high temperature aids in the production of nanographites with a more ordered structure. Other techniques, like as surface functional group inclusion, heat treatment, and physical adsorption, can also be used to increase the electrical conductivity of ACF [134]. The surface and volume resistivity of activated carbon fabric can be determined by the Concentric Electrode Method according to ASTM D257-14 or by the Parallel electrode

method. In the Concentric Electrode Method, direct current is applied at a voltage of 100 ± 5 V across opposite ends of activated carbon fabric and the resultant current flowing across a sample.

The parallel electrode measurement setup is shown in Fig .15. Here, the sample material is clamped in position along its width by a pair of electrodes at both ends, at a specific distance apart, connected to a multimeter that displays the electrical resistance (in ohms) of the material in series. After which, the electrical resistivity (in ohm. cm) is calculated.

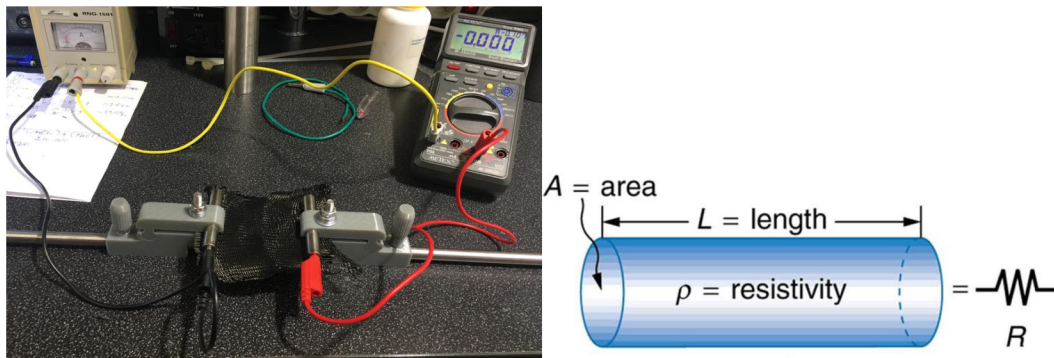


Fig. 17. Parallel electrode measurement setup.

Resistivity is calculated by using the equation,

$$\rho = R \times \frac{A}{L} \quad (8)$$

Where, ρ = Surface Resisivity ($\Omega \cdot m$); R = Electrical resistance (Ω); A = Cross-sectional area of the electrode (m^2); L = Distance between electrodes (m). It has been investigated that both surface and volume resistivity of Kevlar-derived carbon products decreased with increased carbonization temperature, using the concentric electrode method [15]. In another study, the electrical resistivity of the Kevlar fabrics was carbonized to four temperatures ranging from 800–1100 °C, using the parallel electrode measurement setup. It is reported that the electrical resistivity decreased progressively with increasing carbonization temperatures, which is attributed to the higher carbon yield due to carbonization at higher temperatures due to the removal of organic compounds in the form of volatiles [107]. The movement of electrons through each graphite layer or the hopping of electrons across the defects/interfaces between disordered graphite layers can be attributed to the development of electrical conductivity in activated carbon samples [12], [135], [136].

The intrinsic conductivity of individual carbon particles, the resistance of inter-particle contacts, and the volume density of the latter are all factors that have been widely recognized to influence the overall electrical conductivity of activated carbon (AC) and other carbonaceous materials. The electrical conductivity inherent to carbon materials is primarily determined by the voids present within their constituent particles and grains. Evidently, the aforementioned area encompasses the porosity that corresponds to the voids within the particles. The correlation between the total pore volume of the AC sample and its intrinsic electrical conductivity is straightforward. Specifically, an increase in the total pore volume of the AC sample is associated with a decrease in its intrinsic electrical conductivity [137].

The graphitization degree of AC materials is a significant factor that strongly influences their electrical conductivity magnitude, as widely acknowledged. The aforementioned characteristic is predominantly influenced by the precursor substance and the techniques employed in the manufacturing procedure, particularly in the carbonization phase. According to reports, there is a progressive decrease in electrical resistivity as the carbonization temperature increases. This phenomenon is considered to be instigated by the higher carbon yield resulting from carbonization at higher temperatures, which leads to the removal of organic compounds in the form of volatiles [15][123]. The impact of pyrolysis temperature on the DC electrical conductivity of a range of AC pellets [138]. The results indicate a significant rise in conductivity as the carbonization temperatures were increased within the range of 410 to 600 C, as illustrated in Fig. 16(a).

It has been previously reported, the resistivity in unidirectional carbon fiber reinforced polymer composites along the fibers is observed to be low, measuring 0.022 m Ω m, while the resistivity transverse to the fiber direction is comparatively high, measuring 310 m Ω m [139]. The resistivity of carbon fibers varies between 2 and 20 $\mu\Omega$ m, contingent upon the specific type of fiber [140]. According to Zhao et al [141], the incorporation of approximately 1.0 wt% CNTs resulted in an increase in the electrical resistivity of CNT/polymer composites to approximately 0.1 Ω .cm. This study involves the preparation of activated carbon fabrics derived from Kevlar through single-step thermal treatments using three distinct atmospheres. These atmospheres include CO₂ evolved from charcoal (method 1), a mixture of gases from ammonium bicarbonate salt (NH₄HCO₃) (method 2), and Nitrogen gas (N₂) (method 3). The electrical properties exhibited by these activated carbon fabrics are noteworthy (as shown in Fig. 16(b)) [107].

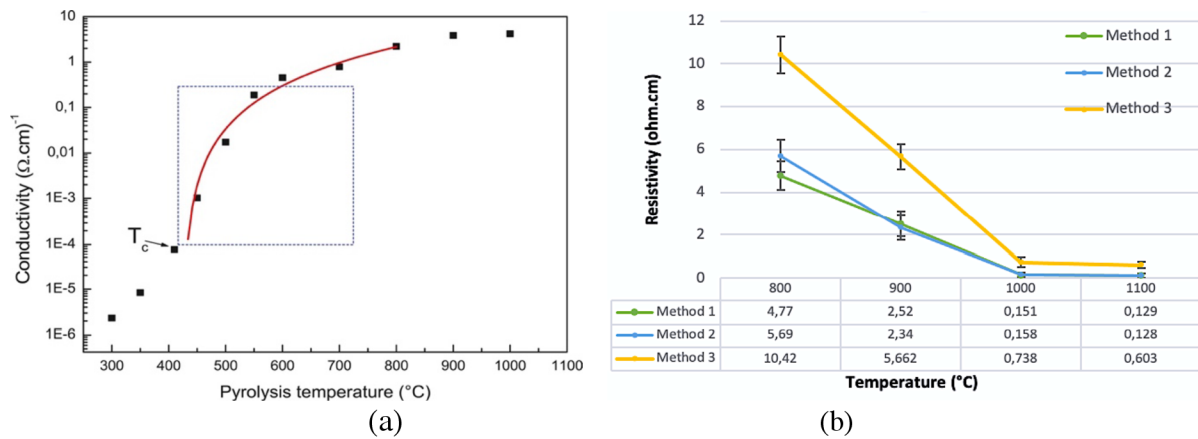


Fig. 18. (a) The direct current, room temperature conductivity versus pyrolysis temperature [138]; and (b) Electrical resistivity of activated carbon fabrics from methods 1, 2, and 3 [107].

The optimization of pyrolysis conditions can be tailored to meet specific electrical property requirements. The present work observed a significant decrease in surface and volume resistivity of approximately 15×10^3 and 25×10^2 times, respectively, for the activated carbon sample activated at 1200 °C compared to the sample activated at 800 °C. The enhanced electrical conductivity of the activated carbon sample at 1200 °C, as depicted in Table 7, can be attributed to the increased graphitization process. The observed impact of temperature could potentially be attributed to the graphitic structure, as higher temperatures can facilitate the development of such a structure and consequently enhance conductivity [142], [143].

Table 6. Effect of carbonization temperature on the electrical conductivity of activated carbon fabric [15], [107].

Concentric Electrode Method - Surface resistivity (ohm)		
800 °C	1000 °C	1200 °C
1.60×10^6	486.15	95.78
Concentric Electrode Method - Volume resistivity (ohm.cm)		
800 °C	1000 °C	1200 °C
967.14×10^3	1251.29	414.14

Parallel Electrode Method (ohm.cm)			
800 °C	900 °C	1000 °C	1100 °C
4.77	2.52	0.151	0.129

The phenomenon of electron tunneling, wherein electrons are capable of traversing the interstitial spaces between closely situated grains and particles, has been widely acknowledged as the principal mode of electrical conduction in carbon-based granular and powder materials [144]. The reduction of inter-particle distances and the consequent increase in inter-grain contact are expected to significantly augment the electrical conductivity of the specimen [145]. In addition, the electrical properties are affected by the oxygen-free Lewis-basic sites present on the graphene sheets that are produced through the heat treatment of AC samples. The hypothesis suggests that the emergence of operative groups and configurations on the surface of activated carbon is due to the interaction between oxygen, which has a high electronegativity, and carbon atoms that donate electrons, which are situated on the periphery of the nanographene sheets. This interaction leads to a specific localization of the conduction electrons, resulting in an elevation of the electrical resistance [144]–[146].

8. Electromagnetic Shielding Effectiveness of Kevlar-derived activated carbon

Although there have been numerous research studies on electromagnetic interference (EMI) shielding materials in the past, the creation of new, lightweight shielding materials with strong absorption and weak secondary reflection has become necessary for improvements in EMI shielding effectiveness that are more environmentally friendly. Although research has focused on the porous morphology, large specific surface area, and increased electrical conductivity of shielding materials as critical variables, there is still a significant challenge in creating lightweight structures with outstanding EMI shielding qualities on an economic basis [147]–[151].

Absorption, reflection, and multiple internal reflections are the three mechanisms contributing to the overall efficiency of electromagnetic radiation or EMI shielding. Typically, reflection serves as the primary EMI shielding technique. A carrier of unpaired electrons or holes, which

interact with the electromagnetic field in the radiation, is required for a material to reflect EMI. As a result, the shielding material must be conductive; however, high conductivity isn't strictly necessary (a volume resistivity of about $1 \text{ } \Omega \text{ cm}$ is usually enough). Absorption, a secondary EMI shielding mechanism, is influenced by the material's thickness. With electric and/or magnetic dipoles in the shield that can interact with the EM radiation, shielding through absorption becomes more effective. Multiple internal reflections, also known as EM radiation reflection occurring from numerous internal surfaces, phase interfaces, and inhomogeneities in the shielding material, is the third EMI shielding method. Foam or porous materials, which have a high specific surface area, or composites made of fillers with high specific surface areas with a large phase interface, are materials with good multiple reflection capacity [74], [152]–[154].

Only the regions near the surface of the electric conductors can be penetrated by high-frequency electromagnetic radiation, known as the ‘skin effect.’ As the electromagnetic wave travels through the conductor, its strength exponentially decreases [155]. The skin depth (δ) is the depth at which the electric field decreases to $1/e$ (e is Euler's number, and $1/e$ is equivalent to 0.37 of the incident value) and is represented as:

$$\delta = \frac{1}{\sqrt{\pi f \sigma \mu}} \quad (9)$$

Where: f – frequency of electromagnetic radiation, σ – shield electric conductivity ($\Omega^{-1} \text{ m}^{-1}$)
 μ – shield magnetic permeability, $\mu = \mu_0 \mu_r$, where μ_r = shield relative magnetic permeability, and μ_0 – permeability of air or free space ($\mu_0 = 4\pi \times 10^{-7} \text{ H m}^{-1}$). It is clear that as the EM wave frequency, magnetic permeability, and conductivity of the shield increase, so does the skin depth. The potential interaction between EM waves and shielding materials is depicted in Fig. 19. When electromagnetic waves (EM) enter a shielding material; they first interact with the surface before penetrating it and entering the inside. Absorption loss (SE_A) occurs when the main body of the material absorbs a portion of the electromagnetic waves. Reflection loss (SE_R) results from EM waves being reflected by a material's surface rather than absorbed by it. Multiple reflection loss (SE_M) occurs when absorbed electromagnetic waves travel to a different shielding material interface and are reflected once more. This is followed by energy dissipation inside the shielding material. The three principal types of losses— SE_R , SE_A and SE_M —all work together to attenuate EM waves; therefore, the sum of the three effects above can be used to compute the total SE of EMI (SET), as indicated in the equation below [156], [157]:

$$SE_T = 10 \log_{10} \frac{P_I}{P_T} = 20 \log_{10} \frac{E_I}{E_T} = 20 \log_{10} \frac{H_I}{H_T} = SE_R + SE_A + SE_M \quad (10)$$

Where P_I , P_T , E_I , E_T , H_I , and H_T stand for the incident power, transmitted power, incident electric field intensity, transmitted electric field intensity, incident magnetic field intensity, and transmitted magnetic field intensity, respectively.

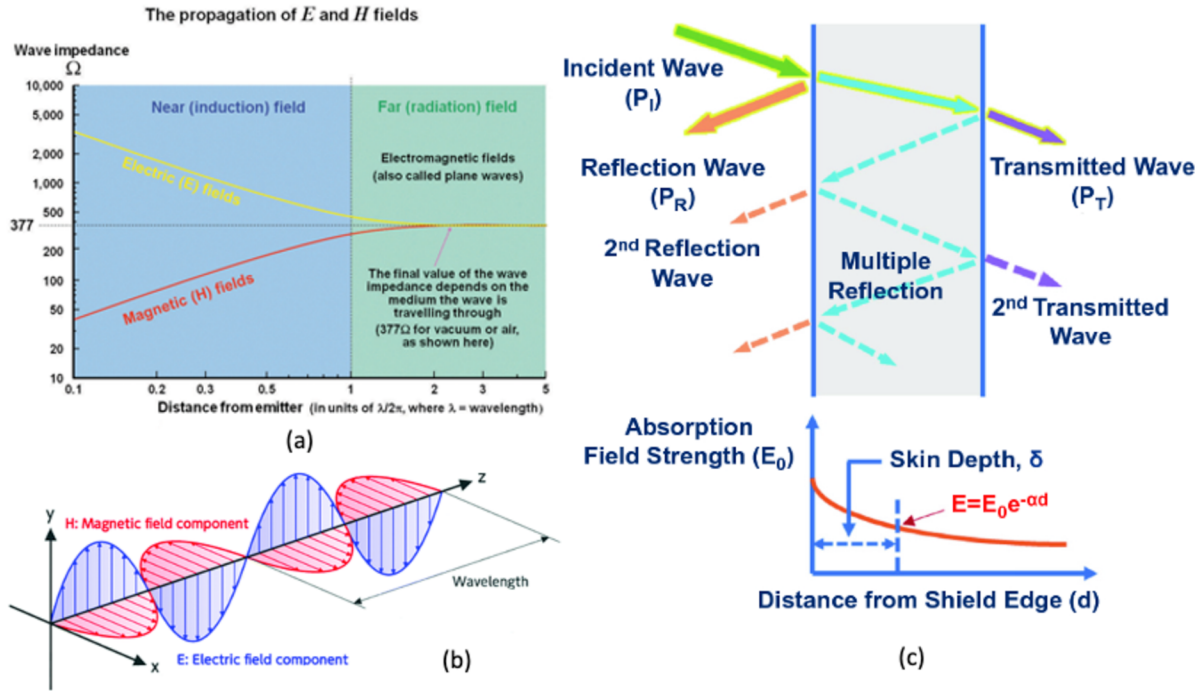


Fig. 19. Schematic representation of the EMI shielding mechanisms (a) Wave impedance and propagation of electric and magnetic fields, (b) electromagnetic transverse oscillating wave, and (c) electromagnetic wave propagation model in EMI shielding materials [155], [156], [158].

The electromagnetic shielding effectiveness of activated carbon structures can be assessed by employing test methods based on two independent principles. The waveguide method, which is used at higher frequencies (e.g., 2.45 GHz), and the coaxial transmission line method, which is used at lower frequencies (e.g., 600 MHz to 1.5 GHz). The waveguide method's measuring setup, which consists of a rectangular hollow waveguide column with electrically conducting walls, is shown in Fig. 20. The test object is positioned at the waveguide column's opening, with a reception antenna inside. A high-frequency analyzer is used to detect electromagnetic signals, and a network analyzer produces electromagnetic waves [123], [147].

According to ASTM D 4935-10, a sample holder with an input and an output that is connected to a network analyzer to produce and receive electromagnetic signals makes up the measuring setup for the coaxial transmission line method, as shown in Fig .21. The fact that the findings obtained in other laboratories are comparable is this technique's main benefit. Additionally, the coaxial transmission line can be utilized to separate each piece of data into its transmitted, reflected, and absorbed components [159].

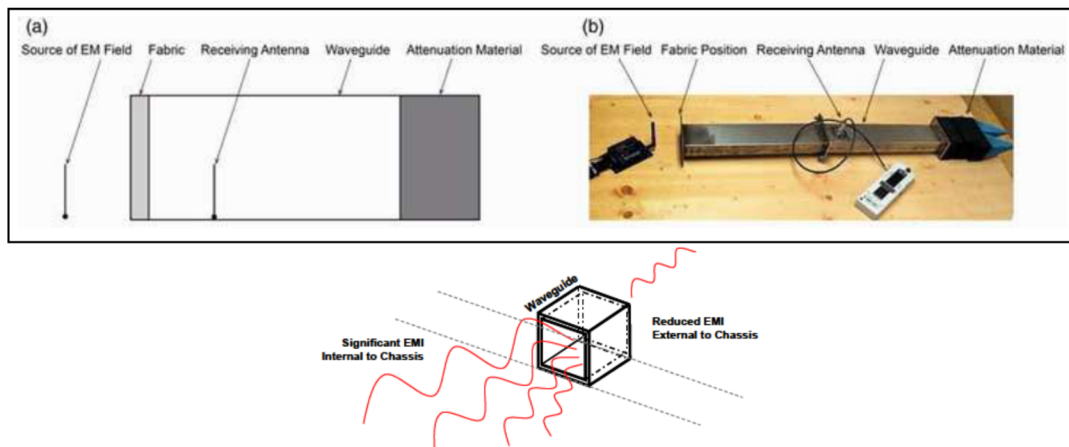


Fig. 20. Measurement setup of waveguide method and its schematic mechanism (bottom) [123], [160].

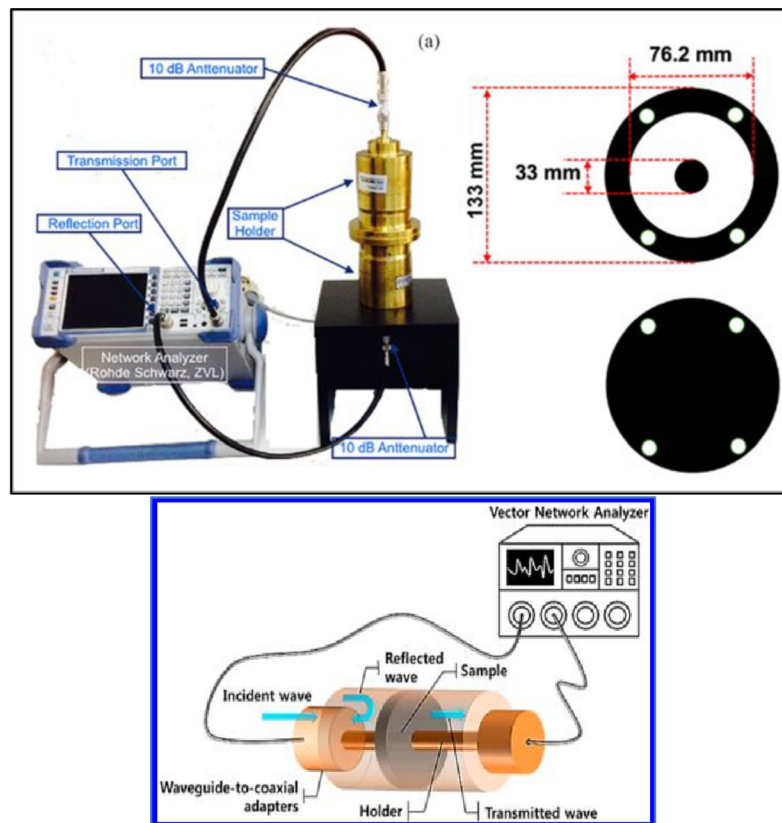


Fig. 21. Measurement set up of coaxial transition line method [150], [161].

The present findings indicate that the activated carbon derived from Kevlar exhibited an increase in electromagnetic shielding efficiency with an increase in carbonization temperature. At a very low carbonization temperature, the shielding efficiency was nearly zero; however, as the carbonization temperature rose, it dramatically increased. A single layer of activated carbon fabric was shown to have EM shielding efficiency of 31 dB, 27 dB, and 5 dB at carbonization temperatures of 1200 °C, 1000 °C, and 800 °C, respectively, at 2.45 GHz frequency as illustrated in Fig. 22 (a). For the most effective shielding efficiency, the percolation threshold is potentially between 1000 °C and 1200 °C carbonization temperatures [15].

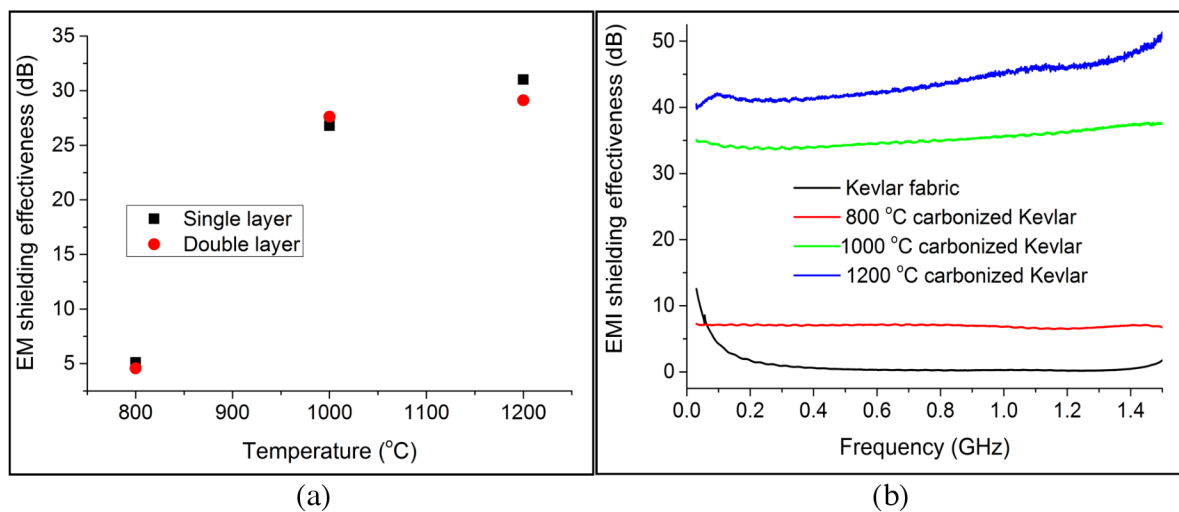


Fig. 22. Electromagnetic shielding effectiveness (a) Effect of carbonization temperature at 2.45 GHz, and (b) Effect of frequency in low-frequency region [15].

Electromagnetic shielding efficiency activated carbon fabrics at different carbonization temperatures in the lower frequency range of 600 MHz, 1 GHz, and 1.5 GHz, is illustrated in Fig. 22 (b). The activated carbon fabric that is produced at a temperature of 800°C exhibited the least effective electromagnetic shielding performance, with a measurement of approximately 5 dB. Upon carbonization of Kevlar fabric at a temperature of 1200 °C, it exhibits shielding capabilities of 42 dB, 45 dB, and 51 dB. The considerably low electrical resistivity of the Kevlar-derived activated carbon fabrics, as discussed in the previous section, enables them to be used as suitable shielding materials Previous studies have indicated that the lower electromagnetic shielding values of activated carbon fabrics derived from Kevlar, in comparison to activated carbon nonwoven web derived from acrylic, can be attributed to both the fiber arrangement and the densification effect induced by gasification [123].

9. Joule heating behavior of Kevlar-derived activated carbon fabrics

The principal theory behind Joule heating also referred to as Ohmic heating or resistive heating, is based on Joule's law of conservation of energy, by a phenomenon known as the Joule's effect (shown in Fig.), which is meant to occur when a voltage difference is applied across a conductive material. This effect occurs when electrical energy is consumed in overcoming the resistance in the material between the electrons and the atoms, causing this energy to be generated in the form of heat. Joule's first law postulates that the quantity of thermal energy generated is directly proportional to the square of electrical current, the resistance of the circuit, and the duration for which the current flows through the circuit [162], shown mathematically as follows:

$$Q = I^2 R t \quad (11)$$

where Q is the heat produced by the material; I is the electrical current flowing through the conductor in amperes; R is the electrical resistance in ohms; t is the elapsed time in seconds. This is one of the distinct properties of material potentially considered for application in thermoregulating intelligent materials. The amount of energy that a substance radiates depends on its surface emissivity and actual surface temperature. The surface emissivity of a material is its effectiveness in emitting energy in the form of thermal radiation. For surfaces with high emissivity, the emissivity factor is considered to be up to 90%.

The one-dimensional steady-state heat transfer equation is chosen as the model to project the temperature distribution of fibers with applied electric power. The expression for electrical power (Q) produced uniformly by the electrical current is as follows:

$$Q = j \times F = \frac{I^2}{A^2 \sigma} \quad (12)$$

Where F is the electrical field equal to the applied voltage divided by the fiber length, σ is the electrical conductivity of the fibers, and j is current density equal to electric current (I) divided by the effective cross-section area (A). Fig. 23 shows a schematic representation of the Joule heating phenomenon. We assume that heat is transported to the environment at the ends of composite fibers and through the surroundings via air convection in addition to being conducted one-dimensionally through the fibers [163].

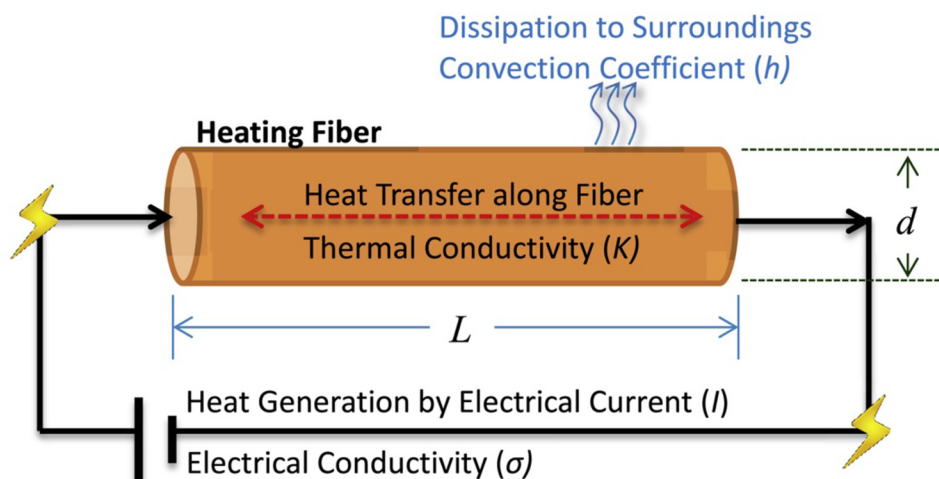


Fig. 23. Schematic diagram of Joule heating phenomenon [163].

In order to produce carbon-rich products suitable for a variety of applications, different polymeric materials have been continuously pyrolyzed and carbonized over time through a process of thermal degradation, where the organic material undergoes aromatic evolution, polymerization, and bond cleavage processes while being subjected to a wide temperature range in an inert environment, the carbonization process removes non-carbon volatiles such as nitrogen, hydrogen, methane, carbon dioxide, carbon monoxide, ammonia, and water, which constitutes about half or more of the precursor's weight. The required type of carbon product and its particular use determine the maximum carbonization temperature, where the chemical composition and the physical characteristics exhibit fundamental changes [54], [83], [97], [164]–[166].

9.1. Temperature – Voltage (T-V) relation

It has been reported that the temperature difference is proportional to the electrical power for electrically conductive fibers [163], [167]. Since the electrical power is also proportional to the square of electrical current, the experimental maximum temperature differences obtained by the infrared camera are expected to be linear when fitted as a function of the square of electrical current, as shown in Fig. 24(a), demonstrating that temperature increased with increasing electrical current. At 1000 μA current, the most significant temperature differential recorded for CNT-based conductive fibers was 153 $^{\circ}\text{C}$ [163]. A similar trend is observed in the present work, for fabrics obtained from carbonization of Kevlar (under CO_2 atmosphere from

charcoal). From Fig. 24(b) it can be seen that in the temperature-voltage (T-V) curves, the surface temperature remained almost the same, without any significant rise in temperature when a low voltage ($V < 3$ V) was supplied. Subsequently, the surface temperature of the fabrics increases with increasing voltage. The fabrics carbonized at 1000°C and 1100 °C, show a considerably steep increase in surface temperature with increasing voltage. At maximum applied voltage (10 V), surface temperatures of ~ 250 °C, for fabrics carbonized at 1000°C can be observed [107].

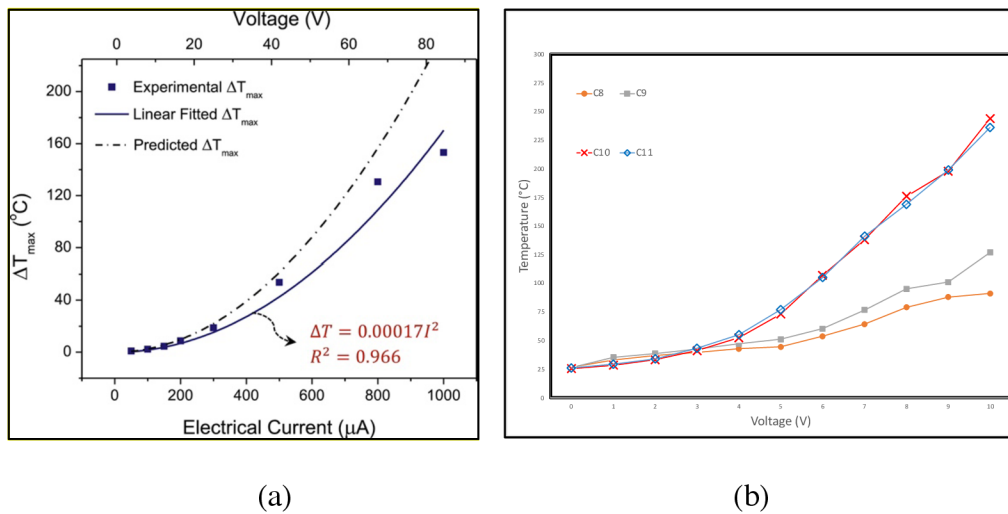


Fig. 24. Temperature-voltage relation. (a) Maximum temperature difference (ΔT_{max}) estimated for electrically conductive fibers at varying input electrical current and voltage [163], (b) Kevlar-derived activated carbon fabrics [107].

9.2. Temperature – Time (T-I) relation: Heating - Cooling Kinetics

The investigation of a heating-cooling cycle through a first-order simple kinetic model can be facilitated by utilizing time-dependent temperature relation curves [107], [168]. The system is comprised of three distinct parameters, specifically the characteristic growth time constant (τ_g), the efficiency of heat transfer (h_{r+c}), and the characteristic decay time constant (τ_d). Fig. 25(a) depicts the time-dependent temperature fluctuations observed in the carbon fabrics derived from Kevlar, which shows a similar trend as compared to time-dependent temperature characteristics of structures containing carbon black at an applied power of 1.5 W/cm³ (Fig. 25(b)). The data indicate that the surface temperature exhibited a sharp initial increase under a consistent voltage supply of 5 V. Subsequently, the rate of temperature increases gradually

decreased over time and ultimately peaked at the 120-second mark. Subsequently, the temperature exhibited a rapid decline towards ambient conditions, reaching room temperature at the 240-second mark, coinciding with the cessation of the applied voltage. The correlation between the steady rise in temperature due to Joule heating and the ultimate carbonization temperature is worth mentioning. Fabrics that have undergone carbonization at temperatures of 1000°C and 1100 °C exhibit a higher leveling-off temperature [107]. Upon conducting additional calculations on the aforementioned parameters, it becomes evident that the values of τ_g and τ_d exhibit a decrease, whereas h_{r+c} displays an increase as the carbonization temperature is raised, due to higher carbon content [168].

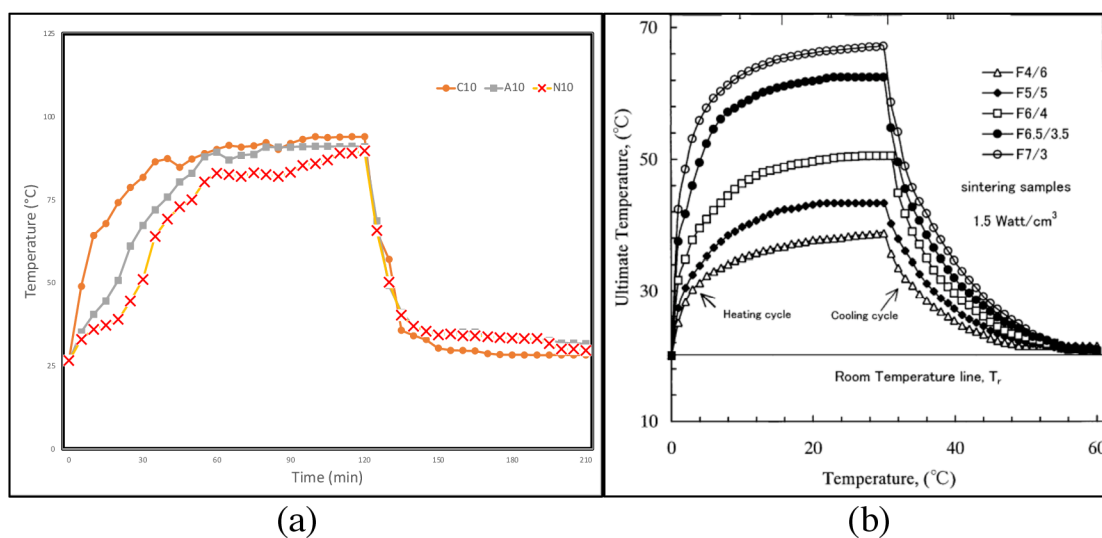


Fig. 25. Temperature – time relation of (a) Kevlar-derived activated carbon fabrics [107], (b) composites with carbon black [168].

10. Conclusion

This dissertation is conceived as a summary of published scientific and professional works, in which the author of this thesis is the main author or co-author. In order to emphasize the topicality of the studied topic, the novelty, and author motivation to research activities, the work is supplemented with citations of other research works published in the given area. Four selected papers with high citation response are listed in the appendix section.

The present work establishes a concentrated study on the thermal degradation of Kevlar and its volatile products of pyrolysis, and it describes the novelty of the utilization of Kevlar fabric

wastes for the development of micro-porous and electrically conductive carbon-based materials by means of a novel, controlled and single-stage processes of carbonization and physical activation, without the requirement of any intermediate stabilization process. In order to achieve this, Kevlar fabric waste was subjected to thermal decomposition under different conditions of pyrolysis environment, temperature, and rate of heating. The present work focused on the influence of different carbonization temperatures, ranging from 500 to 1200 °C, and different atmospheric conditions on the properties of the activated carbon. Here, three different inert atmospheres, namely CO₂ evolved from charcoal, a mixture of gases from ammonium bicarbonate salt (NH₄HCO₃), and Nitrogen gas (N₂), inside a high-temperature furnace were utilized. The following conclusions have been drawn.

- The utilization of Kevlar wastes sourced from industrial processes effectively eliminates the expenses associated with acquiring raw materials. The single-step carbonization process is characterized by reduced time consumption and lower power requirements when compared to other carbonization methods that rely on further activation processes. This feature enhances the importance of upcycling. Moreover, the implementation of charcoal or salts as the heat medium, pyrolysis, and CO₂ atmosphere to augment decomposition, results in a reduction of expenses due to its cost-effectiveness and easy accessibility. These factors significantly impact the expenses associated with manufacturing and production, while simultaneously aligning with the fundamental goal of promoting textile reuse, recycling, and waste management.
- A readily accessible, efficient, and cost-effective experimental arrangement is employed to obtain a preliminary indication of the classes of volatile compounds. This is achieved by utilizing UV-Vis spectroscopy measurements in conjunction with a spectral matrix decomposition algorithm to break down measured spectra into potential spectra of individual components. This algorithm illustrates the progressive changes in concentrations of thermal decomposition products as a function of pyrolysis temperature, as well as their differences in volatility.
- The present work investigated the physical, morphological, and electrical characteristics of Kevlar-derived activated carbon, which was conducted using various techniques such as EDX, SEM, BET analysis, and electrical conductivity measurements. The yield of activated carbon fabric was determined to be 31% at 1200 °C carbonization temperature. Although the mechanical strength of activated carbon fabric greatly declined, it is observed the material retains structural integrity after

carbonization. The results indicate a significant reduction in the electrical resistivity of the activated carbon fabrics for all methods of processing as the carbonization temperature increased. Upon subjecting the material to 1200 °C carbonization temperature, the activated carbon exhibited a significant decrease in both surface and volume resistivity, of nearly 10^4 and 10^3 times, respectively, compared to the activated carbon sample treated at 800 °C, attributed to the presence of a greater amount of graphite, a more uniform distribution of graphite layers.

- The investigation of electromagnetic interference (EMI) shielding efficiency in the high-frequency (2.45 GHz) and low-frequency (1.5 GHz) ranges indicates significant shielding efficiency, attributed to enhanced multiple internal reflections and increased absorption of electromagnetic radiations, consequent to an increased quantity of nomadic charges (most notably, graphite content), uniform dispersion of graphite layers, decreased fiber diameter, an extended mean free path of electrons, larger surface area, higher porosity, and improved conductive network formation in activated carbon subjected to a temperature of 1200 °C.
- Furthermore, activated carbon fabrics were found to exhibit a remarkable joule heating phenomenon, which was dependent on both the applied voltage and time. The results indicate that an increase in voltage ($V > 3$ V) led to a corresponding increase in the surface temperature of the fabrics. Surface temperatures of activated carbon fabrics were determined to be 244 °C and 264 °C at 10 V, attributed to their higher electrical conductivity. The increase in surface temperature through Joule heating in fabrics produced by all three methods was significantly contingent upon the ultimate carbonization temperature. The temperature at which the leveling-off phenomenon occurred was observed to be higher for fabrics that were carbonized at higher temperatures (>1000 °C), at a constant voltage of 5 V. It can be suggested that techniques employing charcoal and ammonium bicarbonate salt exhibited superior electrical and joule heating properties, in addition to being economically viable and environmentally sustainable.

11. Appendix – Full texts



Study on thermal degradation of poly (1,4 phenylene terephthalamide) and its volatile products by unadorned setup of Pyrolysis and subsequent UV–VIS spectroscopy

Daniel Karthik ^{a,*}, Karel Kupka ^b, Jiri Militky ^a, Mohanapriya Venkataraman ^a

^a Department of Material Engineering, Faculty of Textile Engineering, Technical University of Liberec, Studentska 2, Liberec 46117, Czech Republic

^b TriloByte Statistical Software, s.r.o, Staré Hradiště, Pardubice 533 52, Czech Republic

ARTICLE INFO

Keywords:

Pyrolysis
Kevlar
Volatile
UV-Vis spectroscopy
Singular value decomposition
Spectral matrix

ABSTRACT

Pyrolysis involves the elimination of moisture and volatile components from fibrous materials by cleavage of molecular bonds to finally obtain carbon-rich residues. Over the years, there have been numerous studies on the pyrolysis of poly (1,4 phenylene terephthalamide) (Kevlar) and characterization of volatile products by using various analytical techniques. The main objectives of this work were to exhibit a simple and straightforward pyrolysis method using a smelting furnace, concurrently condensing the volatile products on a cold surface, followed by acquiring information on progressive changes in concentrations of decomposition products and their difference in volatility using UV-Vis spectroscopy, and to subsequently demonstrate an interesting algorithm for separation of mixture spectra. Variations in concentration of major elements (C, N, S, and O) were also monitored as a function of pyrolysis temperature. An increase in the concentration of volatile products was observed above 500 °C, reaching maximum at 700 °C and then progressively decreases towards the final temperature of 1100 °C. Separation of mixture spectra was attempted using the concept of spectral matrix decomposition to decompose measured spectra into possible spectra of individual components with the objective of proposing a fast and inexpensive method coupled with computational aid that contributes to kinetic studies of pyrolytic processes.

1. Introduction

The development of carbonaceous materials is influenced by factors such as the nature of precursor used, the application of activating agent and emphatically the process conditions of pyrolysis. In fact, the operational parameters in the pyrolysis process have a discernable effect on the resulting manner of decomposition and on the final characteristics of the product [1–3]. Studies report that after a dehydration phase of the fibers, that eliminates moisture and volatile components present in the raw material, pyrolysis and carbonization provides heat in an inert atmosphere to break molecular bonds and create carbon structures [4,5].

The process of thermal decomposition of materials is of major significance to their structural and thermal properties. Furthermore, the products of decomposition of a material may play a vital role with regard to great temperatures or fire exposure [6–9]. Pyrolysis is a thermally initiated chemical process that generally decomposes organic molecules to smaller ones in an inert atmosphere. The term ‘pyrolysis’ is often restricted to considering a high temperature reaction resulting

only in gases and char, but it also includes thermolysis of organic macromolecules in the temperature range from 250° to 800°C resulting in gaseous, liquid and solid products. Above 800 °C, carbonization phase is realized, where fundamental changes of both chemical composition and physical properties of the organic material can be seen, which is applied as a utilization technology mostly for biomass waste [3]. The initial step of pyrolysis process involves intramolecular endothermic chemical reaction either by rearrangement of chemical bonds followed by elimination of small molecules, and/or cleavage of chemical bonds followed by the stabilization of the unstable fragments (the former reactions occur at around 300 °C, and the latter at above 500 °C) [7], [8], [10].

Poly p-phenylene terephthalamide (PPTA) commercially known as Kevlar® (hereafter referred to as Kevlar) is an aramidic synthetic fiber with a high content of carbon and, typically high strength and high decomposition temperature. Kevlar fibers are fully crystalline with a small fraction of randomly oriented material and the chemical formula is $[-CO-C_6H_4-CO-NH-C_6H_4-NH-]_n$ [6], [8], [11–13].

* Corresponding author.

E-mail address: danielkarthiktex10@gmail.com (D. Karthik).

<https://doi.org/10.1016/j.jaap.2023.105985>

Received 24 November 2022; Received in revised form 6 April 2023; Accepted 27 April 2023

Available online 28 April 2023

0165-2370/© 2023 Elsevier B.V. All rights reserved.

Early studies on pyrolysis of Kevlar were based on the analysis of the chemical composition and of volatile degradation products with evidence of carbon being obtained via non-isotropic and non-graphitizable structures [14–19]. It is reported that Kevlar appears to be chemically stable up to about 545 °C and the main chemical transformation takes place over a narrow temperature range of 550–575 °C, where the maximum rate of weight loss accounted to depolymerization corresponds at 575 °C and further decomposition leads to cleavage of C=O and C-N bonds, progressively leading to polyaromatic compounds over 600 °C [15].

Khanna et al. [20] revealed that volatile degradation products contain one or two aromatic rings whose substituent groups are essentially amino, nitrile, carboxyl and phenyl. Krasnov et al. [21] reported that at 400 °C the main of Kevlar pyrolysis products are H₂O and CO₂ and concluded that the thermal degradation mechanism involved hydrolysis of the NH-CO bonds and subsequent decarboxylation of carboxyl end groups. From a study carried out by Brown and Power [14], the composition of volatiles of Kevlar pyrolysis at temperatures in the range 300–700 °C indicated the occurrence of both homolytic and heterolytic ruptures of the amide unit. The first type of rupture was predominant at high temperatures and the second one at low temperatures [1], [14], [15].

Friedman et al. [22], proposed a mechanism analogous to that for aliphatic polyamides, in which cleavage of the aromatic -NH bonds are considered to be the initial reaction. Kalashik et al. [23] confirmed heterolytic mechanisms at temperatures < 480 °C and parallel homolytic and heterolytic reactions at higher temperatures. A pyrogram of evolved gasses of p-aramid shows that most of the degradation products are released from 550 °C to 650 °C [24]. Schulten et al. [25] identified various aromatic products with one, two or three rings and mainly contained amino and nitrile substituents. Another study reported the evidence of nitrogen oxides being formed during the thermal decomposition of p-aramid [26].

Thermogravimetric analysis (TGA) performed on Kevlar at a heating rate of 10 °C/min under nitrogen showed that about 55 wt% of the material is lost from 550 °C to 650 °C [27]. Also, at heating rate of 10 °C/min, in argon, maximum mass loss initiates lower than 570 °C [28]. However, there are several other analytical techniques that have been explored with, in order to gain more information on the thermal degradation of Kevlar and the volatile products exposed therefrom. The different techniques that is often chosen to identify degradation products majorly include mass spectrometry, Fourier-transform infrared spectrometry [8]; Infrared spectroscopy [15,29]; pyrolysis-gas-chromatography/mass spectrometry (Py-GC/MS) [8], [24]; pyrolysis-field ionization mass spectrometry (Py-FIMS) and pyrolysis-gas chromatography (Py-GC) [25]; Electron paramagnetic resonance (EPR) [26]. In order to identify and measure the constituent compounds of a mixture, gas chromatography-mass spectrometry (GC-MS) is a common analytical technique used globally. However, there are some drawbacks to GC-MS analysis, such as high costs (some labs or applications may find GC-MS systems prohibitively expensive to purchase and maintain) and complex sample preparation (including extraction and cleanup procedures), which can be labor-intensive and expensive and calls for alternative tools of undemanding access, cost and utilization [30].

UV-Vis spectroscopy, applicable to any type of suspension, is one of the most robust and straightforward techniques for quantifying the portion of light lost as it travels through a sample, relative to its blank counterpart [31]. Although UV-Vis spectra are generally inadequate for identifying compounds precisely, this can give us preliminary information about the types or groups of constituent compounds, with which one can determine if another program/technique (such as: GC-MS) is required to precisely identify individual constituent compounds. Furthermore, to the best of our knowledge, UV-Vis spectroscopy has not been used to analyse the volatiles of pyrolysis of Kevlar. The present study involves a relatively simple, straightforward, yet informative

setup to analyse the volatiles of Kevlar pyrolysis.

Our interest is in the solid evolution during thermal treatment, the knowledge of which will allow selection of the optimum conditions for the pyrolysis process prior to ulterior activation of the resulting carbon fibers. These results are also of keen interest with regard to the thermal stability of aramids, Kevlar fibers in particular, as they are used as fire-resistant materials at moderate to high temperature ranges. This work describes a simple and straightforward procedure to pyrolyze Kevlar in a smelting furnace, in an atmosphere containing CO₂, consecutively condensing volatile fumes evolved during pyrolysis on a cold surface, followed by potentially using UV-Vis spectroscopy to demonstrate changes in concentrations of decomposition products and their difference in volatility. Furthermore, this work essentially attempts to demonstrate an interesting algorithm for separation of mixture spectra with a purpose to propose a fast and affordable method coupled with computational aid that contributes to kinetic studies of pyrolytic processes.

2. Experimental

2.1. Materials

The Kevlar 29 fibrous waste was obtained from Veba Textile Mills Ltd (Broumov), Czech Republic in form of discarded short fabrics wastes. The Kevlar had 1710 dtex yarn count, 0.24 m²/g surface area, 1.43 g/cm³ density and 5.2 wt% moisture content. Its elemental analysis was reported as weight percentages on a dry basis 63.85% C, 15.09% N, 0.80% S and 18.84% O.

EDX analysis was carried out using X-Max^N Silicon Drift Detector, Oxford Instruments with a detection limit of ~1 atom%. AZtec software was used to identify and quantify the weight (in percentage) of existing elements.

The reduction in weight of pyrolyzed material obtained at each of the final temperatures was measured with respect to raw Kevlar material. The weight of Kevlar samples was measured on an analytical lab scale weighing balance before and after the pyrolysis procedure, the difference in weight is calculated and represented as a percentage. Material quantities were sampled five times for all characterization procedures.

2.2. Pyrolysis method

Pyrolysis and Carbonization of Kevlar was carried out in a smelting furnace, in a CO₂ atmosphere generated by using ammonium bicarbonate salt. Ammonium bicarbonate is an inorganic compound with formula NH₄HCO₃, decomposes when heated above 36 °C, releasing ammonia, water and carbon dioxide gases as follows: NH₄HCO₃ → NH₃ + H₂O + CO₂ [32]. This potentially provides an inexpensive way of creating a non-reactive atmosphere containing CO₂, without the risk of contact with O₂ in air, thereby, avoiding the possibility of thermo-oxidation.

The smelting furnace (shown in Fig. 2), stations a cylindrical graphite crucible vertically positioned in the center, inside which the Kevlar fabric sample (in rolled form) is placed. 10 g of ammonium bicarbonate salt were added into the crucible containing the Kevlar sample, to potentially create a CO₂ atmosphere. The final temperature is set and the furnace is turned on for the heating to initiate from room temperature. The average heating rate of the pyrolysis process in the smelting furnace for the total time taken to reach the maximum temperatures was ~50 °C/min.

The Kevlar fabric samples were pyrolyzed in the furnace starting from room temperature (21 °C) up to final temperature of 1100 °C. The residual material (char) of the material obtained after pyrolysis and carbonization till final temperature is shown in Fig. 1, in reference to the starting raw material.

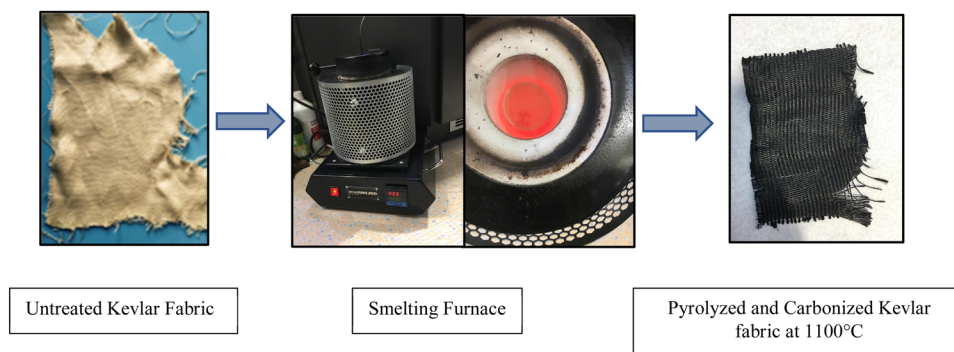


Fig. 1. Representation of pyrolysis process of Kevlar in the smelting furnace.

2.3. Analysis of volatile products by UV–VIS spectroscopy

Volatile products of pyrolysis at temperatures from 500° to 1100°C were collected by condensing the fumes evolved from the furnace on a cold surface (in this case a glass slide) and then dissolved in isopropanol (IUPAC name: Propan-2-ol). The dissolved solutions were placed in a cool and dry place for 24 h to ensure complete dissolution of the condensed volatiles of pyrolysis. Their UV-Vis absorption spectra in isopropanol were measured using Black-comet UV-Vis Spectrophotometer, StellarNet diode array (resolution 2 nm), StellarNet, Inc. A schematic representation of the process involved is described in Fig. 2.

3. Results and discussion

3.1. Energy dispersive X-Ray (EDX) elemental composition analysis

The relative proportion of different elements present in the Kevlar fibers undergoing thermal decomposition were estimated from the EDX analysis. The pyrolysis of fibrous Kevlar materials to final temperatures ranging from 500 °C to 1100 °C, at every 100 °C interval was carried out. The significant elemental composition of the pyrolyzed materials obtained at each of these final temperatures was assessed, as shown in Table 1. The remaining percentage of composition of the pyrolyzed material is made up of insignificant amounts of impurities that include Na, Cu, Cl and Ca. It can be observed, with increase in temperature from 500 °C upto 1100 °C, the percentage of carbon was found to increase. However, oxygen and nitrogen content were found to reduce. This indicated the decomposition of Kevlar macromolecules at higher temperatures and subsequent removal of sulfur, nitrogen and other elements. It must be pointed out that as received fibers, without drying, were used for all thermal treatments. EDX analysis is applied to merely show the increase in the percentage of carbon in the materials due to pyrolysis.

Table 1

Effect of temperature on elemental composition of Kevlar and Kevlar chars.

T (°C)	C (wt%)	N (wt%)	O (wt%)	S (wt%)
20	63.8 ± 0.7	15.0 ± 0.4	18.8 ± 0.3	0.8 ± 0.1
500	69.7 ± 0.6	10.5 ± 0.2	14.2 ± 0.3	0.8 ± 0.1
600	76.1 ± 0.9	8.3 ± 0.3	12.0 ± 0.4	0.9 ± 0.1
700	80.5 ± 0.7	5.1 ± 0.3	10.4 ± 0.2	0.9 ± 0.5
800	83.7 ± 0.6	3.2 ± 0.5	10.3 ± 0.2	0.9 ± 0.1
900	87.1 ± 0.6	2.0 ± 0.4	8.8 ± 0.3	0.7 ± 0.1
1000	88.5 ± 0.8	1.4 ± 0.4	8.3 ± 0.4	0.7 ± 0.1
1100	90.2 ± 0.8	1.3 ± 0.5	6.7 ± 0.3	0.7 ± 0.8

3.2. Reduction in weight with respect to increasing temperature

Kevlar fabrics were pyrolyzed to final temperatures in the range of 500–1100 °C. It can be observed from Fig. 3, that there is significant increase in weight reduction with increasing temperature of pyrolysis majorly in the range of 700–800 °C, indicating the high concentration of volatile products released at these temperatures. The reduction in weight of the material is attributed to the volatile products formed during pyrolysis.

3.3. UV-Vis Spectroscopy Analysis with proposed algorithm for separation of mixture spectra

The absorption spectra shown in Fig. 4, of volatiles collected at different temperatures differ from each other, which suggests the existence of more than one dominant component with abundances dependent on temperature. Using spectral matrix decomposition such as singular value decomposition (SVD) it is possible to decompose measured spectra into possible spectra of individual components [33–35]. This computational procedure is also referred to as “spectral unmixing” and is recently used for image analysis eg. in planetary

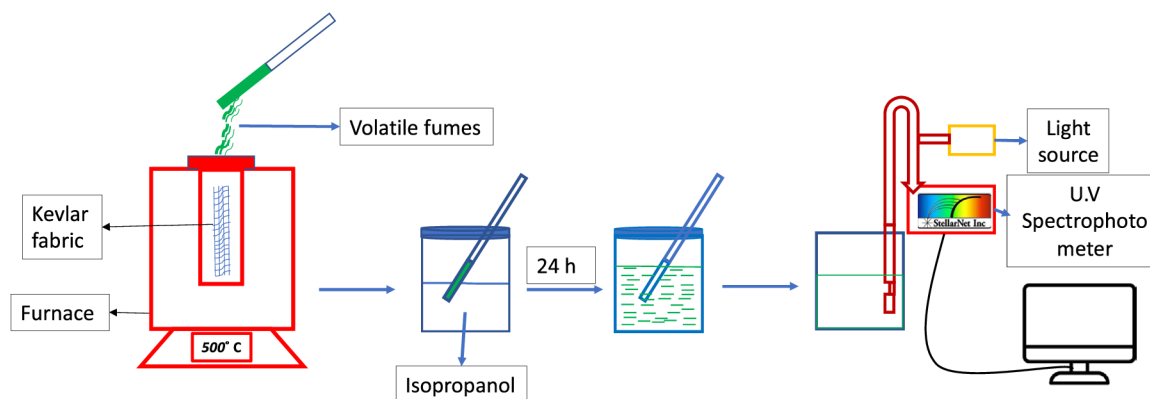


Fig. 2. Schematic representation of condensation of volatile products during pyrolysis of Kevlar fabric and its analysis by UV-Vis Spectroscopy.

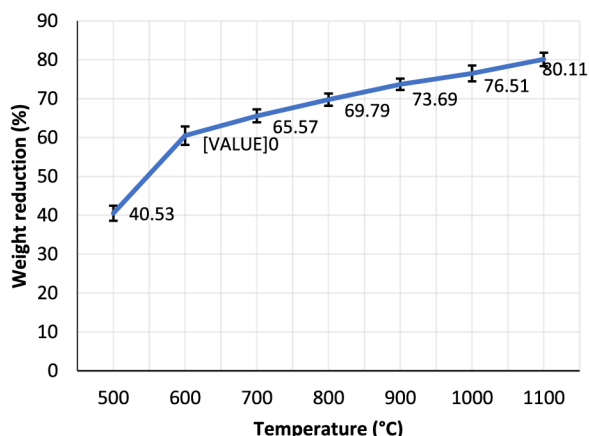


Fig. 3. Weight reduction percentage with increasing temperature.

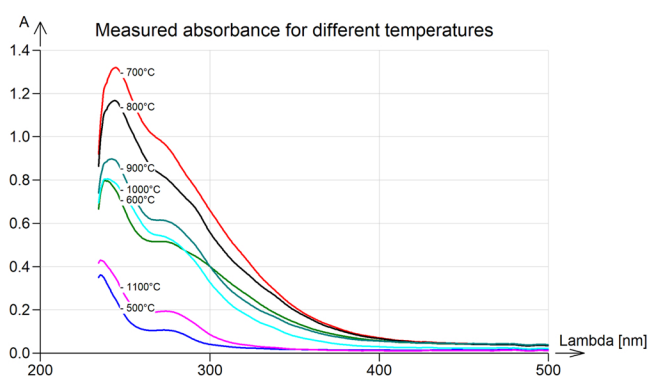


Fig. 4. UV-Vis absorption spectra for different temperatures.

science. It can serve as complementary support to more sophisticated methods, or as preliminary informative analysis with inexpensive equipment taking advantage of better utilization of information contained in simple UV-VIS (-NIR) spectra without FTIR or MS. According to Lambert-Beer's law (for fixed beam length) $A = \epsilon \cdot c$, or in multiple dimensions,

$$\mathbf{A} = \mathbf{S} \mathbf{C} + \mathbf{E} \quad (1)$$

$$\mathbf{A} = \begin{bmatrix} a_{11} & \dots & a_{1j} & \dots & a_{1s} \\ \vdots & & \vdots & & \vdots \\ a_{i1} & \dots & a_{ij} & \dots & a_{is} \\ \vdots & & \vdots & & \vdots \\ a_{n1} & \dots & a_{nj} & \dots & a_{ns} \end{bmatrix} \quad (2)$$

where $\mathbf{A}(n \times s)$ is the matrix of measured absorbances, a_{ij} is the absorbance in j -th sample (spectra) at i -th wavelength, $\mathbf{S}(n \times m)$ is the matrix of absorption coefficients, $\mathbf{C}(m \times s)$ is the concentration matrix, $\mathbf{E}(n \times s)$ is the matrix of errors, n is the number of wavelengths (corresponding to wavelength resolution of the spectrophotometer), s is number of samples (spectra) and m is number of different absorbing compounds present in the samples. Each column of matrix \mathbf{A} is in fact one discrete UV-VIS spectrum corresponding to given sample.

Let $\mathbf{A} = \mathbf{UDV}^{-1}$ be a singular value decomposition of the spectral absorbance matrix \mathbf{A} with $\mathbf{U}(n \times s)$, diagonal $\mathbf{D}(s \times s)$, $\mathbf{V}(s \times s)$ with columns of \mathbf{U} and rows of \mathbf{V}^{-1} sorted in decreasing order of diagonal elements of \mathbf{D} . (containing on diagonal singular values expressing relative importance of individual components of mixture spectrum). Assume that number of real compounds (individual components) is smaller than number of samples and individual concentrations are not in the same

ratios. Then the dimensionality can be reduced to assumed k compounds (individual components in mixture spectrum) by decreasing the size of the matrices (cutting off rows/columns) to $\mathbf{U}_k(n \times k)$, diagonal $\mathbf{D}_k(k \times k)$, $\mathbf{V}_k(s \times k)$ and $\mathbf{A} = \mathbf{UDV}^{-1}$ becomes

$$\mathbf{A} = \mathbf{U}_k \mathbf{D}_k \mathbf{V}_k^{-1} + \hat{\mathbf{E}} \quad (3)$$

Where $\hat{\mathbf{E}}(n \times s)$ can be interpreted as the matrix of estimated errors. By introducing a rotation matrix \mathbf{R} of an appropriate size [36,37], (3) can be re-written as

$$\mathbf{A} = (\mathbf{U}_k \mathbf{D}_k \mathbf{R})(\mathbf{R}^{-1} \mathbf{V}_k^{-1}) + \hat{\mathbf{E}} \quad (4)$$

It can be shown that (1) is a special case of (4) implying that the factors in brackets are reconstructed spectra of the assumed individual compounds and their concentrations in samples for a particular \mathbf{R} .

$$\begin{aligned} (\mathbf{U}_k \mathbf{D}_k \mathbf{R}) &= \mathbf{S}^* \approx \mathbf{S} \\ (\mathbf{R}^{-1} \mathbf{V}_k^{-1}) &= \mathbf{C}^* \approx \mathbf{C} \end{aligned} \quad (5)$$

Since both concentrations and absorption coefficients are non-negative numbers, the rotation matrix should ensure that all elements of the two matrices be non-negative. There exist many strategies how to find optimal \mathbf{R} .

Here we used as a criterion the roots for a minimum of selected column of \mathbf{S} , $\arg \min_{\mathbf{R}} \{(S_j^*)^2\}$. This algorithm is general based on the

Lambert Beer law validity and oriented to decompose spectra into m components according to criterion the roots for a minimum of selected column of matrix \mathbf{S} (Eq. 5). Other programs are obviously decomposing arbitrary spectrum without use the information about their origin (Lambert Beer law) and number of components is not optimized. Two components were here identified automatically as optimal by program. For two assumed components the reconstructed individual spectra and concentrations according to Eq. (5) are shown in the following figures. (Figs. 5 and 6).

The two components identified as optimal by above procedure can be interpreted as two mixtures of absorbing individuals, Component (1) and Component (2). Reconstructed spectra of the two identified components at temperatures 500 – 1100 °C are shown in Fig. 6. The reconstructed spectra: Component (1) has maxima 251 and 297 nm, Component (2) has maxima 235 and 275 nm. These identified absorption wavelengths of the assumed components can be used to potentially indicate the compounds that fall in the category of the specified wavelengths, by the assistance of a database such as Organic Compounds Database compiled by Harold M. Bell at Virginia Tech [38]. In general, each of the reconstructed spectra of the assumed components (two components in our case) may even possibly be a mixture of compounds. Chemical identification of pyrolysis products has been described elsewhere, by various methods [1,6,7,9,10,12,15]. According to Czégény and Blazsó [39], the decomposition pyrograms of Kevlar by Py-GC-MS primarily produced benzonitrile, aniline, benzeneamine and benzoic acid in the range of 600–800 °C, where benzonitrile was potentially

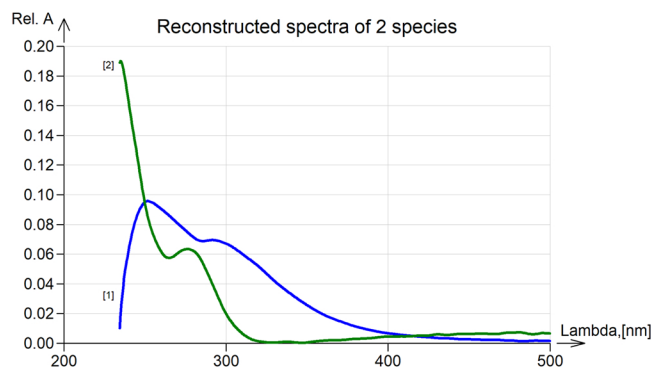


Fig. 5. Reconstructed UV-VIS spectra of the two assumed components.

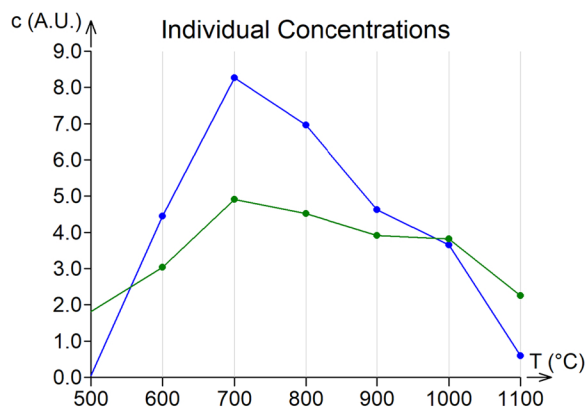


Fig. 6. Reconstructed estimated concentrations of the two identified components at temperatures 500 – 1100 °C.

formed through homolytic cleavage of aromatic -NH bond followed by protonation and dehydration. In another study, benzene and benzonitrile were the main fragments at 600 °C and nearly reached at 80% at 750 °C. Apart from that, benzaldehyde, benzoic acid, benzoate and aniline were produced among many other compounds. [17].

With the aid of the Organic Compounds Database, the constituent class of compounds that are included at the specified wavelength maxima of the two components were obtained and are listed as follows:

Component 1: Benzaldehyde (O-Chlorobenzaldehyde, 2,4-Dichlorobenzaldehyde, O-Bromobenzaldehyde, M-Iodobenzaldehyde); Aniline (N,N-Dimethylaniline, N-Ethylaniline, 3,5-Dichloroaniline, P-Iodoaniline); Styrene (M-Methylstyrene, P-Chlorostyrene, P-Bromostyrene); Nitrotoluene (4-Chloro-3-Nitrotoluene, 4-Chloro-2-Nitrotoluene), Benzoic Acid(2,4-Dihydroxybenzoic Acid).

Component 2: Benzonitrile (Tolunitrile, Chlorobenzonitrile, Bromobenzonitrile), Benzoate (Methyl 2-Methylbenzoate, Methyl 3-Methylbenzoate, Benzyl Benzoate), Benzaldehyde (2,4-Dimethoxybenzaldehyde, 2,4,5-Trimethoxybenzaldehyde), Benzoic Acid (P-Chlorobenzoic Acid, 2,4-Dichlorobenzoic Acid), Toluic Acid, Phenylacetylene, Nitroaniline.

It can be noted, that some of the volatile compounds that were revealed by previous studies, mentioned earlier, classifies into one of the types of volatile compounds obtained in the present work. This indicates the information obtained from spectra of the two components is congruent with the identification of volatile compounds obtained by other methods. From the experimental procedure presented, gaseous products such as CO, CO₂, NH₃, were not detected, but the spectra obtained describes the detection of heavier compounds, condensed at room temperature. The relative molar concentrations at different temperatures are given in arbitrary units (A.U.). True amounts can be estimated eg. from total mass balance.

Although we are unable to confirm precisely the specific constituent compounds in the component mixture, this certainly gives us preliminary indication and knowledge of the types and class of volatile compounds produced during the pyrolysis process. Furthermore, with the support of this estimated information, more suitable techniques (like Py-GC-MC or TGA-FTIR), to accurately identify the constituent compounds, could be essentially employed, if required.

Individual concentrations of the two identified components at temperatures 500 – 1100 °C are shown in Fig.6, where it can be observed that there is significant increase in concentration of both components of the decomposition products > 500 °C upto 700 °C and then gradually decreases heading towards 1100 °C. This information is in close agreement to previous work on decomposition of Kevlar, which includes depolymerization over 500 °C, progressively leading to cleavage of bonds and formation of polyaromatic compounds over 600 °C [15], [24]. The concentration of component (1) is higher than that of

component (2) between temperatures 600–800 °C and steeply decreases from 900 °C onwards.

4. Conclusion

This manuscript mainly focuses on a simple, easily accessible, less time consuming and inexpensive experimental setup that one could determine from, to obtain preliminary indication of the types/class of compounds, by utilizing UV spectroscopy measurement in conjunction with a spectral matrix decomposition algorithm to decompose measured spectra into possible spectra of individual components. A simple and straightforward method of pyrolyzing Kevlar fabric samples was performed using a smelting furnace in an atmosphere containing CO₂, potentially created by the addition ammonium bicarbonate salt. Pyrolysis was carried out starting at room temperature (21 °C) up to 1100 °C, where volatile products of pyrolysis at temperatures from 500° to 1100°C were collected at intervals of 100 °C by condensing on a cold surface (in this case a glass slide) and then dissolved in isopropanol.

UV-Vis absorption spectra in isopropanol were measured to demonstrate changes in concentrations of decomposition products and their difference in volatility and also demonstrate an interesting algorithm for separation of mixture spectra using spectral matrix decomposition such as singular value decomposition to decompose measured spectra into possible spectra of individual components. Here we used as a criterion, the roots for a minimum of selected column of absorption coefficients of measured absorbances to potentially obtain the reconstructed spectra of the assumed individual compounds and their concentrations in samples.

Declaration of Competing Interest

The authors declare that they have no known competing financial interests or personal relationships that could have appeared to influence the work reported in this paper.

Data Availability

The authors are unable or have chosen not to specify which data has been used.

References

- [1] S. Villar-Rodil, A. Martínez-Alonso, J.M.D. Tascón, Studies on pyrolysis of Nomex polyaramid fibers, *J. Anal. Appl. Pyrolysis* vol. 58–59 (2001) 105–115, [https://doi.org/10.1016/S0165-2370\(00\)00124-8](https://doi.org/10.1016/S0165-2370(00)00124-8).
- [2] R.C. Bansal and M. Goyal, *Activated carbon adsorption*. Boca Raton: Taylor & Francis, 2005.
- [3] M. Afshari, Ed., *Electrospun nanofibers*. In Woodhead publishing series in textiles, no. volume number 186. Amsterdam: The Textile Institute; Elsevier, 2017.
- [4] F. Suárez-García, A. Martínez-Alonso, J.M.D. Tascón, Activated carbon fibers from Nomex by chemical activation with phosphoric acid, *Carbon* vol. 42 (8–9) (2004) 1419–1426, <https://doi.org/10.1016/j.carbon.2003.11.011>.
- [5] G. Conte, et al., Assessment of activated carbon fibers from commercial Kevlar® as nanostructured material for gas storage: effect of activation procedure and adsorption of CO₂ and CH₄, *J. Anal. Appl. Pyrolysis* vol. 152 (2020), 104974, <https://doi.org/10.1016/j.jaap.2020.104974>.
- [6] M. Blazsó, Pyrolysis for recycling waste composites. in *Management, Recycling and Reuse of Waste Composites*, Elsevier, 2010, pp. 102–121, <https://doi.org/10.1533/9781845697662.2.102>.
- [7] Yang Ming, Zhu Xiao-ling, Liang Guo zheng, *Pyrolysis Process Kevlar Fibers Thermogravim. Anal. Couple Fourier Transform Infrared Spectrosc* vol. 36 (5) (2016) 1374–1377 (May).
- [8] A. Ramgobin, G. Fontaine, S. Bourbigot, Thermal degradation and fire behavior of high performance polymers, *Polym. Rev.* vol. 59 (1) (2019) 55–123, <https://doi.org/10.1080/15583724.2018.1546736>.
- [9] M. Faraday, “Chemistry and Physics of Fire and Liquid Fuels,” p. 47.
- [10] J.J. Freeman, J.B. Tomlinson, K.S.W. Sing, C.R. Theocharis, Adsorption of nitrogen and water vapour by activated Kevlar® chars, *Carbon* vol. 31 (6) (1993) 865–869, [https://doi.org/10.1016/0008-6223\(93\)90186-E](https://doi.org/10.1016/0008-6223(93)90186-E).
- [11] E. Kowsari, V. Haddadi-Asl, F. Boorboor Ajdari, J. Hemmat, *Aramid Fibers Compos. Innov. Sustain. Mater. Biomed. Appl.* (2019) 173–204, <https://doi.org/10.1016/B978-0-12-816872-1.00006-6>.

- [12] T. Deng, G. Zhang, F. Dai, F. Zhang, Mild surface modification of *para*-aramid fiber by dilute sulfuric acid under microwave irradiation, *Text. Res. J.* vol. 87 (7) (2017) 799–806, <https://doi.org/10.1177/0040517516639831>.
- [13] J. Choma, L. Osuchowski, M. Marszewski, A. Dziura, M. Jaroniec, Developing microporosity in Kevlar®-derived carbon fibers by CO₂ activation for CO₂ adsorption, *J. CO₂ Util.* vol. 16 (2016) 17–22, <https://doi.org/10.1016/j.jcou.2016.05.004>.
- [14] J.R. Brown, A.J. Power, “Thermal degradation of aramids: Part I—Pyrolysis/gas chromatography/mass spectrometry of poly(1,3-phenylene isophthalamide) and poly(1,4-phenylene terephthalamide, *Polym. Degrad. Stab.* vol. 4 (5) (1982) 379–392, [https://doi.org/10.1016/0141-3910\(82\)90044-1](https://doi.org/10.1016/0141-3910(82)90044-1).
- [15] M.E.G. Mosquera, M. Jamond, A. Martinez-Alonso, J.M.D. Tascón, Thermal Transformations of Kevlar Aramid Fibers During Pyrolysis: Infrared And Thermal Analysis Studies, ACS Publications,, 2002. (<https://pubs.acs.org/doi/pdf/10.1021/cm00047a006>).
- [16] I. Tomizuka, Y. Isoda, Y. Amamiya, Carbon fibre from a high-modulus polyamide fibre (Kevlar, TANSO vol. 1981 (106) (1981) 93–101, <https://doi.org/10.7209/tanso.1981.93>.
- [17] G.M. Cai, W.D. Yu, Study on the thermal degradation of high performance fibers by TG/FTIR and Py-GC/MS, *J. Therm. Anal. Calorim.* vol. 104 (2) (2011) 757–763, <https://doi.org/10.1007/s10973-010-1211-0>.
- [18] K.S. Ko, C.W. Park, S.-H. Yoon, S.M. Oh, Preparation of Kevlar-derived carbon fibers and their anodic performances in Li secondary batteries, *Carbon* vol. 39 (11) (2001) 1619–1625, [https://doi.org/10.1016/S0008-6223\(00\)00298-0](https://doi.org/10.1016/S0008-6223(00)00298-0).
- [19] Y. Kawahara, S. Otoyama, K. Yamamoto, Direct carbonization of high-performance aromatic polymers and the production of activated carbon fibers, *J. Text. Sci. Eng.* vol. 05 (06) (2015), <https://doi.org/10.4172/2165-8064.1000219>.
- [20] Y.P. Khanna, et al., Aromatic polyamides. II. Thermal degradation of some aromatic polyamides and their model diamides, *J. Polym. Sci. Polym. Chem. Ed.* vol. 19 (11) (1981) 2817–2834, <https://doi.org/10.1002/pol.1981.170191115>.
- [21] P. Ye, V.M. Krasnov, L.B. Savinov, V.I. Sokolov, V.K. Logunova, Belyakov, T. A. Polyakova, Thermal degradation of isomeric aromatic polyamides, *Polym. Sci. USSR* vol. 8 (3) (1966) 413–421, [https://doi.org/10.1016/0032-3950\(66\)90258-9](https://doi.org/10.1016/0032-3950(66)90258-9).
- [22] L. Friedman, “Mass spectrometric thermal analysis: a review,” p. 29.
- [23] A.T. Kalashik and N.P. Paiikarova, “Comparative analysis of the thermal degradation of poly-p-benzamide and poly-p-phenylene terephthalamide,” p. 9.
- [24] T. Shin, O. Hajima, W. Chuichi, Pyrograms and Thermograms of 163 High Polymers, and MS Data of the Major Pyrolyzates in. *Pyrolysis – GC/MS Data Book of Synthetic Polymers*, Elsevier, 2011, pp. 7–335, <https://doi.org/10.1016/B978-0-444-53892-5.10002-1>.
- [25] H.-R. Schulten, B. Plage, H. Ohtani, S. Tsuge, *Angew. Makromol. Chem.* vol. 155 (1) (1987) 1–20, <https://doi.org/10.1002/apmc.1987.051550101>.
- [26] X.-W. Wang, Z.-M. Hu, Z.-F. Liu, Thermal degradation of meta- and para-aramid fibers in different atmospheres, *Int. Polym. Process.* vol. 23 (1) (. 2008) 81–87, <https://doi.org/10.3139/217.2046>.
- [27] L. Giraldo, Y. Ladino, J.C.M. Pirajánc, M.P. Rodríguez, Synthesis and characterization of activated carbon fibers from Kevlar, *Eclética Quím.* vol. 32 (4) (2007) 55–62, <https://doi.org/10.1590/S0100-46702007000400008>.
- [28] Alberto Castro-MunizAmelia Martinez-AlonsoJuan M.D. Tascón, Modification of the pyrolysis/carbonization of PPTA polymerby intermediate isothermal treatments, *CARBON* vol. 46 (2008).
- [29] S. Villar-Rodil, F. Suárez-García, J.I. Paredes, A. Martínez-Alonso, J.M.D. Tascón, Activated carbon materials of uniform porosity from polyaramid fibers, *Chem. Mater.* vol. 17 (24) (. 2005) 5893–5908, <https://doi.org/10.1021/cm051339t>.
- [30] C. Brännhammar, “Limitations and disadvantages of GC-MS,” *Labio*, Dec. 30, 2022. (<https://labioanalytics.com/limitations-and-disadvantages-of-gc-ms/>) (accessed Apr. 05, 2023).
- [31] P. Alafogianni, K. Dassios, S. Farmaki, S.K. Antiohos, T.E. Matikas, N.-M. Barkoula, On the efficiency of UV–vis spectroscopy in assessing the dispersion quality in sonicated aqueous suspensions of carbon nanotubes, *Colloids Surf. Physicochem. Eng. Asp.* vol. 495 (2016) 118–124, <https://doi.org/10.1016/j.colsurfa.2016.01.053>.
- [32] Nederlandse Vereniging van Veiligheidstechnici and N. Veiligheidsinstituut (Amsterdam Vereniging van de Nederlandse Chemische Industrie, Handling chemicals safely 1980. The Hague: Dutch Association of Safety Experts: Dutch Chemical Industry Association: Dutch Safety Institute, 1980.
- [33] P. Neymeyr, M. Sawall, D. Hess, Pure component spectral recovery and constrained matrix factorizations: concepts and applications, *J. Chemom.* (2010) n/a–n/a, <https://doi.org/10.1002/cem.1273>.
- [34] Y. Zeng, M. Garland, An improved algorithm for estimating pure component spectra in exploratory chemometric studies based on entropy minimization, *Anal. Chim. Acta* vol. 359 (3) (1998) 303–310, [https://doi.org/10.1016/S0003-2670\(97\)00638-7](https://doi.org/10.1016/S0003-2670(97)00638-7).
- [35] R. Heylen, M. Parente, P. Gader, A review of nonlinear hyperspectral unmixing methods, *IEEE J. Sel. Top. Appl. Earth Obs. Remote Sens.* vol. 7 (6) (. 2014) 1844–1868, <https://doi.org/10.1109/JSTARS.2014.2320576>.
- [36] A. Huck, M. Guillaume, J. Blanc-Talon, Minimum dispersion constrained nonnegative matrix factorization to unmix hyperspectral data, *IEEE Trans. Geosci. Remote Sens.* vol. 48 (6) (2010) 2590–2602, <https://doi.org/10.1109/TGRS.2009.2038483>.
- [37] L. Guo, F. Kooli, M. Garland, A general method for the recovery of pure powder XRD patterns from complex mixtures using no a priori information, *Anal. Chim. Acta* vol. 517 (1–2) (2004) 229–236, <https://doi.org/10.1016/j.aca.2004.05.006>.
- [38] Harold M. Bell, *Organic Compounds Database.* (<https://www.colby.edu/chemistry/cmp/cmp.html>) (Accessed 12 June 2022).
- [39] Z. Czégény, M. Blazsó, Thermal decomposition of polyamides in the presence of poly(vinyl chloride), *J. Anal. Appl. Pyrolysis* vol. 58–59 (2001) 95–104, [https://doi.org/10.1016/S0165-2370\(00\)00152-2](https://doi.org/10.1016/S0165-2370(00)00152-2).

Article

Activated Carbon Derived from Carbonization of Kevlar Waste Materials: A Novel Single Stage Method

Daniel Karthik ^{1,*} , Vijay Baheti ², Jiri Militky ¹ , Muhammad Salman Naeem ³, Veronika Tunakova ¹ and Azam Ali ¹

¹ Department of Materials Engineering, Faculty of Textiles, Technical University of Liberec, 46117 Liberec, Czech Republic; jiri.militky@tul.cz (J.M.); veronika.tunakova@tul.cz (V.T.); azam.ali@tul.cz (A.A.)

² Department of Textile Technology, Indian Institute of Technology, Delhi 110016, India; vijaykumar.baheti@gmail.com

³ Faculty of Engineering and Technology, National Textile University, Faisalabad 37610, Punjab, Pakistan; salman.ntu@gmail.com

* Correspondence: daniel.karthik@tul.cz; Tel.: +420-770-649-149

Abstract: The augmented demands of textile materials over time have brought challenges in the disposal of substantial volumes of waste generated during the processing and end of life of such materials. Taking into consideration environmental safety due to discarding of textile waste, it becomes critical to recuperate useful products from such waste for economic reasons. The present work deals with the preparation of porous and electrically conductive activated carbon fabric by a novel single stage method of simultaneous carbonization and physical activation of Kevlar feedstock material procured from local industries, for effective electromagnetic (EM) shielding applications. The Kevlar fabric waste was directly carbonized under a layer of charcoal without any intermediate stabilization step at 800 °C, 1000 °C, and 1200 °C, with a heating rate of 300 °C/h and without any holding time. The physical and morphological properties of the activated carbon, influenced by carbonization process parameters, were characterized from EDX, X-ray diffraction, SEM analysis, and BET analysis. Furthermore, the electrical conductivity was analyzed. Finally, the potential application of the activated material for EM shielding effectiveness was analyzed at low (below 1.5 GHz) and high (2.45 GHz) frequencies. The phenomena of multiple internal reflections and absorption of electromagnetic radiations was found dominant in the case of activated carbon fabric produced at higher carbonization temperatures.

Keywords: activated carbon; carbonization; porous surface; cost effective; Kevlar; textile waste; recycle; electrical conductivity; EMI shielding



Citation: Karthik, D.; Baheti, V.; Militky, J.; Naeem, M.S.; Tunakova, V.; Ali, A. Activated Carbon Derived from Carbonization of Kevlar Waste Materials: A Novel Single Stage Method. *Materials* **2021**, *14*, 6433. <https://doi.org/10.3390/ma14216433>

Academic Editors: Filippo Giannazzo and Ivan Shtepliuk

Received: 3 September 2021

Accepted: 23 October 2021

Published: 27 October 2021

Publisher's Note: MDPI stays neutral with regard to jurisdictional claims in published maps and institutional affiliations.



Copyright: © 2021 by the authors. Licensee MDPI, Basel, Switzerland. This article is an open access article distributed under the terms and conditions of the Creative Commons Attribution (CC BY) license (<https://creativecommons.org/licenses/by/4.0/>).

1. Introduction

The ever-pressing affairs on global warming and ecological complications persistently impact the rising awareness in societies of the importance of sustainability, circular economy, and recyclable/reusable products. [1–3]. With the increasing demand for textiles, the amount of waste generated during the processing and end of life of textile materials has significantly increased, adding to the challenges encountered due to its disposal thereof. Tons of textile waste is produced annually from textile industries. The textile waste generated by European Union (EU) countries equates to approximately 16.5 million tons annually [4]. A vast amount of post-consumer textile waste is thrown into landfills or is incinerated and left to decompose, usually releasing methane, among other toxic fumes, which contributes in the greenhouse effect of global warming. Textile wastes from specific categories of materials, that are expensive and divergent, retains its characteristic properties and, due to economic and ecological reasons, it is essential to pave the way to potentially reuse/recycle the same [5–7]. The typical high value-added products obtained from such wastes are

nanoparticles, nanocomposites activated carbon, and fillers for reinforcements, to mention a few.

Activated carbon is a highly porous product, usually derived from semi crystalline precursors such as viscose rayon, phenolic resins, polyacrylonitrile, or isotropic coal tar pitches, by a number of lengthy and multistep processes [8–10]. Activated carbon has a very high porous structure with a large internal surface area of around 500–2000 m²/g [11]. In recent years, research on exploring alternative, inexpensive sources together with methods for the preparation of activated carbon materials has attracted attention. Activated carbon is an excellent adsorbent for the removal of dyes, heavy metals, hazardous smoke, unnecessary odor, taste, and organic substances from the environment [12]. The large surface area, well-developed internal structure, and presence of various surface functional groups depend on the nature of the raw material used, the nature of the activating agent, and the conditions of the pyrolysis and activation processes [9,13].

Surprisingly, the utilization of highly ordered polymer precursors (i.e., Aramid fibers) which do not need oxidative stabilization, have been studied for activated carbon fiber production [14]. Aramid is a long chain aromatic polyamide where at least 85% of amide linkages are attached directly to two aromatic rings [8]. Freeman et al. [14] first proposed the use of Kevlar to obtain carbons with high surface areas, narrow pore size distributions, and acceptable yields [9,15]. Later, a number of studies focused on the preparation of activated carbon fibers from Nomex and Kevlar fibers by physical activation using CO₂ or steam, and by chemical activation in the presence of small amounts of phosphoric acid [16–20]. More recently, the introduction of intermediate isothermal treatments during the pyrolysis of Aramid fibers have been reported to improve the carbon yield, nitrogen content, and reversible electrical capacity of activated carbon fibers [15,21,22]. Despite all these previous efforts, Aramid fibers are still not attractive precursors of carbon materials due to their sophisticated applications in the aeronautical and aerospace industries. An alternative option of using Kevlar pulp has been employed previously as inexpensive feedstock, but surprisingly there are no studies on carbonization of Aramid fibrous textile waste [23].

For general and more commonly used textile fibers, there are plenty of possibilities and various processes to recycle/reuse fibrous wastes. The approaches include chemical processes to depolymerize polymers, recovery of plastic resins from carpet fibers, direct extrusion of mixed fiber waste, composites as wood substitutes, fibers for concrete and soil reinforcement, waste-to-energy conversion, and carpet as feedstock for cement kilns, to mention a few. However, for high performance fibers, such as Kevlar in particular, it is relatively harder to maintain its original structure during processes intended for reutilization of fibrous wastes.

Numerous efforts have been made in previous studies on surface modifications using chemical etching by mixed acids, ionization, surface irradiation by plasma, ultrasonic treatment, chemical grafting methods, and fluorinated modification [21,22]. However, the decomposition mechanism of Aramid has relatively fewer studies for the development of porosity or surface activation behavior to create micro porous Aramid structures using controlled thermal treatment and carbonization.

In our previous study, Naeem et al. [24], a single stage carbonization and physical activation method, under a layer a charcoal, was employed to produce a porous and electrically conductive activated carbon web from needle punched acrylic fibrous waste, but with the necessity of an additional step of thermal stabilization, wherein dehydrogenation, oxidation, and nitrile cyclization reactions take place prior to subsequent carbonization. The present work focuses on the preparation of porous and electrically conductive activated carbon fabric from Kevlar fabric waste, using the same single stage carbonization and physical activation process, except in this case there is no necessity for a thermal stabilization step. Due to rigid-rod structure and a high degree of aromaticity of Kevlar, the direct carbonization process is used. As described in Figure 1, during the carbonization process at a temperature of about 550–575 °C, the progressive decomposition of amide groups take place, wherein intermediate aryl nitrile species are formed. Above 600 °C,

polyaromatic compounds are created. This is a continuous single stage process, without the need for an additional thermal stabilization step [25,26].

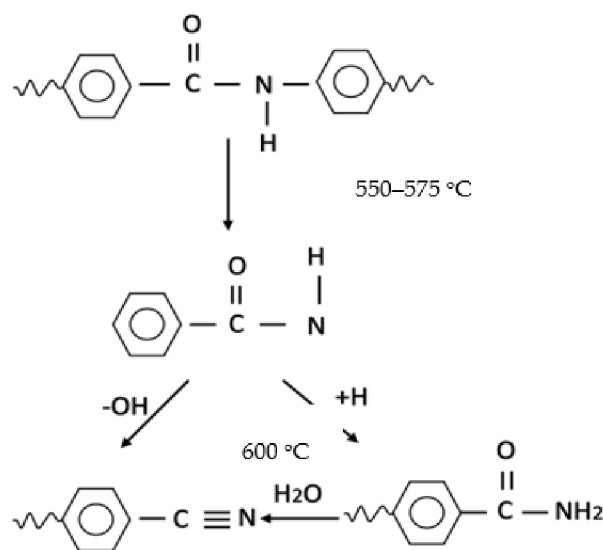


Figure 1. Representation of progressive decomposition process of the Kevlar structure [26].

The carbonization process employed is a less expensive treatment with a lower production time and cost, due to pyrolysis conditions of direct carbonization without intermediate stabilization, in turn leading to less energy consumption, which means less waste. Charcoal, being inexpensive and readily available, was used as the source of heat and to facilitate pyrolysis, which adds to a cheaper production cost.

The positive approach to utilizing textile waste materials in seamless amalgamation with the distinct properties of Kevlar, the novel and faster single stage carbonization process, and the inexpensive and easily obtainable charcoal for purpose of incineration has directed us to the notion of possibly developing a techno-economic product with potential applications. The novelty of present work was the utilization of natural gas for the simultaneous development of porous and electrically conductive Kevlar fibers using controlled physical activation and carbonization. The activated carbon fabrics produced were tested on a waveguide method and a coaxial transmission line method for their end use performance as effective electromagnetic shielding materials. In this way, the large quantity of Kevlar fibrous waste can be utilized for advanced applications to protect the nature.

2. Experimental Methods

2.1. Materials

The Kevlar woven fabric waste was procured from Veba Textile Mills Ltd (Broumov), Czech Republic as short, discarded fabric waste. The Kevlar had a 1710 dtex yarn count, 0.24 m²/g BET surface area, 1.43 g/cm³ density and 5.2 wt% moisture content. Its elemental analysis was reported as weight percentages on a dry basis of 63.85% C, 15.09% N, 0.8% S, and 18.84% O.

2.2. Preparation of Activated Carbon Fabric

The novel single stage carbonization and physical activation of Kevlar fibrous waste was carried out under a layer of charcoal in a high temperature furnace (Elektrické Pece Svoboda, Svetice, Czech Republic). The Kevlar fabric was directly carbonized without any intermediate stabilization step. Temperatures of 800 °C, 1000 °C, and 1200 °C at 300 °C/h heating rate and with no holding time were adopted during the process of carbonization. Figure 2 shows the different stages of production of activated carbon fabric from Kevlar fibrous waste.

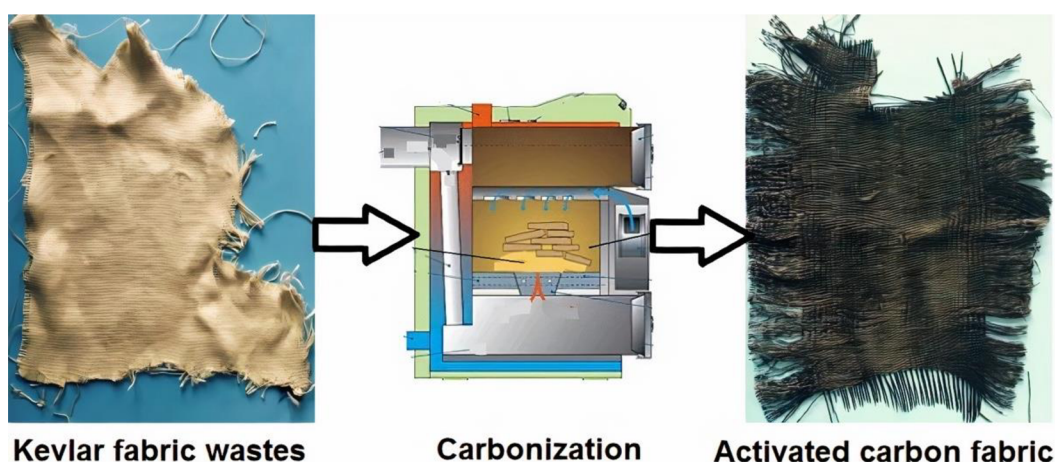


Figure 2. Representation of activated carbon fabric preparation from Kevlar fabric waste.

2.3. Characterization of Activated Carbon Fabric

Characterization of physical properties. The change in yarn count, yarn strength, fabric areal density, thickness, shrinkage, flexibility, and dusting tendency of Kevlar was studied with respect to the increase in the carbonization temperature. The single yarn strength was measured on a TIRA test 2300 LaborTech machine (LaborTech, Opava, Czech Republic) with a gauge length of 20 cm and at a speed of 100 mm/min. The ASTM D 2259 standard [27] was employed for the shrinkage estimation, where change in length of the Kevlar yarn before and after carbonization was measured. For the change in flexibility after carbonization, the bending length was measured by employing the principle of a cantilever bending under its own weight as per ASTM D 1388 standard [28]. The TH-7 instrument (Faculty of Textiles, Technical University of Liberec, Liberec, Czech Republic) was used to measure the bending force of samples and then stiffness was calculated [29]. Lastly, Taber wear and abrasion testers (Taber Industries, New York, NY, USA) were used as per ASTM D 3884 standard [30] to rub the surface of the carbonized Kevlar fabric under 30 rotating cycles, and the amount of generated dust particles were used to evaluate the dusting tendency.

Energy dispersive X-ray (EDX) analysis. An LZ 5 EDX detector, Oxford Instruments, Oxford, UK was used to calculate the relative percentage of different elements in the activated material at three selected carbonization temperatures.

X-ray diffraction (XRD) analysis. The XRD analysis was carried out to confirm the development of crystalline and amorphous regions in prepared activated carbon fabric with respect to the change in carbonization temperature. It was performed on a PANalytical X'Pert PRO MPD diffraction system.

SEM analysis. The porosity characteristics in activated carbon fabric were observed under the field emission scanning electron microscope Sigma, Zeiss, Germany. The 2-kV accelerated voltage and 1000 \times magnification was employed to obtain the surface micrographs of activated carbon fabrics produced at 800 $^{\circ}$ C, 1000 $^{\circ}$ C, and 1200 $^{\circ}$ C carbonization temperatures. The activated carbon fabric obtained was electrically conductive, so its metallization was not needed before testing. Nevertheless, the received Kevlar fabric was metallized by sputter coating.

BET surface area. An Autosorb iQ, Quantachrome Instruments, Boynton Beach, CA, USA was employed to measure the specific surface area of carbonized Kevlar fabrics from N₂ adsorption–desorption isotherms at 77.35 K. The relative pressure range P/P_0 from 0.02 to 1 was adopted for the collection of adsorption/desorption isotherm measurements. Before the adsorption analysis, the produced activated carbon samples were pre-treated in an oven at 45 $^{\circ}$ C for 5 h and then out gassed overnight at 300 $^{\circ}$ C. Lastly, the specific surface area was determined from the calculations of obtained adsorption and desorption isotherms.

Characterization of electrical resistivity. The surface and volume resistivity of activated carbon fabric prepared at 800 °C, 1000 °C, and 1200 °C was determined by using a Hewlett Packard 4339 B resistance meter at a relative humidity of 40%, at a temperature of 22 °C, and at 100 V according to ASTM D257-14 [31]. The direct current was applied at a voltage of 100 ± 5 V at opposite ends of the activated carbon fabric and the resultant current passing through the sample was measured after 15 ± 1 s.

2.4. Electromagnetic Shielding Effectiveness of Activated Carbon Fabric

The two different measurement principles were employed to estimate the electromagnetic shielding effectiveness of prepared activated carbon fabric. The waveguide method was used at a higher frequency (i.e., 2.45 GHz), whereas the coaxial transmission line method for a lower frequency range (i.e., 600 MHz to 1.5 GHz) was used.

Waveguide method. A receiving antenna was placed inside of a rectangular hollow waveguide having electrically conductive walls, whereas a sample was placed at the entrance to the waveguide. The electromagnetic waves were generated by a network analyzer Agilent E 4991A. A high frequency analyzer HF-38B (Gigahertz Solutions, Langenzenn, Germany) was used to receive the electromagnetic signals. The complete details of this measurement method can be found in previous work [32]. The Equation (1) was used to estimate the electromagnetic shielding effectiveness, SE [dB]

$$SE = 10 \log \frac{P_t}{P_i} \quad (1)$$

where P_t and P_i is power density (W/m^2) measured in presence of sample (transmitted), and without the sample (incident,) respectively.

Coaxial transmission line method. The insertion-loss principle, according to ASTM D 4935-10 standard, was employed to determine the EM shielding effectiveness in this method. The measurement set-up consisted of a sample holder with its input and output connected to the network analyzer. A shielding effectiveness test fixture (Electro-Metrics, Inc., model EM-2107A, Johnstown, NY, USA) was used to hold the sample. The network analyzer (Rohde & Schwarz ZN3, Rohde & Schwarz, Columbia, MD, USA) was used to generate and receive the electromagnetic signals.

3. Results and Discussions

3.1. Physical Properties of Activated Carbon Fabric

Table 1 shows the effect of carbonization temperature on physical characteristics of Kevlar derived activated carbon fabrics. The yarn count, areal density, and thickness of Kevlar fabrics were found to drop by more than 50% after the carbonization at 1200 °C. During the carbonization, the main chemical transformation occurred, involving the formation of intermediate aryl nitriles at 500–600 °C, and then progressive aromatization/ring condensation, leading to polyaromatic compounds above 600 °C. This resulted in isotropic, non-graphitizable carbon fibers at first and then into activated carbon by activation with oxidizing natural gas [33]. The yield of activated carbon reduced with an increase in carbonization temperature, and 31% yield was obtained after 1200 °C carbonization. These results are in agreement with previous studies [15,22].

Table 1. Effect of carbonization temperature on physical properties of activated carbon fabric.

Sample	Yarn Count (dtex)	Areal Density (g/m^2)	Thickness (mm)	Shrinkage	Flexibility	Dusting	Yield (%)
Kevlar	1710	1031	1.16	-	-	-	-
800 °C	715	600.5	0.61	Good	Average	Good	58.24
1000 °C	450	368	0.54	Good	Good	Average	35.69
1200 °C	410	322.5	0.46	Average	Excellent	Poor	31.28

When shrinkage testing was carried out, the Kevlar fabrics showed a negligible change in length upon carbonization, unlike our previous experience on acrylic fibers [24]. This indicated better thermal stability of Kevlar fabrics due to the highly ordered arrangement of macromolecules. Nevertheless, the dusting tendency of Kevlar was observed to be similar to the case of acrylic fibers with an increase in carbonization temperature. Interestingly, the flexibility of carbonized Kevlar was found to be superior to the regular carbon and Kevlar fabric (See Figure 3). This indicated better drape properties of the produced activated carbon fabrics and, thus, increased comfort when used as personal protective fabrics.

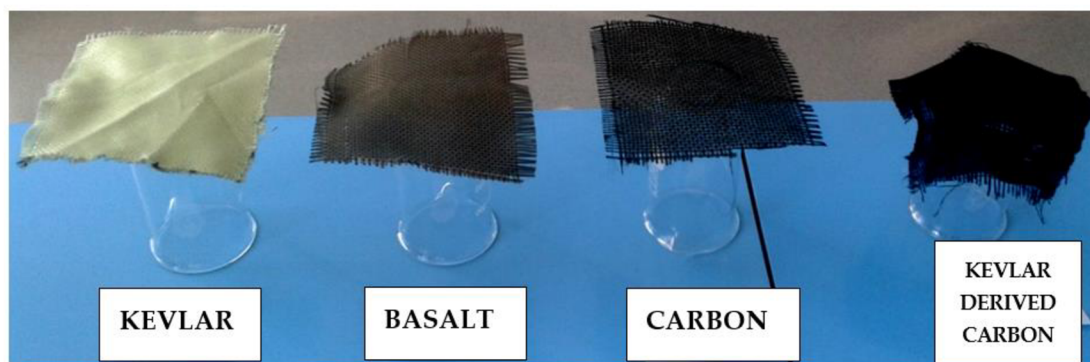


Figure 3. Flexibility of produced activated carbon fabric and other regular fabrics.

To know the draping and the physical comfort of Kevlar derived activated carbon fabrics, the stiffness was measured from the bending properties of the fabric using bending length and flexural rigidity. As shown in Table 2, the stiffness was found to reduce with an increase in carbonization temperature. This behavior was attributed to increased porosity, reduced inter-fiber/yarn friction, and abrasion at fiber/yarn cross-over points due to the decomposition of organic substances from Kevlar fabric during the carbonization.

Table 2. Effect of carbonization temperature on mechanical properties of activated carbon fabric.

Sample	Stiffness (N.m)	Breaking Force (N)	Breaking Elongation (%)
Kevlar	40.92 ± 8.13	126.74 ± 9.07	1.79 ± 0.23
800 °C	8.48 ± 1.17	2.7 ± 1.30	1.15 ± 0.49
1000 °C	5.38 ± 1.01	2.25 ± 1.06	1.07 ± 0.49
1200 °C	4.16 ± 0.93	2.09 ± 1.01	0.94 ± 0.27

Finally, when mechanical properties were investigated, the single yarn strength of Kevlar was found to reduce heavily after the carbonization (Figure 4). The maximum reduction in yarn strength was observed in the case of 1200 °C carbonized Kevlar fabric, where breaking force decreased from 127 N to 2 N and breaking elongation decreased from 1.79% to 0.94%. This behavior was attributed to the formation of additional pores or rough surfaces on Kevlar fibers after the carbonization (see Figure 5).

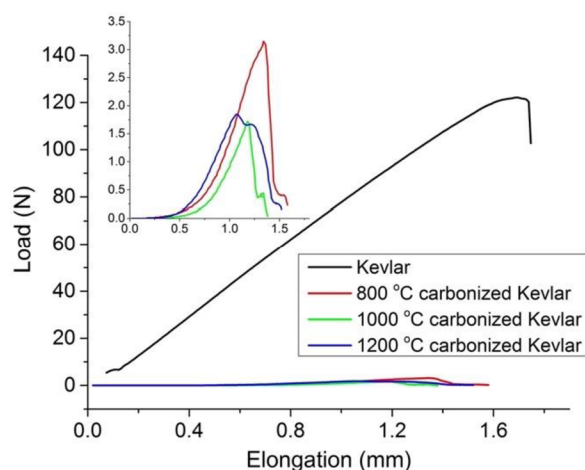


Figure 4. Load elongation curve for carbonized Kevlar fabrics.

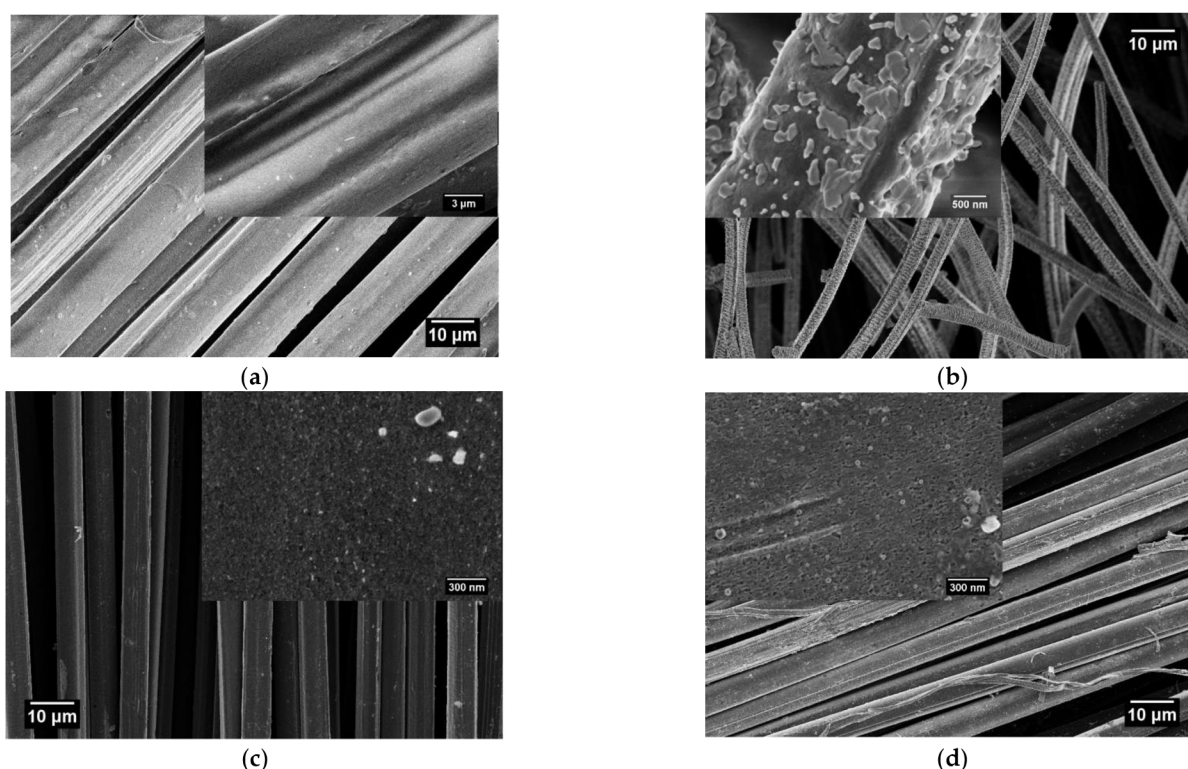


Figure 5. Microstructure of Kevlar fibers after different carbonization temperatures. (a) Kevlar fabric; (b) activated carbon fabric at 800 °C; (c) activated carbon fabric at 1000 °C; and (d) activated carbon fabric at 1200 °C.

3.2. Characterization of Activated Carbon Fabric

BET analysis. The absorption of electromagnetic radiations depends on the specific surface area of materials; therefore, the BET analysis was performed on samples of Kevlar derived carbon obtained at 800 °C, 1000 °C, and 1200 °C carbonization temperatures. From the nitrogen adsorption/desorption isotherm of activated carbon fabrics shown in Figure 6, a rapid rise in the adsorption–desorption isotherm can be observed. This confirmed the type I isotherm based on the classification of the International Union of Pure and Applied Chemistry (IUPAC) [34,35] and the formation of micropore in carbonized Kevlar fabrics. Moreover, the constant slope at intermediate relative pressures with increasing carbonization temperatures indicated the presence of uniform micropore sizes [13]. More clear observation of the isotherm indicated some contribution of type IV with a type H4

hysteresis loop. With an increase in carbonization temperature, the type H4 hysteresis loop was found to become narrow. This indicated a negligible effect of an increase in carbonization temperature on the development of mesoporosity in the structure [36,37]. The marginal increase in specific surface area with an increase in carbonization temperature was observed. The specific surface area for activated carbon fabric prepared at 1200 °C, 1000 °C, and 800 °C obtained was 248 m²/g, 174 m²/g, and 109 m²/g, respectively. This behavior was attributed to the opening of previously inaccessible pores through the removal of tars and disorganized carbon by the gradual reaction of atmospheric oxygen with carbonized Kevlar fibrous waste [38]. Nevertheless, the smaller values of maximum surface areas compared to literature can be associated to possible collapse or closure of pores by a gasification-induced densification at higher carbonization temperature [24].

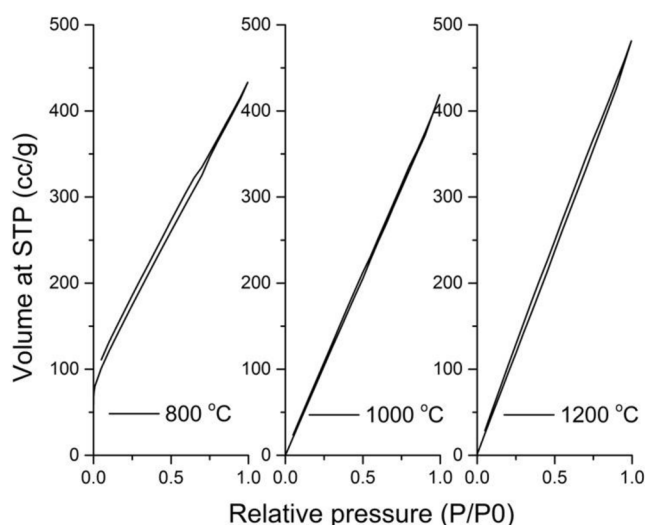


Figure 6. Nitrogen adsorption-desorption isotherm of carbonized Kevlar fabrics.

Mechanism of pore formation. The porosity and surface area created during physical activation can be attributed to the loss of small molecules (CO and CO₂) by gasification of non-graphitic carbon and heteroatoms, the reaction with graphitic carbon, and the reorganization of layers of pseudo-graphitic planes. The development of micro porosity in the present work can be related to selective gasification of the less ordered fractions of the carbonaceous material and an increase in the thickness of the layers of graphitic planes after the carbonization [37]. Moreover, the tendency to attain a limit in pore development with an increase in carbonization temperature can be explained in terms of the gasification-induced densification effect [12].

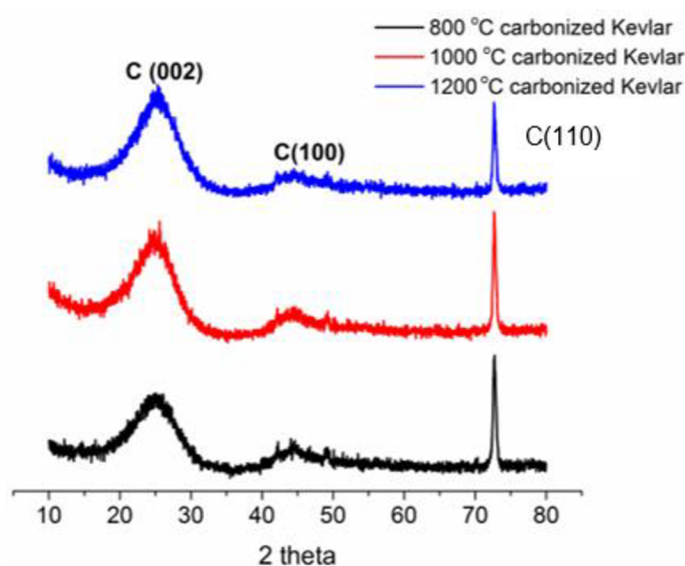
SEM morphology. The formation of porosity in carbonized Kevlar fibrous waste was observed from the Kevlar fiber surface before and after carbonization. The SEM images of Kevlar fibers at different carbonization temperatures of 800 °C, 1000 °C, and 1200 °C can be seen in Figure 5a–d. The Kevlar fibers showed a prominent rough surface after the carbonization, and the surface roughness was increased with increasing carbonization temperature. Therefore, development of a more porous structure was confirmed post physical activation of Kevlar fibers during the carbonization process [14].

EDX analysis. The relative proportion of different elements present in the activated carbon fibers was estimated from the EDX analysis. With an increase in carbonization temperature from 800 °C to 1200 °C, the carbon content was found to increase and the oxygen content was found to reduce (See Table 3). This indicated the decomposition of Kevlar macromolecules at a higher temperature and the subsequent removal of hydrogen, sulfur, nitrogen, and other elements [39]. The 89.26% carbon content and 5.87% oxygen content were estimated for the activated carbon obtained at 1200 °C.

Table 3. Effect of carbonization temperature on elemental composition of activated carbon fabric.

Wt.%	C	N	O	Na	S	Cl	K	Ca
Kevlar	63.85	15.09	18.84	1.20	0.84	0.10	0.01	0.08
800 °C	69.17	8.66	13.19	4.86	2.07	0.18	0.79	1.07
1000 °C	83.47	5.68	7.81	0.45	0.69	0.02	1.68	0.20
1200 °C	89.26	2.56	5.87	0.16	0.60	0.15	1.22	0.17

XRD analysis. The XRD analysis was carried out to know the development of crystallinity with an increase in carbonization temperature. The nature of peaks observed in the XRD pattern can be used to identify the crystallinity of activated carbon samples produced at 800 °C, 1000 °C, and 1200 °C temperature (Figure 7). The development of a higher crystallinity at a higher carbonization temperature was confirmed based on the increase in intensity and sharpness of peaks with an increase in carbonization temperature. The presence of a hexagonal graphitic structure due to C (002) reflection was confirmed from the location of the strongest diffraction peak found at 25.5° [40]. The other diffraction peak found at 43° was associated with C (100) diffraction of the graphitic structure. Furthermore, more transformation of the amorphous structure into graphitized structure can be expected due to the reduced spread of XRD spectra with an increase in carbonization temperature. Therefore, higher electrical conductivity of activated carbon samples can be expected when they are produced at a higher carbonization temperature.

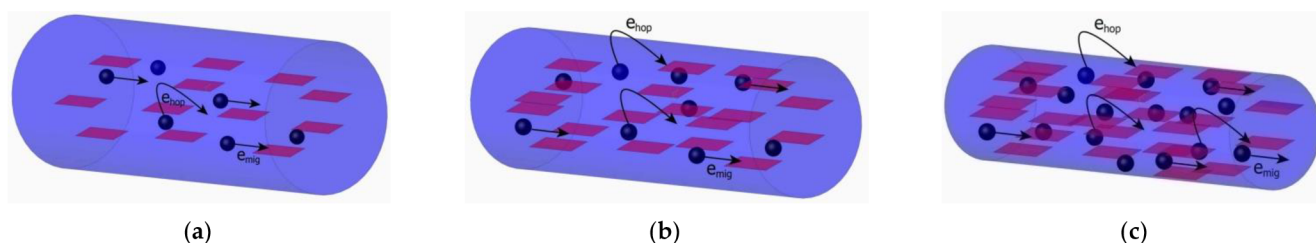
**Figure 7.** Effect of carbonization temperature on crystallinity of activated carbon fabric.

Electrical conductivity. The electrical conductivity was measured to estimate the performance of EM shielding recorded by the reflection of EM radiations. The effect of carbonization temperature on electrical conductivity of activated carbon fabrics is shown in Table 4. With an increase in carbonization temperature, both surface and volume resistivity values were found to decrease. Almost 15,000- and 2500-times reduction in surface and volume resistivity, respectively, was observed for the 1200 °C activated carbon sample in comparison to the 800 °C activated carbon sample. The formation of more graphitization, confirmed by the existence of a sharp diffraction peak in XRD spectra (Figure 7), can be related to the higher electrical conductivity of the 1200 °C activated carbon sample.

Table 4. Effect of carbonization temperature on electrical resistivity of activated carbon fabric.

Carbonization Temperature	Surface Resistivity (ohm)	Volume Resistivity (ohm.cm)
800 °C	1.60×10^6	967.14×10^3
1000 °C	486.15	1251.29
1200 °C	95.78	414.14

Mechanism of charge transport. The movement of electrons through one graphite layer or their hopping across the defects/interfaces between disordered graphite layers can be attributed to the development of electrical conductivity in activated carbon samples [41–43]. Therefore, the two potential means of electron transport (migration and hopping) in the activated carbon fabric produced at 800, 1000, and 1200 °C, respectively are shown in Figure 8a–c. The migration and hopping of electrons were responsible for the higher electrical conductivity of the 1200 °C activated carbon fabric than the 800 and 1000 °C activated carbon. This was possible due to a higher graphite content, uniform distribution of graphite layers, and reduced fiber diameter, which finally resulted in the formation of a more compact micro-current network in the 1200 °C activated carbon fabric [44,45].

**Figure 8.** Mechanism of charge transport in activated carbon fabric [24] at (a) 800 °C, (b) 1000 °C, and (c) 1200 °C.

3.3. Electromagnetic Shielding Ability

Waveguide method. The electromagnetic shielding effectiveness of the prepared activated carbon fabric was measured in single and double layers at 2.45 GHz frequency using the waveguide method. When the carbonization temperature was increased, the Kevlar derived activated carbon exhibited an increase in the electromagnetic shielding effectiveness (see Figure 9). At the carbonization temperatures of 1200 °C, 1000 °C, and 800 °C, the EM shielding effectiveness of 31 dB, 27 dB, and 5 dB was found, respectively, for a single layer of activated carbon fabric. The shielding effectiveness was almost zero at a very low carbonization temperature, however, it increased drastically with the increase in carbonization temperature. For maximum shielding effectiveness, the location of the percolation threshold can be expected between 1000 °C and 1200 °C carbonization temperatures. In this temperature range, the carbonized Kevlar showed higher electrical conductivity, higher porosity, and higher surface area, and therefore increased multiple internal reflections and stronger absorption of electromagnetic radiations [46]. Nevertheless, the effect of increasing the number of layers was found to be negligible for increasing the shielding effectiveness (see Figure 9b). These results are not in agreement of our previous work on activated carbon web produced from acrylic fibrous waste. This behavior can be explained due simple interlacing of Kevlar warp and weft in woven fabrics, unlike more intermingled random arrangements of acrylic fibers in needle punched nonwoven webs of previous work [24].

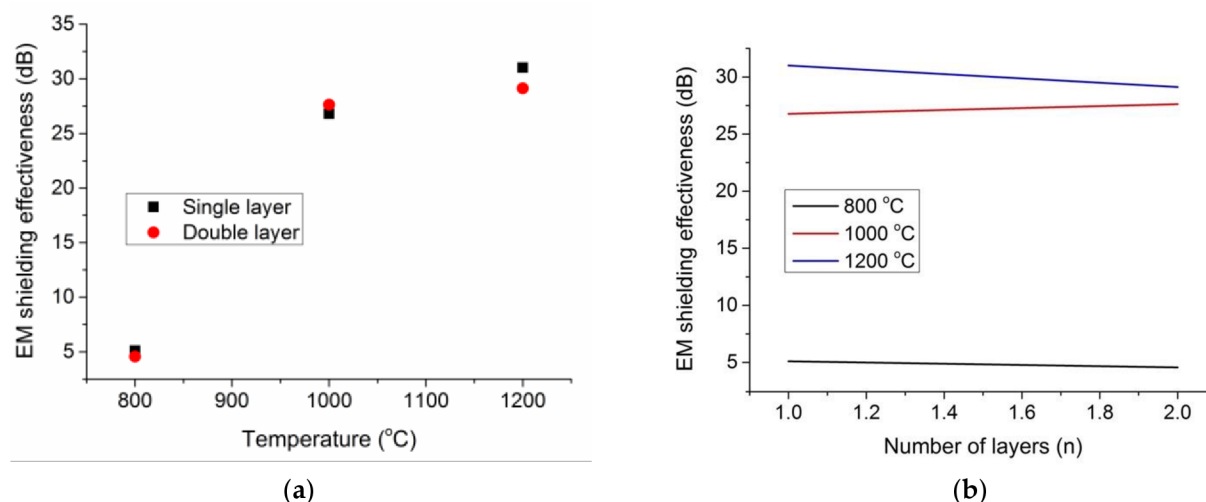


Figure 9. Electromagnetic shielding effectiveness at 2.45 GHz; (a) effect of carbonization temperature; and (b) effect of number of layers.

Coaxial transmission line method. This method was employed to estimate the electromagnetic shielding effectiveness of activated carbon samples in frequencies of 600 MHz, 1 GHz, and 1.5 GHz. From Figure 10a,b, it can be seen that the shielding effectiveness increased with increase in the carbonization temperature. The lowest electromagnetic shielding effectiveness, of about 5 dB, was observed for the single layer of activated carbon fabrics produced at 800 °C. However, when the Kevlar fabric was carbonized at 1200 °C, the shielding ability of 42 dB, 45 dB, and 51 dB was found for respective frequencies of 600 MHz, 1 GHz, and 1.5 GHz. As discussed in the previous section, the similar reasons for the fiber arrangement and gasification-induced densification effect can be attributed to overall lower values of electromagnetic shielding for Kevlar derived activated carbon fabrics than the acrylic derived activated carbon nonwoven web in previous work [24].

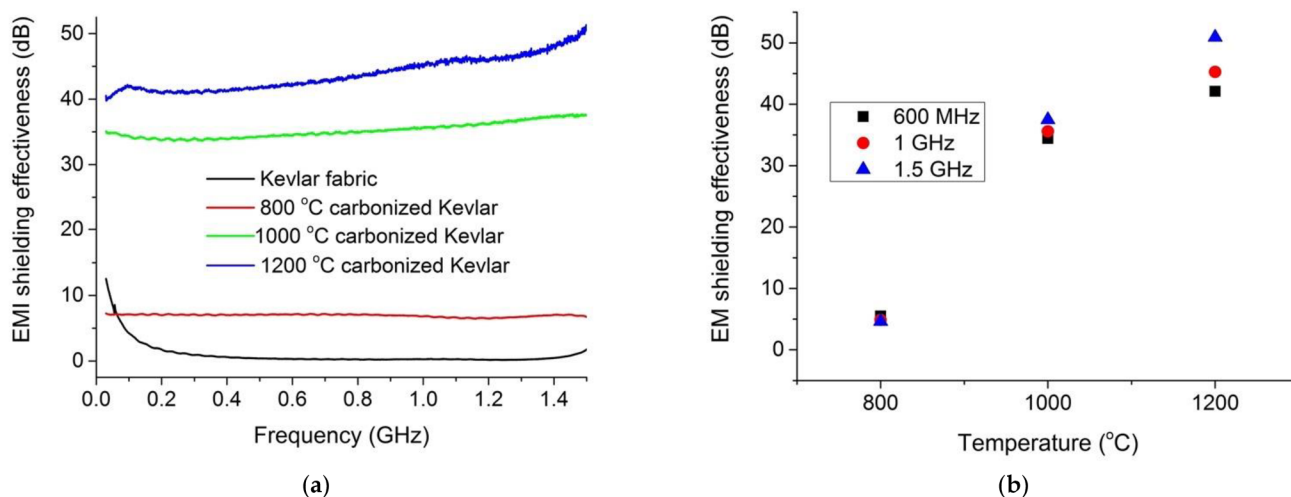


Figure 10. Electromagnetic shielding effectiveness in low frequency region; (a) effect of frequency; and (b) effect of carbonization temperature.

Mechanism of EM shielding. The EM shielding efficiency of materials is governed by the means of reflection, absorption, and multiple internal reflections of EM radiations. The cause of mismatch in impedance between air and material is due to the availability of mobile or nomadic charge carriers (electrons or holes) on the surface. The reflection of electromagnetic radiations [41,45]. The thickness of the material decides the second important mechanism of absorption of electromagnetic radiations caused by Ohmic loss

and polarization loss [44]. The dissipation of energy by nomadic charges through conduction, hopping, and tunneling mechanisms results into the ohmic loss. Polarization is derived from functional groups, defects, and interfaces within the material, which leads to polarization loss from the energy required for overcoming the momentum to reorient the dipoles in each half cycle of the EM wave. Lastly, the inhomogeneity and huge interfacial area of materials contribute to the mechanism of multiple internal reflections due to the scattering effect within the shielding material [46].

In present work, the higher EM shielding properties of the 1200 °C activated carbon fabric can be attributed to the increased multiple internal reflection and stronger absorption of EM waves. This is because the carbonization of Kevlar at a higher carbonization temperature produced a heterogeneous surface with increased electrical conductivity and porosity. This can be explained further from the increased graphite content, uniform dispersion of graphite layers, reduced fiber diameter, etc., of the 1200 °C activated carbon fabric shown in Figures 4, 6d and 7. The dissipation of more electrical energy and, thus, higher Ohmic loss can be expected from the greater number of nomadic charges (from increased graphite content in Figure 8) coupled with their uniform state of dispersion for elongated electrons' mean free paths and enhanced conductive network [47]. Further, the dissipation of the incident EM wave can be expected from the reduced fiber diameter (Table 1) and larger conductive surface area (Figure 5d). Lastly, the higher polarization loss can be expected due to non-homogeneous surface characteristics of the 1200 °C activated carbon fabric shown in Figure 5d.

4. Conclusions

The Kevlar fibrous waste obtained from an industry was successfully converted into activated carbon by a simultaneous process of carbonization and physical activation in the presence of atmospheric air and CO₂ (created by charcoal), using controlled thermal treatment in a high temperature furnace. The Kevlar fibrous waste was heated under a layer of charcoal using a novel single stage carbonization and physical activation. No intermediate stabilization step was employed and direct carbonization of Kevlar fibrous waste was carried out at 800 °C, 1000 °C, and 1200 °C temperatures with the heating rate of 300 °C h⁻¹ and without any holding time.

The pyrolysis at 1200 °C resulted in activated carbon having a higher specific surface area and higher electrical conductivity. The lower heating rate was found to have a significant effect on the development of porous morphology with higher surface area. This behavior is attributed to gradual reaction of atmospheric oxygen and CO₂ with carbonized acrylic fibrous waste. The yield of activated carbon was found to be 31% after the 1200 °C carbonization. The reduced stiffness of carbonized Kevlar was attributed to increased porosity, reduced inter-fiber/yarn friction, and abrasion at fiber/yarn cross-over points due to decomposition of organic substances during the carbonization. This limit in pore development with an increase in carbonization temperature can be explained due to gasification-induced densification effect in Kevlar fibers. The 1200 °C activated carbon sample exhibited almost 10⁴ and 10³ times reduction in surface and volume resistivity, respectively, over the 800 °C activated carbon sample, which is attributed to a higher graphite content, uniform distribution of graphite layers, and reduced fiber diameter in the 1200 °C activated carbon fabric. The greater number of nomadic charges (i.e., graphite content), uniform dispersion of graphite layers, reduced fiber diameter, elongated electrons' mean free paths, larger surface area, higher porosity, and enhanced conductive network formation were responsible for the increase in multiple internal reflections and stronger absorption of EM radiations in the 1200 °C activated carbon. The use of Kevlar waste material collected from industries removes raw material procurement costs. The single-step carbonization process is less time consuming and, hence, uses relatively less power in comparison to the other procedures for carbonization through physical activation. Finally, the utilization of charcoal as the medium for heat, pyrolysis, and CO₂ atmosphere to enhance decomposition further reduces the costs as it is cheaper, more common, and easily

available. These aspects strongly contribute to the manufacturing and production costs, whilst effectively keeping in line with the primary objective of textile re-use, recycling, and waste management.

Author Contributions: Conceptualization, V.B.; methodology, V.B., Muhammad Salman Naeem and D.K.; validation, J.M., V.B.; formal analysis, V.B., M.S.N. and D.K.; investigation, V.B., D.K., J.M., A.A. and V.T.; resources, J.M., M.S.N. and V.T.; data curation, V.B., D.K., M.S.N. and V.T.; writing—original draft preparation, V.B., D.K.; writing—review and editing, J.M., A.A.; visualization, V.B., D.K.; supervision, V.B., J.M.; project administration, V.B., J.M.; funding acquisition, J.M. All authors have read and agreed to the published version of the manuscript.

Funding: The research was funded by the project “Modular platform for autonomous chassis of specialized electric vehicles for freight and equipment transportation”, Reg. No. CZ.02.1.01/0.0/0.0/16_025/0007293.

Institutional Review Board Statement: Not applicable.

Informed Consent Statement: Not applicable.

Data Availability Statement: Not applicable.

Acknowledgments: This work was supported by the project “Modular platform for autonomous chassis of specialized electric vehicles for freight and equipment transportation”, Reg. No. CZ.02.1.01/0.0/0.0/16_025/0007293.

Conflicts of Interest: The authors declare no conflict of interest.

References

- Pensupa, N.; Leu, S.-Y.; Hu, Y.; Du, C.; Liu, H.; Jing, H.; Wang, H.; Lin, C.S.K. Recent Trends in Sustainable Textile Waste Recycling Methods: Current Situation and Future Prospects. *Top. Curr. Chem.* **2017**, *375*, 76. [CrossRef]
- Overcash, M. A Comparison of Reusable and Disposable Perioperative Textiles: Sustainability State-of-the-Art 2012. *Anesth. Analg.* **2012**, *114*, 1055–1066. [CrossRef]
- Huang, Z.; Yilmaz, E.; Cao, S. Analysis of Strength and Microstructural Characteristics of Mine Backfills Containing Fly Ash and Desulfurized Gypsum. *Minerals* **2021**, *11*, 409. [CrossRef]
- Free Analysis: Carbon Fiber Market. Available online: <https://www.zionmarketresearch.com/market-analysis/carbon-fiber-market> (accessed on 22 June 2020).
- Faruk, O.; Bledzki, A.K.; Fink, H.-P.; Sain, M. Biocomposites reinforced with natural fibers: 2000–2010. *Prog. Polym. Sci.* **2012**, *37*, 1552–1596. [CrossRef]
- Recycling in Textiles—1st Edition. Available online: <https://www.elsevier.com/books/recycling-in-textiles/wang/978-1-85573-952-9> (accessed on 22 June 2020).
- Recycling Textile and Plastic Waste—1st Edition. Available online: <https://www.elsevier.com/books/recycling-textile-and-plastic-waste/horrocks/978-1-85573-306-0> (accessed on 22 June 2020).
- Cao, K.; Siepermann, C.P.; Yang, M.; Waas, A.M.; Kotov, N.A.; Thouless, M.D.; Arruda, E.M. Reactive aramid nanostructures as high-performance polymeric building blocks for advanced composites. *Adv. Funct. Mater.* **2013**, *23*, 2072–2080. [CrossRef]
- Castro-Muñiz, A.; Martínez-Alonso, A.; Tascón, J.M.D. Modification of the pyrolysis/carbonization of PPTA polymer by intermediate isothermal treatments. *Carbon* **2008**, *46*, 985–993. [CrossRef]
- Bhat, G.S.; Cook, F.L.; Abhiraman, A.S.; Peebles, L.H. New aspects in the stabilization of acrylic fibers for carbon fibers, Carbon. *Carbon* **1990**, *28*, 377. [CrossRef]
- Theydan, S.K.; Ahmed, M.J. Optimization of preparation conditions for activated carbons from date stones using response surface methodology. *Powder Technol.* **2012**, *224*, 101. [CrossRef]
- Deng, H.; Yang, L.; Tao, G.; Dai, J. Preparation and characterization of activated carbon from cotton stalk by microwave assisted chemical activation—Application in methylene blue adsorption from aqueous solution. *J. Hazard. Mater.* **2009**, *166*, 514–521. [CrossRef]
- Zięzio, M.; Charnas, B.; Jedynek, K.; Hawryluk, M.; Kucio, K. Preparation and characterization of activated carbons obtained from the waste materials impregnated with phosphoric acid(V). *Appl. Nanosci.* **2020**, *10*, 4703–4716. [CrossRef]
- Freeman, J.; Tomlinson, J.; Sing, K.; Theocharis, C. Adsorption of nitrogen and water vapour by activated kevlar chars. *Carbon* **1993**, *31*, 865–869. [CrossRef]
- Castro-Muñiz, A.; Martínez-Alonso, A.; Tascón, J.M.D. Effect of PPTA pre-impregnation with phosphoric acid on the porous texture of carbons prepared by CO₂ activation of PPTA chars. *Microporous Mesoporous Mater.* **2009**, *119*, 284–289. [CrossRef]
- Choma, J.; Osuchowski, L.; Marszewski, M.; Dziura, A.; Jaroniec, M. Developing microporosity in Kevlar®-derived carbon fibers by CO₂ activation for CO₂ adsorption. *J. CO₂ Util.* **2016**, *16*, 17–22. [CrossRef]
- Villar-Rodil, S.; Denoyel, R.; Rouquerol, J.; Martínez-Alonso, A.; Tascón, J.M.D. Characterization of aramid based activated carbon fibres by adsorption and immersion techniques. *Carbon* **2002**, *40*, 1376–1380. [CrossRef]

18. Suárez-García, F.; Martínez-Alonso, A.; Tascón, J.M.D. Activated carbon fibers from Nomex by chemical activation with phosphoric acid. *Carbon* **2004**, *42*, 1419–1426. [CrossRef]
19. Suárez-García, F.; Martínez-Alonso, A.; Tascón, J.M.D. Nomex polyaramid as a precursor for activated carbon fibres by phosphoric acid activation. Temperature and time effects. *Microporous Mesoporous Mater.* **2004**, *75*, 73–80. [CrossRef]
20. Suárez-García, F.; Martínez-Alonso, A.; Tascón, J.M.D. Beneficial effects of phosphoric acid as an additive in the preparation of activated carbon fibers from Nomex aramid fibers by physical activation. *Fuel Process. Technol.* **2002**, *77–78*, 237–244. [CrossRef]
21. Castro-Muñiz, A.; Suárez-García, F.; Martínez-Alonso, A.; Tascón, J.M.D. Activated carbon fibers with a high content of surface functional groups by phosphoric acid activation of PPTA. *J. Colloid Interface Sci.* **2011**, *361*, 307–315. [CrossRef]
22. Ko, K.S.; Park, C.W.; Yoon, S.H.; Oh, S.M. Preparation of Kevlar-derived carbon fibers and their anodic performances in Li secondary batteries. *Carbon* **2001**, *39*, 1619–1625. [CrossRef]
23. Lu, Z.; Dang, W.; Zhao, Y.; Wang, L.; Zhang, M.; Liu, G. Toward high-performance poly(para-phenylene terephthalamide) (PPTA)-based composite paper via hot-pressing: The key role of partial fibrillation and surface activation. *RSC Adv.* **2017**, *7*, 7293–7302. [CrossRef]
24. Naeem, S.; Baheti, V.; Tunakova, V.; Militky, J.; Karthik, D.; Tomkova, B. Development of porous and electrically conductive activated carbon web for effective EMI shielding applications. *Carbon* **2017**, *111*, 439–447. [CrossRef]
25. Mark, H.F. *Encyclopedia of Polymer Science & Technology, Concise*; J. Wiley: Hoboken, NJ, USA, 2007; ISBN 978-0-470-04610-4.
26. Mosquera, M.E.G.; Jamond, M.; Martínez-Alonso, A.; Tascón, J.M.D. Thermal Transformations of Kevlar Aramid Fibers during Pyrolysis: Infrared and Thermal Analysis Studies. Available online: <https://pubs.acs.org/doi/pdf/10.1021/cm00047a006> (accessed on 4 October 2021).
27. ASTM D2259-21, Standard Test Method for Shrinkage of Yarns, ASTM International, West Conshohocken, PA. 2021. Available online: <http://www.astm.org/cgi-bin/resolver.cgi?D2259> (accessed on 4 October 2021).
28. ASTM D1388-18, Standard Test Method for Stiffness of Fabrics, ASTM International, West Conshohocken, PA. 2018. Available online: <http://www.astm.org/cgi-bin/resolver.cgi?D1388> (accessed on 4 October 2021).
29. Fridrichová, L. A New Apparatus for Measuring the Bending Rigidity. *Adv. Mater. Res.* **2013**, *746*, 440–443. [CrossRef]
30. ASTM D3884-09(2017), Standard Guide for Abrasion Resistance of Textile Fabrics (Rotary Platform, Double-Head Method), ASTM International, West Conshohocken, PA. 2017. Available online: <http://www.astm.org/cgi-bin/resolver.cgi?D3884> (accessed on 4 October 2021).
31. ASTM D257-14(2021)e1, Standard Test Methods for DC Resistance or Conductance of Insulating Materials, ASTM International, West Conshohocken, PA. 2021. Available online: <http://www.astm.org/cgi-bin/resolver.cgi?D257> (accessed on 4 October 2021).
32. Šafářová, V.; Tunák, M.; Truhlář, M.; Militký, J. A new method and apparatus for evaluating the electromagnetic shielding effectiveness of textiles. *Text. Res. J.* **2016**, *86*, 44–56. [CrossRef]
33. Martínez-Alonso, A.; Jamond, M.; Montes-Morán, M.A.; Tascón, J.M.D. Microporous texture of activated carbon fibers prepared from aramid fiber pulp. *Microporous Mater.* **1997**, *11*, 303–311. [CrossRef]
34. Ghorbani, H.; Tavanai, H.; Morshed, M. Fabrication of activated carbon nanoparticles from PAN precursor. *J. Anal. Appl. Pyrolysis* **2014**, *110*, 12–17. [CrossRef]
35. Jiang, Q.; Zhao, Y. Effects of activation conditions on BET specific surface area of activated carbon nanotubes. *Microporous Mesoporous Mater.* **2004**, *76*, 215–219. [CrossRef]
36. Castro-Muñiz, A.; Martínez-Alonso, A.; Tascón, J.M.D. Microporosity and mesoporosity of PPTA-derived carbons. Effect of PPTA thermal pretreatment. *Microporous Mesoporous Mater.* **2008**, *114*, 185–192. [CrossRef]
37. Blanco López, M.C.; Villar-Rodil, S.M.; Martínez-Alonso, A.; Tascón, J.M.D. Effect of some precursor characteristics on the porous texture of activated carbon fibres prepared from Nomex aramid fibres. *Microporous Mesoporous Mater.* **2000**, *41*, 319–321. [CrossRef]
38. Baheti, V.; Naeem, S.; Militky, J.; Okrasa, M.; Tomkova, B. Optimized preparation of activated carbon nanoparticles from acrylic fibrous wastes. *Fibers Polym.* **2015**, *16*, 2193–2201. [CrossRef]
39. Ma, Y.Z.; Yin, X.W.; Li, Q. Effects of heat treatment temperature on microstructure and electromagnetic properties of ordered mesoporous carbon. *Trans. Nonferrous Met. Soc. China Engl. Ed.* **2013**, *23*, 1652–1660. [CrossRef]
40. Kim, J.H.; Jeong, E.; Lee, Y.S. Preparation and characterization of graphite foams. *J. Ind. Eng. Chem.* **2015**, *32*, 21–33. [CrossRef]
41. Cao, M.S.; Song, W.L.; Hou, Z.L.; Wen, B.; Yuan, J. The effects of temperature and frequency on the dielectric properties, electromagnetic interference shielding and microwave-absorption of short carbon fiber/silica composites. *Carbon* **2010**, *48*, 788–796. [CrossRef]
42. Song, W.L.; Cao, M.S.; Hou, Z.L.; Fang, X.Y.; Shi, X.L.; Yuan, J. High dielectric loss and its monotonic dependence of conducting-dominated multiwalled carbon nanotubes/silica nanocomposite on temperature ranging from 373 to 873 K in X-band. *Appl. Phys. Lett.* **2009**, *94*, 233110. [CrossRef]
43. Wen, B.; Cao, M.S.; Hou, Z.L.; Song, W.L.; Zhang, L.; Lu, M.M.; Jin, H.B.; Fang, X.Y.; Wang, W.Z.; Yuan, J. Temperature dependent microwave attenuation behavior for carbon-nanotube/silica composites. *Carbon* **2013**, *65*, 124–139. [CrossRef]
44. Arjmand, M.; Chizari, K.; Krause, B.; Pötschke, P.; Sundararaj, U. Effect of synthesis catalyst on structure of nitrogen-doped carbon nanotubes and electrical conductivity and electromagnetic interference shielding of their polymeric nanocomposites. *Carbon* **2016**, *98*, 358–372. [CrossRef]

45. Arjmand, M.; Sundararaj, U. Electromagnetic interference shielding of Nitrogen-doped and Undoped carbon nanotube/polyvinylidene fluoride nanocomposites: A comparative study. *Compos. Sci. Technol.* **2015**, *118*, 257–263. [[CrossRef](#)]
46. Sano, E.; Akiba, E. Electromagnetic absorbing materials using nonwoven fabrics coated with multi-walled carbon nanotubes. *Carbon* **2014**, *78*, 463–468. [[CrossRef](#)]
47. Cao, M.-S.; Wang, X.-X.; Cao, W.-Q.; Yuan, J. Ultrathin graphene: Electrical properties and highly efficient electromagnetic interference shielding. *J. Mater. Chem. C* **2015**, *3*, 6589–6599. [[CrossRef](#)]



Development of porous and electrically conductive activated carbon web for effective EMI shielding applications



Salman Naem, Vijay Baheti*, Veronika Tunakova, Jiri Militky, Daniel Karthik, Blanka Tomkova

Department of Material Engineering, Faculty of Textile Engineering, Technical University of Liberec, Studentska 2, Liberec 46117, Czechia

ARTICLE INFO

Article history:

Received 21 August 2016
Received in revised form
10 October 2016
Accepted 12 October 2016
Available online 13 October 2016

Keywords:

Textile recycling
Acrylic fibrous wastes
Activated carbon
Electrical conductivity
Electromagnetic shielding
Physical activation
Specific surface area

ABSTRACT

In present work, porous and electrically conductive activated carbon needle punched nonwoven web was produced by heating acrylic fibrous wastes under the layer of charcoal using novel single stage carbonization and physical activation. The influence of 800 °C, 1000 °C and 1200 °C carbonization temperature on physical and morphological properties of activated carbon web was studied from EDX, X-ray diffraction, SEM, X-ray tomography and BET analysis. Additionally, the electrical conductivity was also measured. At the end, the utility of prepared activated carbon web was investigated for electromagnetic shielding ability in high frequency (i.e. at 2.45 GHz) and low frequency regions (i.e. below 1.5 GHz) using waveguide method and coaxial transmission line method, respectively. The activated carbon web produced at 1200 °C showed maximum shielding effectiveness in both high and low frequency regions. For single layers of 1200 °C web, the electromagnetic shielding effectiveness of 63.26 dB, 66.75 dB, and 75.44 dB was found for respective frequencies of 600 MHz, 1 GHz, and 1.5 GHz. This behavior was attributed to the increased multiple internal reflections and stronger absorption of electromagnetic radiations in 1200 °C activated carbon web.

© 2016 Elsevier Ltd. All rights reserved.

1. Introduction

In recent years, research on electromagnetic interference (EMI) shielding materials has attracted significant attention due to increase in electromagnetic population from widespread applications of computer and telecommunication technologies [1,2]. Electromagnetic interference refers to the radiant electromagnetic signals emitted by electrical instruments during their operation. The emitted electromagnetic radiations are concerns since they interfere with the working of other appliances as well as cause serious health risks to the human [3]. The EMI shielding efficiency of materials is governed by reflection, absorption and multiple internal reflections of incident electromagnetic radiations [4–6]. Reflection is commonly used shielding mechanism by high electrically conductive materials such as metals and their nanoparticles. However, high density, lack of flexibility, easy corrosion, costly processing and weak microwave absorption are main drawbacks of metals [7]. Recently, the carbon nanostructures and graphene are

reported as promising alternatives to metal-based shielding materials [3,8].

For eco-friendly advancements in EMI shielding effectiveness, the development of new light weight shielding materials having strong absorption and weak secondary reflection is necessary [9,10]. This can be achieved by porous morphology, large specific surface area and higher electrical conductivity of shielding materials [11]. For instance, carbon-based shielding foams are considered predominant in effective shielding mechanism due to their light weight and the synergetic effect of electrical conductivity and multiple reflections. As a result, many lightweight polymer foams with graphene, CNTs, or carbon nano-fibers were produced [11–15]. Nevertheless, the addition of high concentration of electrically conductive nanofillers was found to cause undesirable effects on the foam ability of the polymers for formation of porous structure [16]. Therefore, the numbers of studies in recent years focused on the development of lightweight EMI shielding materials using various new approaches. Yan et al. proposed a combination of high-pressure compression molding plus salt-leaching method to fabricate porous graphene/polystyrene composites [17]. In addition, the chemical vapor deposition and self assembly of highly aligned graphene sheets into 3D graphene porous structures was

* Corresponding author.

E-mail address: vijaykumar.baheti@gmail.com (V. Baheti).

found to be efficient in improving the EMI shielding properties [18]. The development of carbon aerogels was attempted by some researchers to get maximum electromagnetic shielding due to their ultra-low density, ultra-high specific surface area, and large open pores [19].

Although number of research studies focused on development of porous carbon based EMI shielding materials, the construction of lightweight structures with excellent EMI shielding properties by simple and affordable method is still a big challenge. This work presented the simple and novel method for preparation of porous and electrically conductive activated carbon nonwoven web from acrylic fibrous wastes. The prepared activated carbon is advantageous over carbon made from other materials because of low cost, high density, better purity, and virtually dust-free nature of acrylic fibers [20]. The activated carbon web was prepared by sequential action of carding, needle punching and physical activation of acrylic fibrous wastes in presence of air. The carbonization was performed under the layer of charcoal at 800 °C, 1000 °C and 1200 °C with the heating rate of 300 °C h⁻¹ and without any holding time. Further, electrical conductivity, EDX, X-ray diffraction, SEM, X-ray tomography and BET analysis was carried out to study the effect of carbonization temperature on physical and morphological properties of activated carbon web. At the end, the electromagnetic shielding ability of the produced three webs was investigated with respect to change in carbonization temperature and thickness of material using two different measurement approaches (i.e. waveguide method and coaxial transmission line method). In this way, the present study served to utilize large quantity of acrylic fibrous wastes for development of effective electromagnetic shielding materials.

2. Experimental methods

2.1. Materials

The acrylic fibrous waste was obtained from Grund Industries, Czech Republic in form of short lengths generated during mechanical processing of bath mats. The acrylic fibers are anionic copolymers containing 85–89% of acrylonitrile. Table 1 shows the physical properties of acrylic fibrous wastes.

2.2. Preparation of activated carbon nonwoven web

The short segments of acrylic fibers were removed from bath mats using mechanical cutting method. The compact dense structure of nonwoven web having thickness 11.6 mm and density 2.78 g/cm³ was prepared by opening of short fibers on Carding Machine (Laboratory Roller Card, Befama, Poland) with subsequent action of Needle Punching Machine (Hansa, Germany). The pre-determined size of acrylic nonwoven web was cut and transferred to high temperature furnace (Elektrické Pece Svoboda, Czech Republic) for carbonization in two stages. The sample was initially stabilized at 250 °C with heating rate of 35 °C h⁻¹ and under pre-determined tension. Further, the stabilized web was carbonized at 800 °C, 1000 °C and 1200 °C with heating rate of 300 °C h⁻¹ and without any holding time. The controlled physical activation was

carried out by carbonization under the layer of charcoal. The novel part of this study is single stage carbonization and physical activation in presence of air. The schematic of synthesis of activated carbon web from acrylic short fiber waste is shown in Fig. 1.

2.3. Characterization of activated carbon web

The physical properties of acrylic fibrous and activated carbon nonwoven web were determined in terms of shrinkage, flexibility and dusting tendency. The shrinkage measurement was performed as per ASTM D 2259 standard available for testing textile fibers. The shrinkage was evaluated from change in length of acrylic fiber web before and after carbonization. The flexibility or stiffness was evaluated from bending length by employing the principle of cantilever bending of the web under its own weight as per ASTM D 1388 standard. The dusting tendency was evaluated from amount of generated dust particles after rubbing the surface of web on Taber wear and abrasion tester as per ASTM D 3884 standard. The rotary rubbing action was performed for 30 cycles under controlled conditions of pressure and abrasive action.

2.3.1. Energy dispersive x-ray (EDX) analysis

It was performed on Oxford Instruments, LZ 5 EDX detector, UK to know the change in relative proportion of different elements with respect to change in carbonization temperature.

2.3.2. X-ray diffraction (XRD) analysis

It was carried out on a PANalytical X' Pert PRO MPD diffraction system. The development of crystalline and amorphous regions in prepared activated carbon web was investigated with respect to change in carbonization temperature.

2.3.3. SEM analysis

The field emission scanning electron microscope Sigma, Zeiss, Germany was employed to investigate the morphology of acrylic fibrous web and prepared activated carbon web of 800 °C, 1000 °C and 1200 °C carbonization temperature. This helped to understand the development of porosity characteristics of activated carbon web with change in carbonization temperature. The micrographs were taken at 2 kV accelerated voltage and 1000× magnification. As prepared activated carbon web was electrically conductive, so it was not metalized before test. However, the acrylic fibrous nonwoven web was metalized by sputter coating.

2.3.4. X-ray micro-computed tomography

In order to observe the three dimensional view of prepared activated carbon, the X-ray micro computerized tomography was performed on SKYSCAN 1272 of BRUKER. The micro graph of 1200 °C activated carbon web was compared with acrylic fibrous web at a pixel resolution of 1.60 μm. The scanned images of 5 mm length sample size were reconstructed using NRecon into three dimensional object, which was further analyzed for structural properties using CTan. A suitable thresholding was applied to remove the back ground noise. DE speckling function was operated to remove noise and to fill small holes within the fibers structure. Shrink-wrap technique was used to limit the region of interest boundaries as per the fiber spread contours. The CTvox and Data Viewer tools were utilized for visualization and measurement of image database.

2.3.5. BET surface area

The specific surface area of 1200 °C activated carbon web was measured from N₂ adsorption–desorption isotherms at 77.35 K using Autosorb iQ, Quantachrome Instruments, USA. The adsorption/desorption isotherm measurements were collected in the

Table 1
Physical properties of acrylic short fiber wastes.

Physical properties	
Fineness (Denier)	13
Tenacity (GPD)	2.7
Elongation (%)	45
Shrinkage (%)	2.5

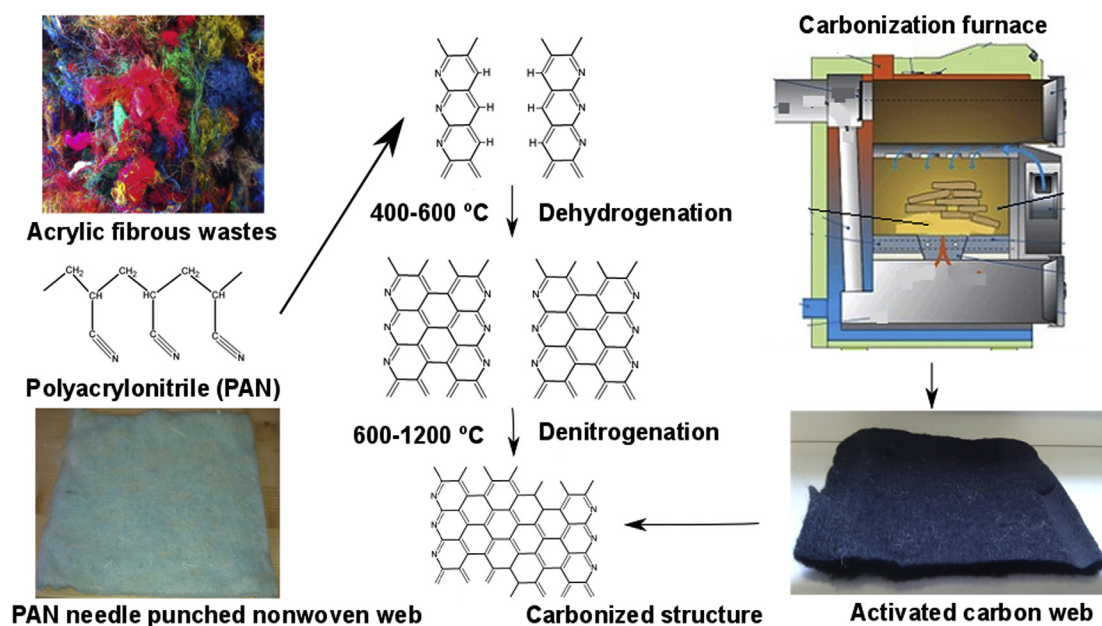


Fig. 1. Schematic of preparation of activated carbon from acrylic fibrous wastes. (A colour version of this figure can be viewed online.)

relative pressure range P/P_0 from 0.02 to 1, where P_0 is saturated pressure of nitrogen gas at 77.35 K temperature (i.e. 1 Atm). The samples were pre-treated in an oven at 45 °C in dry-room for at least 5 h and then out gassed overnight at 300 °C prior to the adsorption analysis. Both adsorption and desorption isotherms were obtained and the specific surface area was determined.

2.3.6. Electrical conductivity

Hewlett Packard 4339 B high resistance meter was used to measure the volume electrical resistivity of activated carbon web samples according to ASTM D257-14 at temperature 22 °C and relative humidity 40%. The specific voltage potential of 100 ± 5 V using direct current was applied across opposite ends of activated carbon web and resultant current flowing across the sample was measured after 15 ± 1 s.

2.4. Electromagnetic shielding effectiveness of activated carbon web

The electromagnetic shielding effectiveness of prepared activated carbon web was determined from two different measurement principles (i.e. waveguide method and coaxial transmission line method).

2.4.1. Waveguide method

The waveguide method examined the electromagnetic shielding ability at 2.45 GHz. This device consisted of a rectangular hollow waveguide having electrically conductive walls. A receiving antenna was placed inside of this waveguide, while a sample was placed at the entrance to the waveguide. A network analyzer Agilent E 4991A was used to generate, and a high frequency analyzer HF-38B (Gigahertz Solutions) was used to receive the electromagnetic signals. More details of this measurement method can be found in [21]. The electromagnetic shielding effectiveness SE [dB] was calculated based on Equation (1).

$$SE = 10 \log \frac{P_t}{P_i} \quad (1)$$

where P_t and P_i is power density (W/m^2) measured in presence of

sample (transmitted), and without the sample (incident) respectively.

2.4.2. Coaxial transmission line method

The coaxial transmission line method examined the electromagnetic shielding ability in frequency range of 600 MHz to 1.5 GHz. This device determined electromagnetic shielding effectiveness using the insertion-loss method according to ASTM D 4935-10 standard [21]. The measurement set-up consisted of a sample holder with its input and output connected to the network analyzer. A shielding effectiveness test fixture (Electro-Metrics, Inc., model EM-2107A) was used to hold the sample. The network analyzer (Rohde & Schwarz ZN3) was used to generate and receive the electromagnetic signals.

3. Results and discussions

3.1. Effect of carbonization parameters on properties of activated carbon web

3.1.1. Effect of carbonization temperature

The physical characteristics of activated carbon webs prepared at 800 °C, 1000 °C and 1200 °C of temperature, under 300 °C h^{-1} heating rate and without any holding time are shown in Table 2. The stabilization of acrylic fibers at 250 °C leads to cyclization, dehydrogenation, and oxidation of polyacrylonitrile structure (Fig. 1) [22]. During this stage, nitrile groups form non-meltable ladder structure, which further enhances mechanical properties and final carbon yield. During subsequent carbonization of stabilized web, the ladder polymer further cross links to form turbo-static carbon structure and the orientation of basal planes leads

Table 2
Effect of carbonization temperature on physical properties of activated carbon web.

Temperature (°C)	Yield (%)	Shrinkage	Flexibility	Dusting
800	61.7	Good	Good	Good
1000	57.12	Good	Average	Average
1200	45	Average	Poor	Poor

to graphite like structure.

From Fig. 2, the specific surface area of prepared activated carbon web was found to increase with increase in carbonization temperature. The activated carbon web prepared at 1200 °C, 1000 °C and 800 °C exhibited the specific surface area of 278 m²/g, 190 m²/g and 120 m²/g respectively. This behavior was attributed to gradual reaction of atmospheric oxygen with carbonized acrylic fibrous waste, which resulted into the opening of previously inaccessible pores through the removal of tars and disorganized carbon [20]. Therefore, the increased surface area at high temperature was indication of increase in porosity due to free spaces created by decomposition of organic matter.

3.1.2. Effect of pre-tension during stabilization

The pre-tension applied on the web during stabilization was found to affect the shrinkage, flexibility and dusting behavior of prepared activated carbon web. Fig. 3 shows the significant amount of shrinkage exhibited by carbonized sample (1200 °C temperature, 300 °C h⁻¹ of heating rate and no holding time) when there was no pre-tension applied during the stabilization. This behavior can be explained from higher entropic and chemical shrinkage occurred in absence of pre-tension. The entropic shrinkage resulted from strain relaxation of molecular chains, whereas chemical shrinkage resulted from formation of cyclized ladder structure. The rate and

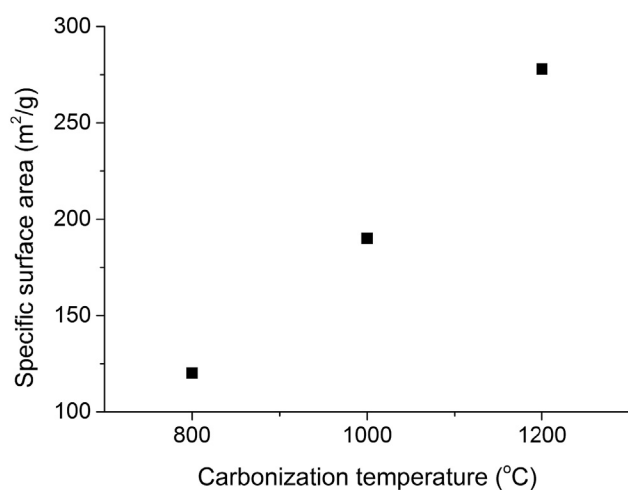


Fig. 2. Effect of carbonization temperature on specific surface area of activated carbon web.



Fig. 3. Activated carbon from stabilization (a) without any pre-tension, (b) with applied pre-tension. (A colour version of this figure can be viewed online.)

magnitude of this shrinkage depends on various factors such as surrounding atmosphere, applied load and heating rate etc [22].

3.2. Characterization of activated carbon web

3.2.1. EDX analysis

Energy disperse x-ray spectroscopy was performed to know the relative proportion of different elements present in the activated carbon webs. From Table 3, the increase in carbon content and reduction in oxygen content was found with increase in carbonization temperature from 800 °C to 1200 °C. The activated carbon web produced at 1200 °C exhibited 92.49% carbon content and 6.61% oxygen content. This behavior was attributed to removal of hydrogen, sulfur, nitrogen and other elements due to decomposition at higher temperature [23].

3.2.2. XRD analysis

In order to know the development of crystallinity with increase in carbonization temperature, the XRD analysis was carried out. Fig. 4 shows the XRD pattern of different activated carbon samples produced at 800 °C, 1000 °C and 1200 °C temperature. The crystallinity of material can be identified from nature of peaks present in the XRD pattern. The intensity and sharpness of peak was found to increase with increase in carbonization temperature. This confirmed the development of higher crystallinity in activated carbon samples produced at higher temperature. The strongest diffraction peak was found at 25.5°, which confirmed the presence of hexagonal graphitic structure due to C (002) reflection [10]. The other diffraction peaks found at 43° and 52.5° were associated with C (100) and C (004) diffraction of graphitic structure. The presence of sharp and intense peak for 1200 °C activated carbon sample showed more transformation of amorphous structure into graphitized structure. This is useful observation to support the results of increased electrical conductivity of activated carbon samples described in further sections.

3.2.3. SEM morphology

In order to know the development of porosity after carbonization of acrylic fibrous wastes, the surface morphology of acrylic fibers before and after carbonization was studied from SEM images. Fig. 5(a–d) show the SEM images of acrylic fibrous web and activated carbon web produced at temperature of 800 °C, 1000 °C and 1200 °C respectively. The activated carbon web showed noticeable rough surface as compared to acrylic fibrous web. The surface roughness was found to increase with increase in carbonization

Table 3

Effect of carbonization temperature on elemental composition of activated carbon web.

Element	App conc.	Intensity	Weight %	Atomic %
800 °C				
C K	0.26	2.12	0.13	91.76
O K	0.01	0.761	0.01	8.24
1000 °C				
C K	0.37	2.12	0.18	91.87
O K	0.02	0.760	0.02	8.13
1200 °C				
C K	0.18	2.10	0.09	92.49
O K	0.01	0.744	0.01	6.61
Ca K	0.00	0.902	0.00	0.90

temperature, which indicated the development of more porous structure after physical activation of acrylic fibrous wastes.

3.2.4. Three dimensional morphology

The three dimensional morphology of acrylic fibrous and 1200 °C activated carbon web can be seen from Fig. 6 (a) and (b) respectively. The diameter of individual fibers in the web was found to become thinner after carbonization. For measurement of diameter distribution, the obtained images were processed and analyzed using image analysis software. The background noise was removed and morphological operations were performed using DE speckling function. After careful thresholding of images, the number of fibers for particular range of fiber diameter was examined. Fig. 7 shows the diameter distribution of fibers for acrylic fibrous and activated carbon web. The number of smaller diameter fibers in activated carbon web was found in higher quantity than the acrylic fibrous web. This further justified the development of higher surface area after controlled carbonization of acrylic fibers.

3.2.5. BET analysis

For electromagnetic shielding effectiveness to be achieved through absorption of radiations, the knowledge of pore characteristics and specific surface area of samples is necessary. Fig. 8 shows the nitrogen adsorption/desorption isotherm of activated carbon web prepared at 1200 °C of carbonization temperature, 300 °C h⁻¹ of heating rate and no holding time. A rapid rise in the adsorption–desorption isotherm was found at low relative pressures, which was followed by a horizontal plateau at higher relative pressures. This behavior indicated type I isotherm based on the classification of the International Union of Pure and Applied Chemistry (IUPAC) [24,25]. The type I isotherm confirmed that

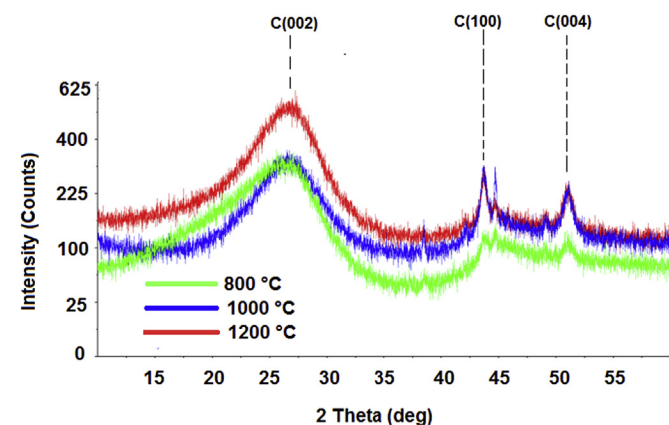


Fig. 4. Effect of carbonization temperature on crystallinity of activated carbon web. (A colour version of this figure can be viewed online.)

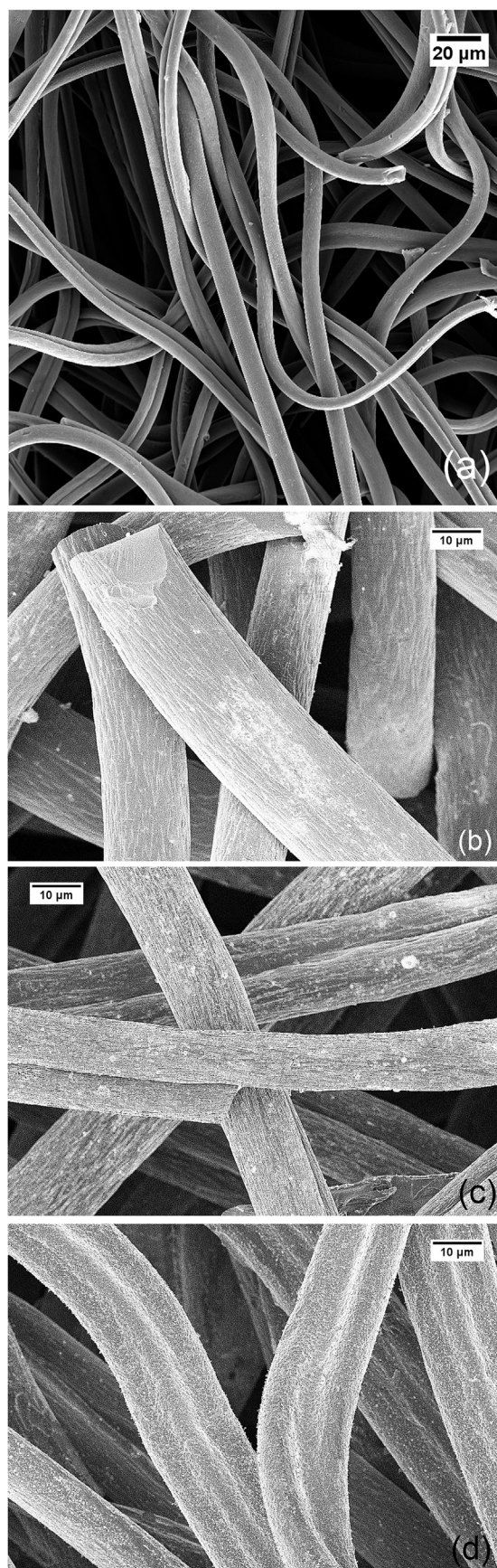


Fig. 5. SEM image of (a) acrylic fibrous web (b) 800 °C activated carbon web (c) 1000 °C activated carbon web (d) 1200 °C activated carbon web.

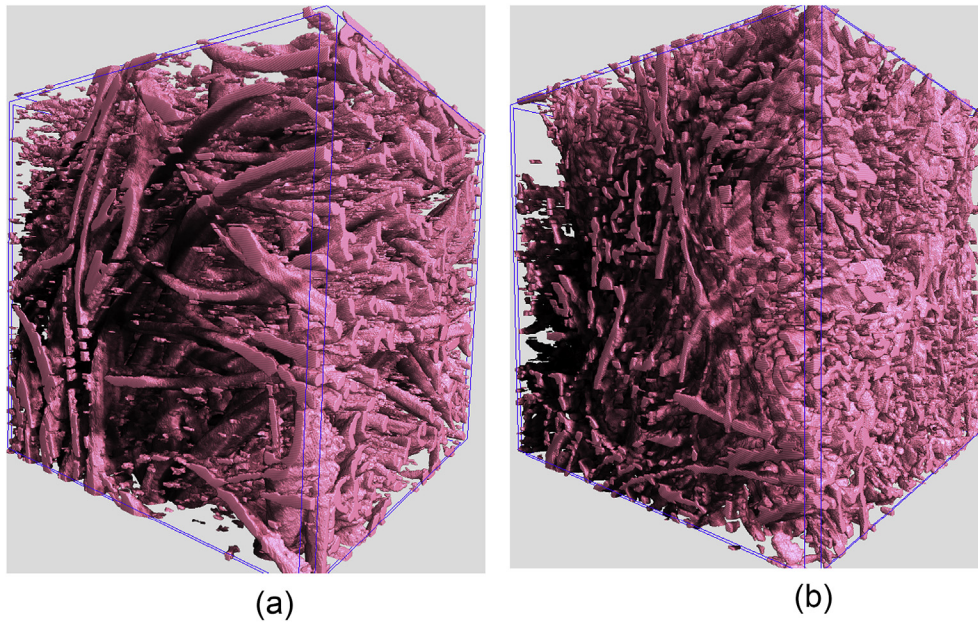


Fig. 6. Three dimensional view at 500 μm scale for (a) acrylic fibrous web (b) 1200 $^{\circ}\text{C}$ activated carbon web. (A colour version of this figure can be viewed online.)

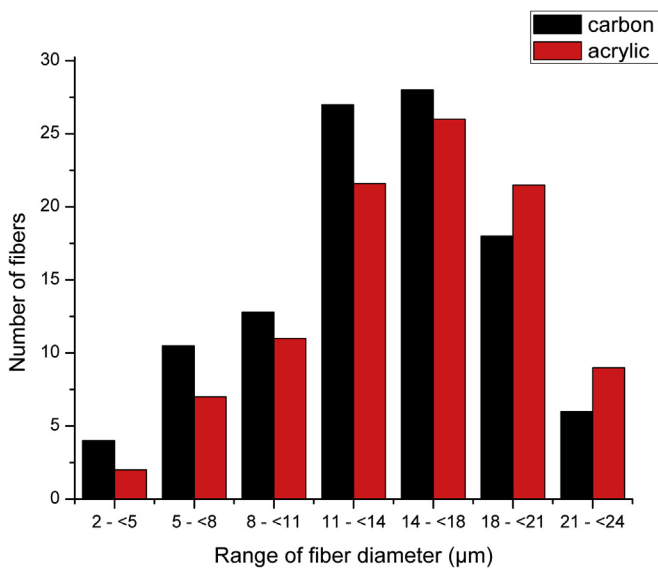


Fig. 7. Distribution of fiber diameter evaluated from computed tomography images. (A colour version of this figure can be viewed online.)

micropore was developed in the activated carbon web produced at 1200 $^{\circ}\text{C}$. The pore volume and pore diameter of this activated carbon web was found 0.437 cc/g and 3.062 nm, respectively from BJH analysis. In accordance to IUPAC classification, the adsorbent pores are classified into three groups: micropore (diameter < 2 nm), mesopore (2–50 nm), and macropore (>50 nm) [26]. Therefore, the prepared activated carbon at 1200 $^{\circ}\text{C}$ predominantly exhibited mesoporous nature.

3.2.6. Electrical conductivity

For electromagnetic shielding effectiveness to be achieved through reflection of EM radiations, the knowledge of electrical conductivity of samples is necessary. Fig. 9 shows the average values in 95% confidence interval for electrical resistivity of

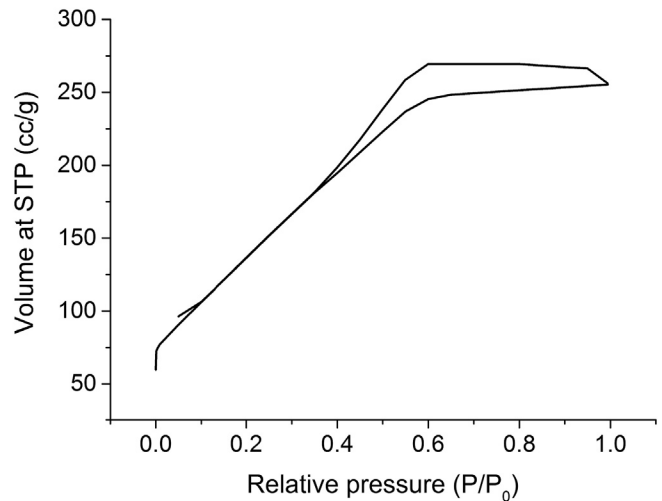


Fig. 8. Nitrogen adsorption-desorption isotherm of 1200 $^{\circ}\text{C}$ activated carbon web.

activated carbon web samples. The electrical resistivity was found to decrease with increase in carbonization temperature. The linear regression model was applied and 76.15% coefficient of determination was found between carbonization temperature and achieved electrical resistivity. The 1200 $^{\circ}\text{C}$ activated carbon sample exhibited 1000 times reduction in electrical resistivity over 800 $^{\circ}\text{C}$ activated carbon sample. The higher electrical conductivity of 1200 $^{\circ}\text{C}$ activated carbon sample was attributed to more graphitization, which was confirmed from presence of sharp diffraction peak observed in XRD spectra (Fig. 4).

3.2.7. Mechanism of charge transport

Fig. 10(a–c) show the two possible modes of electron transport (i.e., migration and hopping) in the activated carbon web produced at 800, 1000 and 1200 $^{\circ}\text{C}$, respectively. The development of electrical conductivity can be explained from the migration of electrons in one graphite layer or their jumping across the defects/interfaces

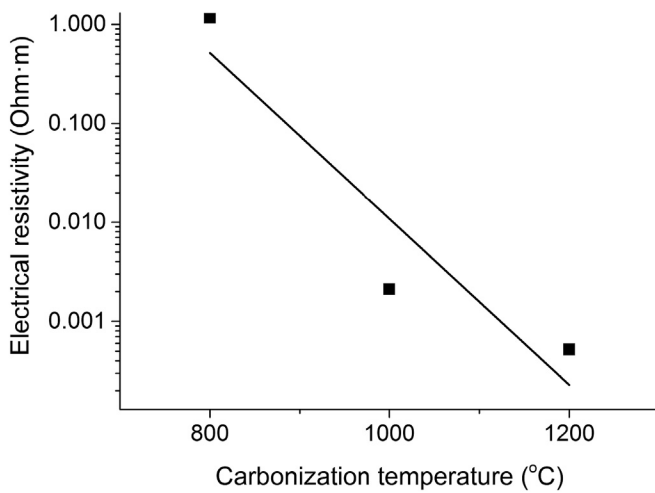


Fig. 9. Effect of carbonization temperature on electrical conductivity of activated carbon web.

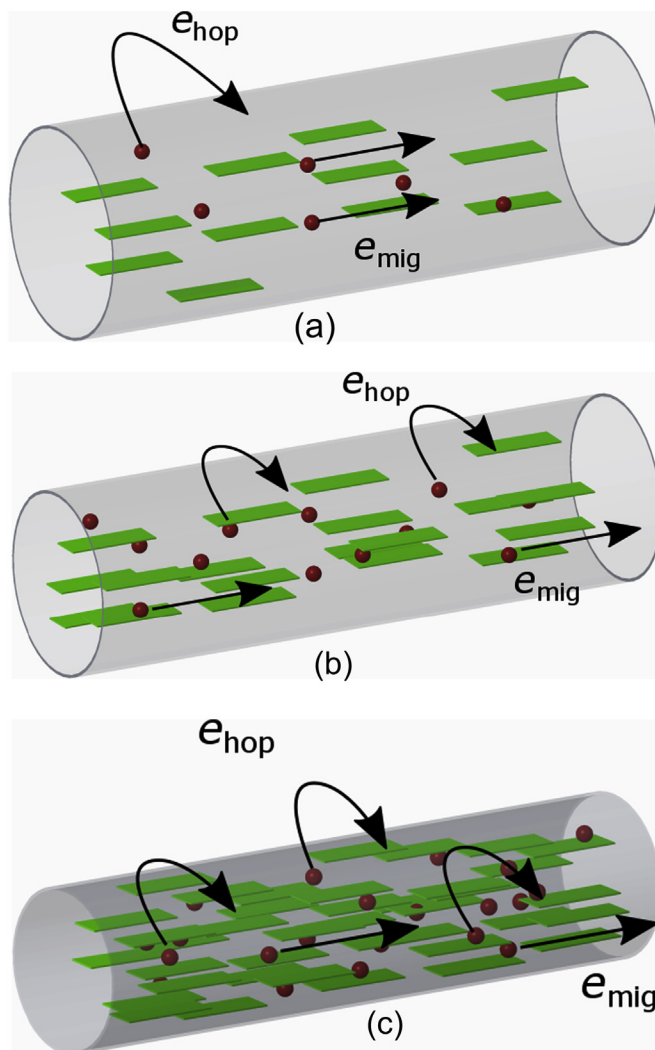


Fig. 10. Mechanism of charge transport in (a) 800 °C activated carbon (b) 1000 °C activated carbon (c) 1200 °C activated carbon. (A colour version of this figure can be viewed online.)

between disordered graphite layers [27–29]. The higher electrical conductivity indicated relatively easier migration and hopping of electrons in case of 1200 °C activated carbon than 800 and 1000 °C activated carbon samples. This behavior can be attributed to their higher graphite content, uniform distribution of graphite layers, reduced fiber diameter, etc shown in Fig. 10, which ultimately resulted into the formation of dense micro-current network in 1200 °C activated carbon structure [30,6].

3.3. Electromagnetic shielding ability

3.3.1. Waveguide method

Fig. 11 (a–b) show the average values in 95% confidence interval for electromagnetic shielding effectiveness of prepared activated carbon web in single and double layers measured at 2.45 GHz frequency. The electromagnetic shielding effectiveness was found to increase with increase in number of layers and increase in carbonization temperature. The electromagnetic shielding effectiveness of 28.29 dB, 26.06 dB and 3.34 dB was exhibited by single layers of activated carbon web produced at 1200 °C, 1000 °C and 800 °C, respectively. At very low carbonization temperature, the shielding effectiveness remained similar to that of non-carbonized

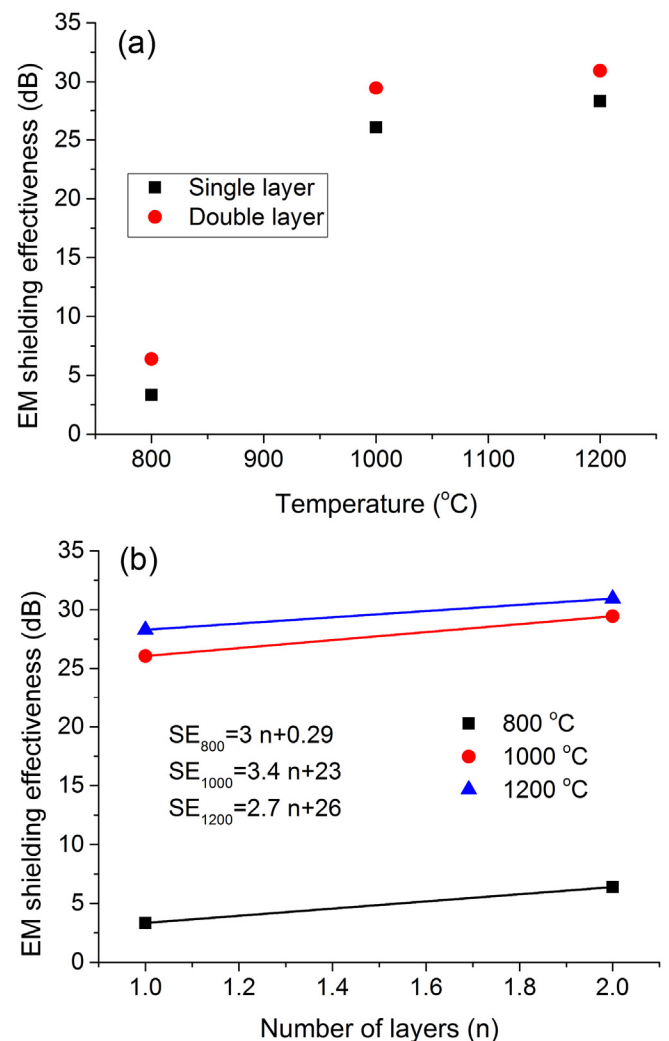


Fig. 11. (a). Effect of carbonization temperature on electromagnetic shielding effectiveness at 2.45 GHz (b). Effect of number of layers on electromagnetic shielding effectiveness at 2.45 GHz. (A colour version of this figure can be viewed online.)

polyacrylonitrile substrate (i.e. zero). Then, the shielding effectiveness was found to increase dramatically over a very narrow range of carbonization temperature, which was connected to the amount of carbon/graphite phase present in the structure. This point is called the percolation threshold, which showed minimum carbonization temperature required for maximum increase in conductivity for higher shielding effectiveness. In present study, the percolation threshold was found between the range of 800 °C and 900 °C carbonization temperature. The maximum shielding effectiveness in this range was attributed to increased multiple internal reflections and stronger absorption of electromagnetic radiations due to higher electrical conductivity, higher porosity and higher surface area [4]. The dramatic increase of shielding ability could not be expected with further increase of carbonization temperature ($T > 1100$ °C). Therefore, the usage of 1000 °C carbonization temperature was considered optimal with regard to its relatively high electromagnetic shielding ability and satisfactory mechanical properties. The similar trend was found for double layers of activated carbon, where shielding effectiveness was increased by 13% in case of 1000 °C activated carbon web. This behavior was attributed to increase in thickness with increase in number of layers.

3.3.2. Coaxial transmission line method

Fig. 12 (a–b) show the mean values of electromagnetic shielding effectiveness for single layers of activated carbon samples in frequencies of 600 MHz, 1 GHz and 1.5 GHz. The increase in shielding effectiveness with increase in carbonization temperature was observed. The single layer of 800 °C activated carbon web revealed the lowest electromagnetic shielding effectiveness of about 5 dB in frequency range of 600 MHz–1.5 GHz. On the other hand, the 1200 °C activated carbon web exhibited the shielding ability of 63.26 dB, 66.75 dB and 75.44 dB for respective frequencies of 600 MHz, 1 GHz and 1.5 GHz.

3.3.3. Mechanism of EMI shielding

The phenomena of reflection, absorption and multiple internal reflections of electromagnetic radiations contribute to the EMI shielding efficiency. The reflection is related to the impedance mismatch between air and absorber. The presence of surface nomadic charges or mobile charge carriers (electrons or holes) is considered as the most important factor for the reflection mechanism [27,6]. Absorption is the second important mechanism and it depends on the thickness of the shield. Absorption arises from Ohmic loss and polarization loss [30]. Ohmic loss comes from the dissipation of energy by nomadic charges through conduction, hopping and tunneling mechanisms, whereas polarization loss originates from the energy required for overcoming the momentum to reorient the dipoles in each half cycle of the EM wave. The polarization is derived from functional groups, defects and interfaces within the material. The third mechanism is multiple internal reflections which represent scattering effect within the shielding material due to its inhomogeneity and huge interfacial area [4].

The 1200 °C activated carbon web exhibited higher EMI shielding properties due to increased multiple internal reflection and stronger absorption of EM waves. This behavior was attributed to the development of heterogeneous surface with increased electrical conductivity and porosity at higher carbonization temperature. This can be explained further from Figs. 4, 7, 10 (c), where 1200 °C activated carbon web showed increased graphite content, uniform dispersion of graphite layers, reduced fiber diameter, etc. The greater number of nomadic charges (from increased graphite content in Fig. 4) coupled with their uniform state of dispersion led to elongated electrons' mean free paths and enhanced conductive network which consequently dissipated more electrical energy and

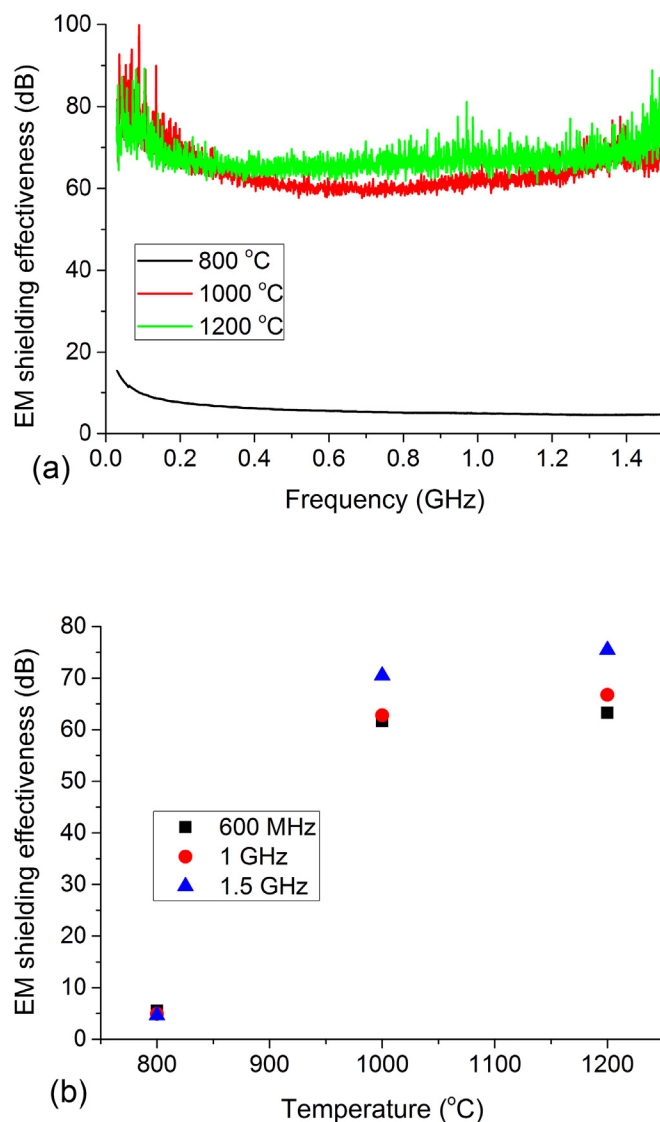


Fig. 12. (a). Effect of frequency on electromagnetic shielding effectiveness. (b). Effect of carbonization temperature on electromagnetic shielding effectiveness in low frequency region. (A colour version of this figure can be viewed online.)

thus higher Ohmic loss [5]. The reduced fiber diameter in Fig. 7 provided larger conductive surface area for dissipation of incident EM wave. Moreover, non-homogeneous surface characteristics of 1200 °C activated carbon web in Fig. 5 (d) could indicate enhanced EMI shielding further from higher polarization loss [31].

4. Conclusions

The present study was focused on development of porous and electrically conductive activated carbon based electromagnetic shielding materials from acrylic fibrous wastes. The simple and novel approach was employed to introduce absorption and reflection properties of electromagnetic radiations into the shielding materials. This was achieved by physical activation of needle punched nonwoven web of acrylic fibers. The carbonization was performed under the layer of charcoal at 800 °C, 1000 °C and 1200 °C with the heating rate of 300 °C h⁻¹ and without any holding time. Further, the influence of carbonization temperature on physical and morphological properties of activated carbon web

was studied from EDX, X-ray diffraction, SEM, X-ray tomography and BET analysis. In the end, the utility of prepared activated carbon web was investigated for electromagnetic shielding ability in high frequency (i.e. 2.45 GHz) and low frequency regions (i.e. below 1.5 GHz) using waveguide method and coaxial transmission line method, respectively. At 2.45 GHz, the electromagnetic shielding effectiveness of 28.29 dB, 26.06 dB and 3.34 dB was exhibited by single layers of activated carbon web produced at 1200 °C, 1000 °C and 800 °C, respectively. On the other hand, for low frequency regions, the 1200 °C activated carbon web exhibited the shielding ability of 63.26 dB, 66.75 dB and 75.44 dB for respective frequencies of 600 MHz, 1 GHz and 1.5 GHz. This behavior was attributed to increased multiple internal reflections and stronger absorption of electromagnetic radiations, which resulted from greater number of nodamic charges (i.e. graphite content), uniform dispersion of graphite layers, reduced fiber diameter, elongated electrons' mean free paths, larger surface area, higher porosity and enhanced conductive network formation in 1200 °C activated carbon.

Acknowledgement

This study was supported under the student grant scheme (SGS-21044) by Technical University of Liberec, Czech Republic.

References

- [1] V. Šafářová, M. Tunák, J. Militký, Prediction of hybrid woven fabric electromagnetic shielding effectiveness, *Text. Res. J.* 85 (2015) 673–686, <http://dx.doi.org/10.1177/0040517514555802>.
- [2] V. Šafářová, J. Militký, Electromagnetic shielding properties of woven fabrics made from high-performance fibers, *Text. Res. J.* 84 (2014) 1255–1267, <http://dx.doi.org/10.1177/0040517514521118>.
- [3] D.D.L. Chung, Electromagnetic interference shielding effectiveness of carbon materials, *Carbon N Y* 39 (2001) 279–285, [http://dx.doi.org/10.1016/S0008-6223\(00\)00184-6](http://dx.doi.org/10.1016/S0008-6223(00)00184-6).
- [4] E. Sano, E. Akiba, Electromagnetic absorbing materials using nonwoven fabrics coated with multi-walled carbon nanotubes, *Carbon N Y* 78 (2014) 463–468, <http://dx.doi.org/10.1016/j.carbon.2014.07.027>.
- [5] M.-S. Cao, X.-X. Wang, W.-Q. Cao, J. Yuan, Ultrathin graphene: electrical properties and highly efficient electromagnetic interference shielding, *J. Mater. Chem. C Mater. Opt. Electron. Devices* 3 (2015), <http://dx.doi.org/10.1039/C5TC01354B>. Ahead of Print.
- [6] M. Arjmand, U. Sundararaj, Electromagnetic interference shielding of Nitrogen-doped and Undoped carbon nanotube/polyvinylidene fluoride nanocomposites: a comparative study, *Compos. Sci. Technol.* 118 (2015) 257–263, <http://dx.doi.org/10.1016/j.compscitech.2015.09.012>.
- [7] V. Rubežiene, J. Baltušnikaitė, S. Varnaite-Žuravliova, A. Sankauskaite, A. Abraitienė, J. Matuzas, Development and investigation of electromagnetic shielding fabrics with different electrically conductive additives, *J. Electrostat.* 75 (2015) 90–98, <http://dx.doi.org/10.1016/j.elstat.2015.03.009>.
- [8] L.L. Wang, B.K. Tay, K.Y. See, Z. Sun, L.K. Tan, D. Lua, Electromagnetic interference shielding effectiveness of carbon-based materials prepared by screen printing, *Carbon N Y* 47 (2009) 1905–1910, <http://dx.doi.org/10.1016/j.carbon.2009.03.033>.
- [9] M. Inagaki, J. Qiu, Q. Guo, Carbon foam: preparation and application, *Carbon N Y* 87 (2015) 128–152, <http://dx.doi.org/10.1016/j.carbon.2015.02.021>.
- [10] J.H. Kim, E. Jeong, Y.S. Lee, Preparation and characterization of graphite foams, *J. Ind. Eng. Chem.* 32 (2015) 21–33, <http://dx.doi.org/10.1016/j.jiec.2015.09.003>.
- [11] Y. Li, B. Shen, X. Pei, Y. Zhang, D. Yi, W. Zhai, et al., Ultrathin carbon foams for effective electromagnetic interference shielding, *Carbon N Y* 100 (2016) 375–385, <http://dx.doi.org/10.1016/j.carbon.2016.01.030>.
- [12] S. Farhan, R. Wang, K. Li, Electromagnetic interference shielding effectiveness of carbon foam containing in situ grown silicon carbide nanowires, *Ceram. Int.* 42 (2016) 11330–11340, <http://dx.doi.org/10.1016/j.ceramint.2016.04.054>.
- [13] A. Fletcher, M.C. Gupta, K.L. Dudley, E. Vedeler, Elastomer foam nanocomposites for electromagnetic dissipation and shielding applications, *Compos. Sci. Technol.* 70 (2010) 953–958, <http://dx.doi.org/10.1016/j.compscitech.2010.02.011>.
- [14] B. Shen, Y. Li, D. Yi, W. Zhai, X. Wei, W. Zheng, Microcellular graphene foam for improved broadband electromagnetic interference shielding, *Carbon N Y* 102 (2016) 154–160, <http://dx.doi.org/10.1016/j.carbon.2016.02.040>.
- [15] X. Sun, X. Liu, X. Shen, Y. Wu, Z. Wang, J.K. Kim, Graphene foam/carbon nanotube/poly(dimethyl siloxane) composites for exceptional microwave shielding, *Compos. Part A Appl. Sci. Manuf.* 85 (2015) 199–206, <http://dx.doi.org/10.1016/j.compositesa.2016.03.009>.
- [16] H. Wang, K. Zheng, X. Zhang, X. Ding, Z. Zhang, C. Bao, et al., 3D network porous polymeric composites with outstanding electromagnetic interference shielding, *Compos. Sci. Technol.* 125 (2016) 22–29, <http://dx.doi.org/10.1016/j.compscitech.2016.01.007>.
- [17] D.-X. Yan, P.-G. Ren, H. Pang, Q. Fu, M.-B. Yang, Z.-M. Li, Efficient electromagnetic interference shielding of lightweight graphene/polystyrene composite, *J. Mater. Chem.* 22 (2012) 18772, <http://dx.doi.org/10.1039/c2jm32692b>.
- [18] Z. Chen, W. Ren, L. Gao, B. Liu, S. Pei, H.-M. Cheng, Three-dimensional flexible and conductive interconnected graphene networks grown by chemical vapour deposition, *Nat. Mater.* 10 (2011) 424–428, <http://dx.doi.org/10.1038/nmat3001>.
- [19] W.-L. Song, X.-T. Guan, L.-Z. Fan, W.-Q. Cao, C.-Y. Wang, M.-S. Cao, Tuning three-dimensional textures with graphene aerogels for ultra-light flexible graphene/texture composites of effective electromagnetic shielding, *Carbon N Y* 93 (2015) 151–160, <http://dx.doi.org/10.1016/j.carbon.2015.05.033>.
- [20] V. Baheti, S. Naeem, J. Militký, M. Okrasa, B. Tomkova, Optimized preparation of activated carbon nanoparticles from acrylic fibrous wastes, *Fibers Polym.* 16 (2015) 2193–2201, <http://dx.doi.org/10.1007/s12221-015-5364-0>.
- [21] V. Safarova, M. Tunak, M. Truhlar, J. Militky, A new method and apparatus for evaluating the electromagnetic shielding effectiveness of textiles, *Text. Res. J.* 86 (2016) 44–56, <http://dx.doi.org/10.1177/0040517515581587>.
- [22] Y. Liu, Y.H. Choi, H.G. Chae, P. Gulgunje, S. Kumar, Temperature dependent tensile behavior of gel-spun polyacrylonitrile and polyacrylonitrile/carbon nanotube composite fibers, *Polym. Guildf.* 54 (2013) 4003–4009, <http://dx.doi.org/10.1016/j.polymer.2013.05.051>.
- [23] Y. MA, X. YIN, Q. LI, Effects of heat treatment temperature on microstructure and electromagnetic properties of ordered mesoporous carbon, *Trans. Nonferrous Met. Soc. China* 23 (2013) 1652–1660, [http://dx.doi.org/10.1016/S1003-6326\(13\)62644-8](http://dx.doi.org/10.1016/S1003-6326(13)62644-8).
- [24] H. Ghorbani, H. Tavanai, M. Morshed, Fabrication of activated carbon nanoparticles from PAN precursor, *J. Anal. Appl. Pyrolysis* 110 (2014) 12–17, <http://dx.doi.org/10.1016/j.jaap.2014.07.008>.
- [25] Q. Jiang, Y. Zhao, Effects of activation conditions on BET specific surface area of activated carbon nanotubes, *Microporous Mesoporous Mater.* 76 (2004) 215–219, <http://dx.doi.org/10.1016/j.micromeso.2004.08.020>.
- [26] B.D. Zdravkov, J.J. Čermák, M. Šefara, J. Janků, Pore classification in the characterization of porous materials: a perspective, *Cent. Eur. J. Chem.* 5 (2007), <http://dx.doi.org/10.2478/s11532-007-0039-3>, 1158–1158.
- [27] M.S. Cao, W.L. Song, Z.L. Hou, B. Wen, J. Yuan, The effects of temperature and frequency on the dielectric properties, electromagnetic interference shielding and microwave-absorption of short carbon fiber/silica composites, *Carbon N Y* 48 (2010) 788–796, <http://dx.doi.org/10.1016/j.carbon.2009.10.028>.
- [28] W.L. Song, M.S. Cao, Z.L. Hou, X.Y. Fang, X.L. Shi, J. Yuan, High dielectric loss and its monotonic dependence of conducting-dominated multiwalled carbon nanotubes/silica nanocomposite on temperature ranging from 373 to 873 K in X-band, *Appl. Phys. Lett.* 94 (2009) 1–4, <http://dx.doi.org/10.1063/1.3152764>.
- [29] B. Wen, M.S. Cao, Z.L. Hou, W.L. Song, L. Zhang, M.M. Lu, et al., Temperature dependent microwave attenuation behavior for carbon-nanotube/silica composites, *Carbon N Y* 65 (2013) 124–139, <http://dx.doi.org/10.1016/j.carbon.2013.07.110>.
- [30] M. Arjmand, K. Chizari, B. Krause, P. Pötschke, U. Sundararaj, Effect of synthesis catalyst on structure of nitrogen-doped carbon nanotubes and electrical conductivity and electromagnetic interference shielding of their polymeric nanocomposites, *Carbon N Y* 98 (2016) 358–372, <http://dx.doi.org/10.1016/j.carbon.2015.11.024>.
- [31] K.L. Kaiser, *Electromagnetic Shielding*, CRC Press, Boca Raton, 2006, pp. 1–52.



Article

Joule Heating of Carbon-Based Materials Obtained by Carbonization of *Para*-Aramid Fabrics

Daniel Karthik * , Jiri Militky , Yuanfeng Wang and Mohanapriya Venkataraman

Department of Material Engineering, Technical University of Liberec, Studentska 1402/2,
46117 Liberec, Czech Republic

* Correspondence: daniel.karthik@tul.cz

Abstract: The Joule heating behavior of carbon-based materials obtained by the process of carbonization of industrial para-aramid fabric wastes are investigated in the present work. Carbonization involves a process of thermally decomposing organic material, thereby altering its physical and chemical properties to obtain carbon-rich materials that are electrically conductive and display Joule heating behavior. The principle of Joule heating is based on the intrinsic electrical resistance of the material across an applied voltage. Here, para-aramid woven fabric wastes are converted into activated carbon materials through straightforward, controlled, single-step thermal treatments by three different kinds of atmosphere, i.e., in the CO₂ evolved from charcoal, a mixture of gases from ammonium bicarbonate salt (NH₄HCO₃), and Nitrogen gas (N₂), respectively, inside a high-temperature furnace. The carbonization temperatures were varied from 800 to 1100 °C. The carbonization process variables were optimized to obtain carbon-rich materials with lower electrical resistivity. The results of electrical resistivity measurements show that for all three methods, the electrical resistivity decreases with increasing carbonization temperatures. An experimental setup consisting of an infrared (IR) camera, positioned over the surface of the fabric specimen to record the surface temperature of the material connected to a DC power supply, was employed. The kinetics of Joule heating and subsequent cooling were also analyzed at a fixed voltage of 5 V by recording the changes in surface temperature with respect to time. The heating–cooling cycle is described by a simple kinetic model of first order.

Keywords: Joule heating; carbonization; activated carbon; electrical resistivity; para-aramid wastes



Citation: Karthik, D.; Militky, J.; Wang, Y.; Venkataraman, M. Joule Heating of Carbon-Based Materials Obtained by Carbonization of *Para*-Aramid Fabrics. *C* **2023**, *9*, 23. <https://doi.org/10.3390/c9010023>

Academic Editor: Gil Gonçalves

Received: 12 January 2023

Revised: 10 February 2023

Accepted: 13 February 2023

Published: 15 February 2023



Copyright: © 2023 by the authors. Licensee MDPI, Basel, Switzerland. This article is an open access article distributed under the terms and conditions of the Creative Commons Attribution (CC BY) license (<https://creativecommons.org/licenses/by/4.0/>).

1. Introduction

In recent years, the growing demand for more multi-functional, techno-economic and sustainable materials for various applications has attracted enormous research interest. Electrothermal and Ohmic heating performance of textiles in particular have compelled much attention in various heating applications. Carbonaceous materials in various forms (fibers, fabrics, or particles) have drawn considerable attention as effective heating elements due to their intrinsic thermal and electrical properties [1,2]. These materials have versatile applications in areas such as smart sensors, grounding materials to dissipate static charge, structural health monitoring, de-icing in aerospace and wind-turbine structures, and electromagnetic interference (EMI) shielding materials, among others [3–6].

Joule heating (also referred to as Ohmic heating or resistive heating), based on the law of conservation of energy, is a phenomenon that occurs when a voltage difference is applied across a conductive material such that electrical energy is consumed in overcoming the resistance in the material between the electrons and the atoms, causing this energy to be generated in the form of heat. This heating is referred to as Joule's effect. The amount of heat produced by the material is proportional to the square of the current, the resistance of the circuit, and the duration for which the current flows through the circuit [7], shown mathematically as follows:

$$Q = I^2 R t \quad (1)$$

where Q is the heat produced by the material in joules; I is the electrical current flowing through the conductor, in amperes; R is the electrical resistance, in ohms; t is the elapsed time, in seconds. Joule heating has been extensively used in various applications where thermal energy produced by the resistance in the conductor is put to use in the form of conduction, convection, or radiation.

It is quite rhetorical to query how the processes of pyrolysis and carbonization of various polymeric materials have been constantly carried out over time, in order to obtain carbon-rich products conducive to various areas of application. Thermal decomposition through these two phases involves aromatic evolution and polymerization of the organic material, through bond cleavage reactions and the rearrangement of compounds in an inert atmosphere over a wide temperature range [8–12]. Non-carbon volatiles in the form of nitrogen, hydrogen, methane, carbon dioxide, carbon monoxide, ammonia, water, etc., are eliminated during the process of carbonization, which contributes to almost 50 percent or more by weight of the precursor material. The maximum temperature of carbonization depends on the required type of carbon and its specific application. Fundamental modifications can be observed in the chemical composition as well as the physical properties [13–17].

The type of the precursor and the selected process parameters greatly influence the final product of carbonization. Having said that, para-aramids (1, 4 p-phenylene terephthalamide), more commonly recognized as Kevlar, have shown to be suitable precursors to obtain carbon fibers by various methods of carbonization and activation (physical and chemical) [10,18,19]. The carbonaceous materials obtained displayed significant electrical and thermal properties. In the present experiment, we utilized feedstock material, gathered from a local industry, as Kevlar fabric wastes and carbonized them to obtain carbon fabric produce.

In the present study, a comparative analysis of the Ohmic heating behavior and electrical properties of carbon fabrics obtained by the carbonization of para-aramid fabrics by three different procedures was conducted. Here, we utilize charcoal and ammonium bicarbonate salt (in separate methods), which are inexpensive and commonly available, in comparison to N_2 gas, in order to potentially create an oxygen-free atmosphere inside the furnace to support activation during the carbonization process. The electrical resistivity and Joule heating behavior of the activated carbon are analyzed. A kinetics model is further used to analyze the heating and cooling cycles of the Joule-heated materials with respect to voltage and time. The para-aramid fabrics used for this study were industrial feedstock material, hence contributing towards sustainability and the potential utilization of textile wastes.

2. Experimental

2.1. Materials

Kevlar 29 para-aramid woven fabric was obtained from Veba Textile Mills Ltd. (Broumov), Czech Republic, in the form of discarded short fabric wastes with a yarn count of 1710 dtex, density of 1.43 g/cm^3 , and 5.2 wt % moisture content (parameters specified by the manufacturing company).

2.2. Methodology

Carbonization of Kevlar was carried out using three different methods based on the atmosphere created in the furnace during the process of pyrolysis, as described below.

Method 1: Charcoal Method

The carbonization of Kevlar fibrous wastes was carried out under the layer of charcoal, creating a CO_2 atmosphere, in a high-temperature furnace. The Kevlar fabric was directly carbonized without any intermediate stabilization step. The final temperatures of $800 \text{ }^\circ\text{C}$, $900 \text{ }^\circ\text{C}$, $1000 \text{ }^\circ\text{C}$, and $1100 \text{ }^\circ\text{C}$, with heating rate of $300 \text{ }^\circ\text{C/h}$ and without any holding time, were adopted during the process of carbonization. This method is described more precisely in our previous work [20].

Method 2: Ammonium bicarbonate salt Method

Carbonization of Kevlar was carried out in a smelting furnace in a combined gas atmosphere generated by using ammonium bicarbonate salt. Ammonium bicarbonate is an inorganic compound with formula NH_4HCO_3 , and it decomposes when heated above 36°C , releasing ammonia, water, and carbon dioxide gases as follows: $\text{NH}_4\text{HCO}_3 \rightarrow \text{NH}_3 + \text{H}_2\text{O} + \text{CO}_2$, so the atmosphere created inside the furnace is mainly a mixture of gasses: CO_2 and NH_3 , replacing air.

The Kevlar fabric samples in rolled form, were placed inside a cylindrical crucible, positioned in the center of the furnace. A total of 10 g of ammonium bicarbonate salt was added into the crucible containing the Kevlar sample, in order to create a mixed gas atmosphere. The Kevlar fabric samples were carbonized to four final temperatures from 800 to 1100°C , with an interval of 100°C .

Method 3: N_2 Method

Carbonization of Kevlar was carried out in a high-temperature furnace, in the presence of an inert N_2 flow atmosphere; a heating rate of $10^\circ\text{C}/\text{min}$ and holding time of 20 min at the final temperature was adopted. The Kevlar fabric samples were carbonized to four final temperatures from 800 to 1100°C , with an interval of 100°C .

The carbon samples obtained from the three methods mentioned above are listed in Table 1, with details of their yields in percentages. For all three methods, the final product at every selected final carbonization temperature, although weak, retained its fabric form and possessed structural integrity, making it suitable to handle for further investigations.

Table 1. Details of carbonized samples.

Sample Code	Atmosphere Type	Carbonization Method	Final Carbonization Temperature ($^\circ\text{C}$)	Fabric Yield (%)	Carbon Yield (%)
C8	CO_2	1	800	58.24 ± 1.3	69.1 ± 0.9
C9	CO_2	1	900	47.26 ± 1.6	76.4 ± 1.2
C10	CO_2	1	1000	35.69 ± 2.1	83.4 ± 0.8
C11	CO_2	1	1100	31.44 ± 1.8	89.1 ± 0.4
A8	Gas mixture	2	800	30.21 ± 1.1	83.7 ± 0.6
A9	Gas mixture	2	900	26.31 ± 1.7	87.1 ± 0.6
A10	Gas mixture	2	1000	23.49 ± 2.5	88.5 ± 0.8
A11	Gas mixture	2	1100	19.89 ± 2.8	90.2 ± 0.8
N8	Nitrogen	3	800	46.23 ± 1.1	67.2 ± 0.9
N9	Nitrogen	3	900	41.79 ± 1.2	73.4 ± 0.8
N10	Nitrogen	3	1000	34.47 ± 1.9	84.1 ± 0.6
N11	Nitrogen	3	1100	30.60 ± 1.5	88.2 ± 0.8

Energy dispersive X-ray (EDX) analysis was carried out using an LZ 5 EDX detector, Oxford Instruments, High Wycombe, UK, in order to calculate the relative percentages of different elements in the activated material after the carbonization process at different temperatures. The elemental analysis of the starting material, Kevlar, in terms of weight percentages on dry basis, was 63.85% C, 15.09% N, 0.8% S, and 18.84% O [20]. Thermal degradation advances with increasing temperatures by the removal of volatile compounds. The increase in carbon content (as a percentage) is of primary importance when enhancing the electrical conductivity and Joule heating of the final product (shown in Table 1). The remaining composition of the carbon fabrics obtained after carbonization is made up of trivial amounts of impurities such as Na, K, Cl, and Ca.

2.3. Ohmic Heating Measurement

The Joule heating behavior of the carbon fabric samples were characterized using a test setup as illustrated in Figure 1. The test sample was clamped in position along its width by a pair of 6 cm long electrodes at both ends, which were 8 cm apart. These electrodes were connected to a DC power supply (TIPA PS3010), TIPA, spol. s.r.o, Opava, Czech Republic. An IR camera (FLIR-E6390), Teledyne FLIR LLC, Oregon, USA. was placed above the test sample at a height of 40 mm, in order to monitor the surface temperature and heat distribution on the sample surface. The current 1 A was kept constant, and the voltage was gradually increased from 0 V to 10 V, at intervals of 1 V, with a holding time of 10 s, and the average temperature over the middle section of the material between the two sets of electrodes was considered.

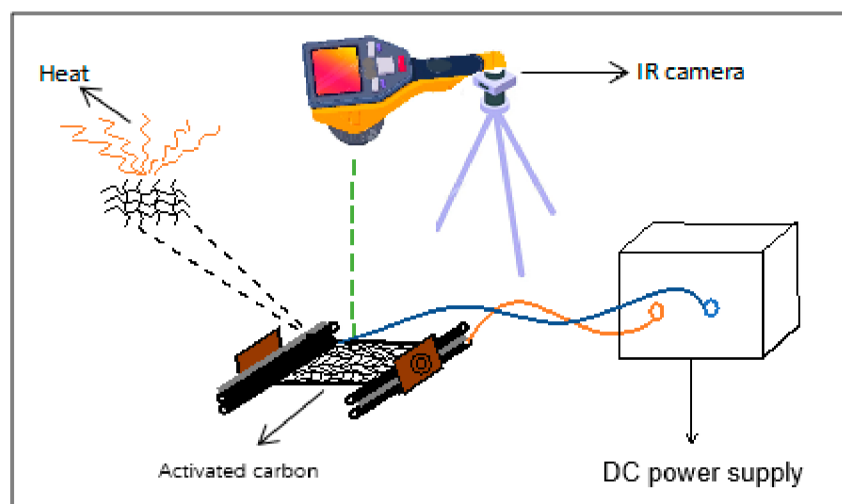


Figure 1. Joule heating measurement setup.

Furthermore, to investigate the Joule heating performance of the carbon fabrics obtained by different methods of carbonization, a constant voltage of 5 V was applied to evaluate the heating/cooling kinetics based on the time-temperature characteristics of the materials.

2.4. Electrical Resistivity

Correspondingly, the test sample was clamped the same way as mentioned in the previous section to measure the Joule heating and was connected to a digital multimeter, which displayed the electrical resistance (in ohms) of the material. A current flow of 1 A was set by regulating the voltage and the resistance value was recorded after 10 s. Furthermore, the electrical resistivity (in ohm.cm) was calculated mathematically as follows [7]:

$$\rho = \frac{A \times R}{L} \quad (2)$$

where ρ is the electrical resistivity (in ohm.cm); A is the cross-sectional area (along the width of the fabric sample in our case); R is the resistance measured (by the multimeter); and L is the length of the fabric sample.

3. Results and Discussions

3.1. Electrical Resistivity

Figure 2 shows the electrical resistivity of the fabrics carbonized to four final temperatures ranging from 800–1100 °C, using methods 1, 2, and 3. The electrical resistivity of all samples was measured five times per sample. It is evident that for all three methods, the electrical resistivity decreased progressively with increasing carbonization temperatures.

This is attributed to the higher carbon yield due to carbonization at higher temperatures, due to the removal of organic compounds in the form of volatiles [21,22]. These carbon-rich fabrics acquire a dense micro current network and create a better passage for current flow. Migration and hopping of electrons through the fibrous network, being a potential means of electron transport, is thought to be responsible for the higher electrical conductivity or lower resistivity [20,23]. For all three methods, there was no significant difference in the resistivity between fabrics carbonized at 800 °C to 1000 °C. The electrical resistivity of fabrics processed by methods 1 and 2 were nearly the same at 1000 °C and 1100 °C carbonization temperatures. Overall, in all three methods the carbonized fabrics displayed lower resistivity, or rather greater conductivity at higher carbonization temperatures, which indicates higher current flow through these materials, thus contributing to increased Joule heating.

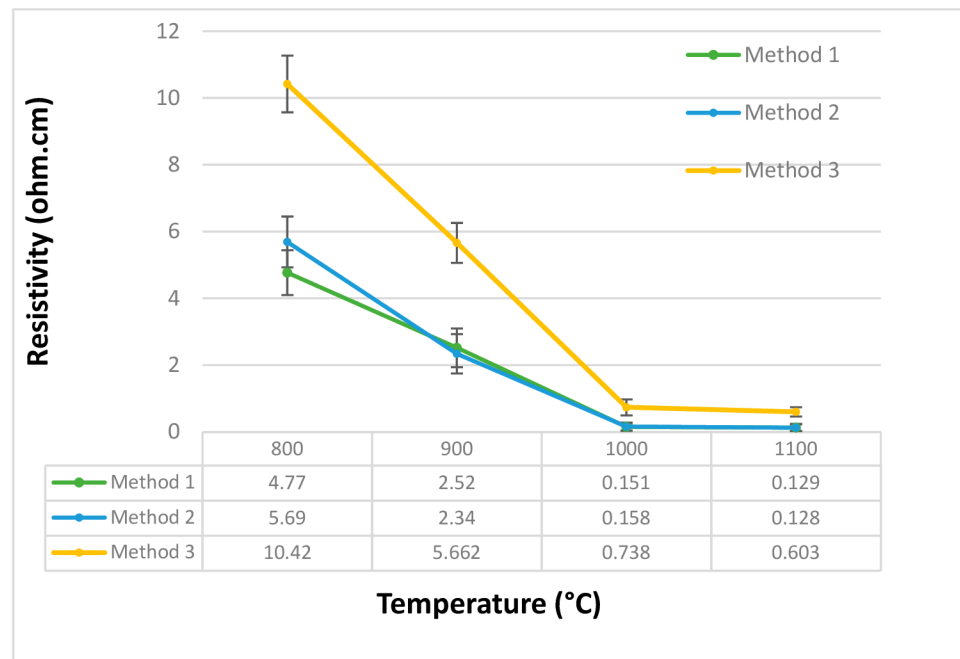
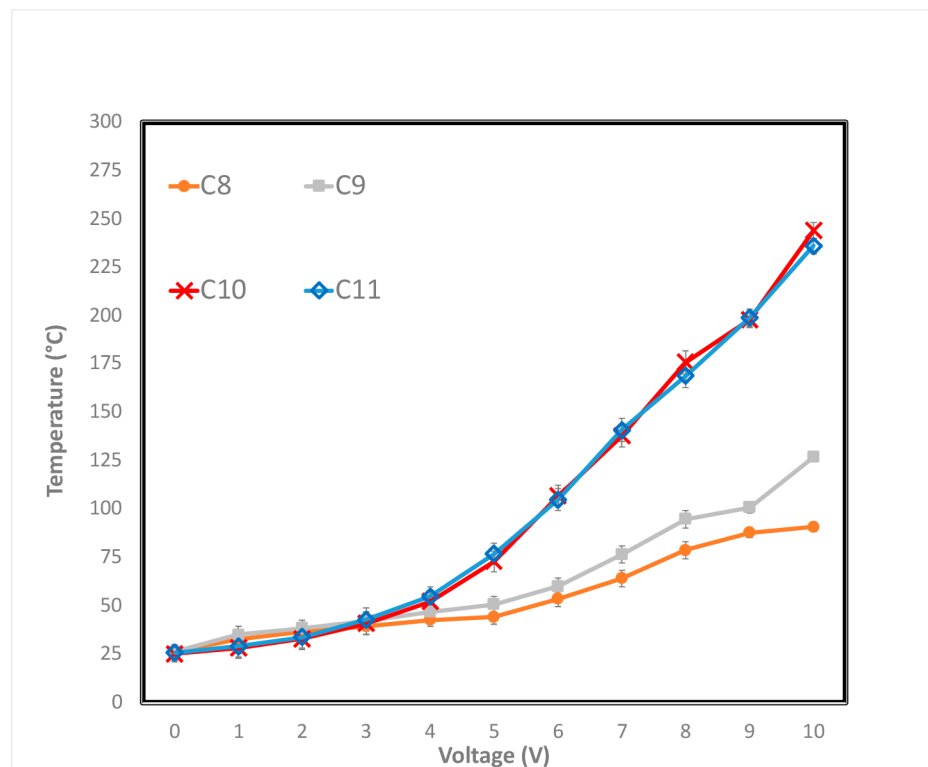


Figure 2. Electrical resistivity of activated carbon fabrics from methods 1, 2, and 3.

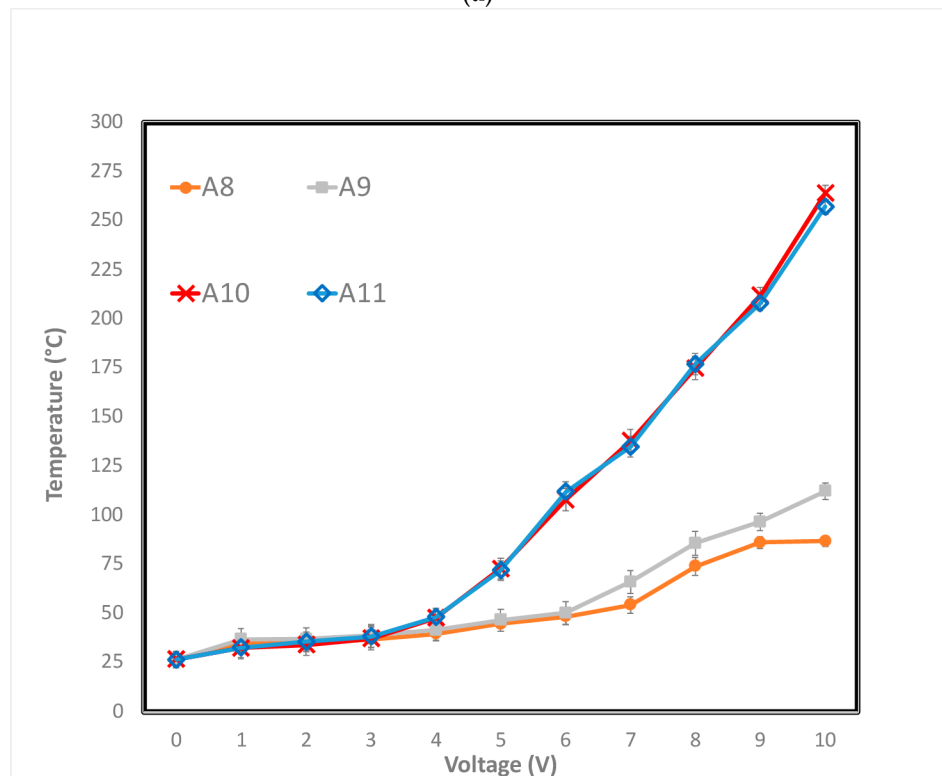
3.2. Joule Heating Characteristics

Temperature–Voltage (T–V) relation

The surface temperature of activated carbon fabrics was investigated at applied voltages ranging from 0 to 10 V, at intervals of 1 V for constant current $I = 1$ A; the surface temperature was recorded 10 s after setting the specific voltage. Figure 3a–c show the T–V curves of the fabrics carbonized by methods 1, 2, and 3, respectively. For each sample, the average value of five test measurements was considered. For fabrics obtained by all three methods, observations made from the T–V curves demonstrate that, initially, the surface temperatures stayed nearly the same, without a significant rise in temperature when a low voltage ($V < 3$ V) was supplied. Subsequently, with increasing voltage, the surface temperature of the fabrics gradually increased. Similarly, for all three methods, the fabrics carbonized at 1000 °C and 1100 °C showed a considerably steep increase in surface temperature with increasing voltage. The surface temperatures for fabrics carbonized at 1000 °C and 1100 °C were nearly alike over the entire range of applied voltage (0–10 V). At the maximum applied voltage (10 V), methods 1, 2, and 3 showed surface temperatures of 244 °C, 264 °C, and 210 °C, for fabrics carbonized at 1000 °C.



(a)



(b)

Figure 3. Cont.

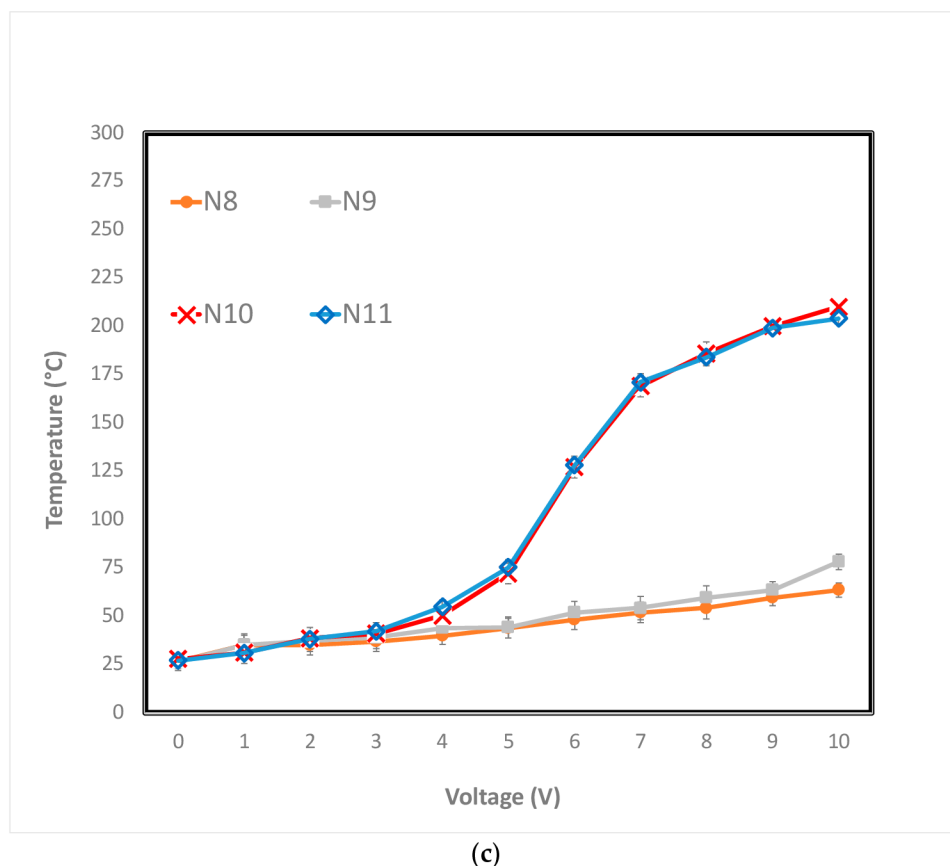


Figure 3. Temperature–voltage relation of activated carbon fabrics from (a) method 1; (b) method 2; and (c) method 3.

Heating/Cooling Kinetics: Temperature–Time (T–t) relation

The purpose of this segment was to analyze the kinetics of continuous heating and cooling of the carbon fabrics, obtained by time-dependent temperature (T–t) relation curves (shown in Figure 4). For each sample, the average value of five test measurements was considered. It is evident that for all the samples, the surface temperature increased steeply once the voltage (set at 5 V) was applied starting at 0 s, and then, after 30 s, the rate of temperature growth gradually increased and reached the maximum temperature at 120 s. Consecutively, after switching off the electrical power supply, the temperature decreased rapidly to room temperature. The stable increase in temperature by Joule heating for fabrics obtained by all three methods greatly depended on the final carbonization temperature. Furthermore, the leveling-off temperature was higher for fabrics carbonized at 1000 °C and 1100 °C, for all three methods at the same applied voltage (5 V). It is clear that under the same applied voltage, the magnitudes of the maximum temperatures were nearly the same for fabrics carbonized at 1000 °C and 1100 °C for all three methods. For this reason, the fabrics carbonized at 1000 °C, using the three methods (C10, A10, and N10), were taken into consideration for comparison (Figure 4d). The maximum temperature of C10 was slightly higher than that of A10 and N10. Furthermore, the initial increase in surface temperature with respect to time was significantly higher for C10 than for A10 and N10. This can be attributed to the more uniform distribution of graphite layers with the fibrous structures for higher current flow. The delay in the increase of surface temperature before reaching a maximum, especially for A10 and N10, is possibly due to the initial heat loss due to convection or radiation, which means it takes longer for current to be distributed uniformly as possible, throughout the surface of the fabric, and thus takes longer to stabilize and reach the maximum temperature.

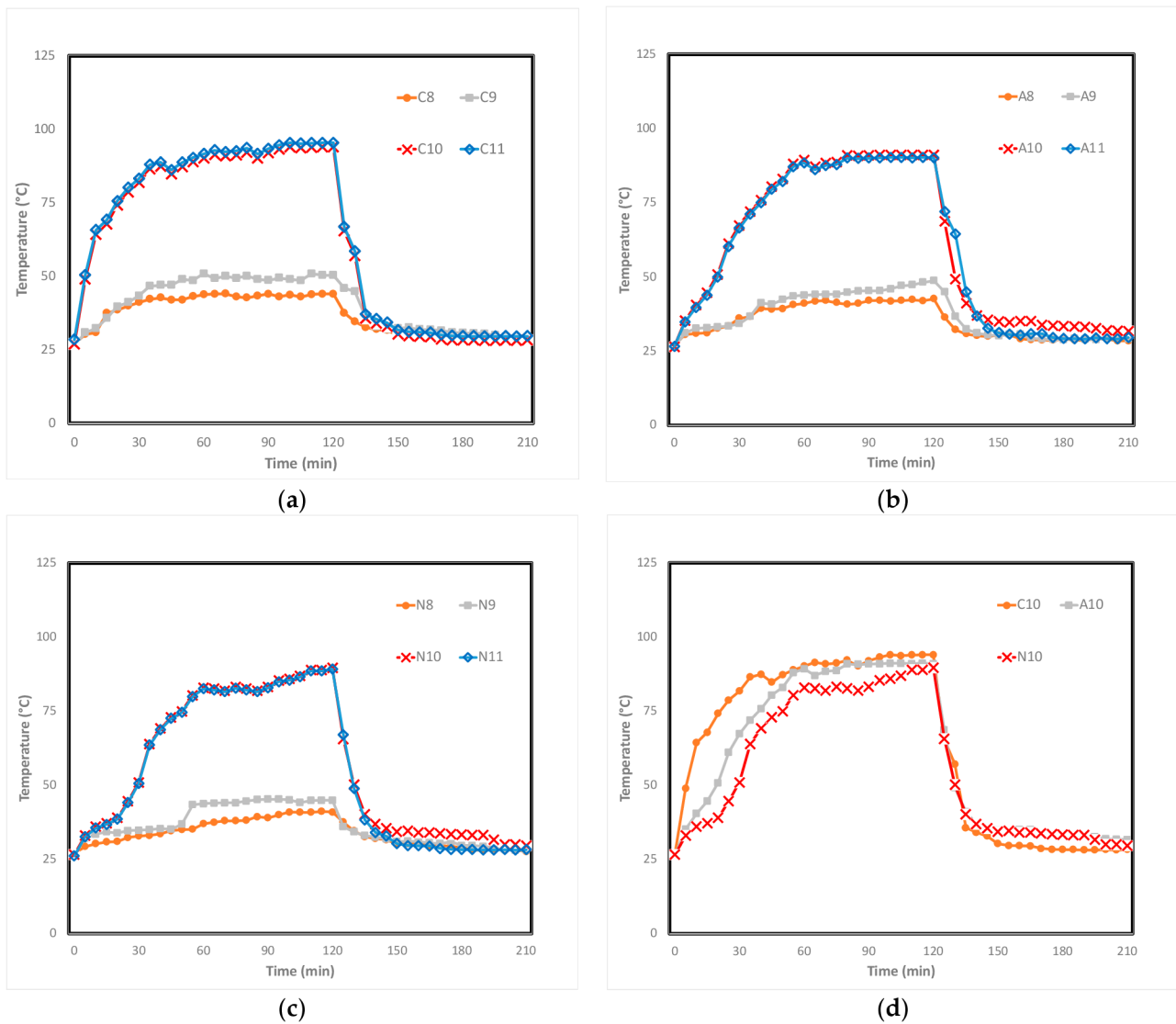


Figure 4. Temperature–time relation of activated carbon fabrics from (a) method 1; (b) method 2; (c) method 3; and (d) comparison of the three methods for fabrics carbonized at 1000 °C.

Here, three heating/cooling kinetic parameters, namely, heating time constant, efficiency of heat transfer, and cooling time constant were obtained to further investigate the Joule heating properties of the carbon fabrics. The T–I curves for fabrics obtained by all three methods shown in Figure 4 can be divided into three sections: (i) temperature growth (heating; 0–60 s), (ii) the region of equilibrium (maximum temperature; 60–120 s), and (iii) temperature decay (cooling; 120–210 s) [24,25].

The heating/cooling kinetics can be simply expressed by a rate equation of the first order, where rate of temperature change dT/dt is proportional to actual temperature T . For the heating phase, the rate equation is of the form [24,25]:

$$\frac{dT}{dt} = -k_h(T_m - T) \tag{3}$$

where T_m is maximum temperature in equilibrium and k_h is the rate constant of heating, which is evidently replaced by the time constant $\tau_g = 1/k_h$. Integration of this differential

equation in the range from ambient temperature T_0 , at time $t = 0$, to temperature T_t , at time t , leads to the following equation [24,25]:

$$\frac{T_t - T_0}{T_m - T_0} = 1 - \exp(-t/\tau_g) \tag{4}$$

The initial heating segment is expressed by Equation (4) and the parameters T_m, τ_g are obtained by nonlinear regression.

For the cooling phase, starting from time t_0 , it can be shown that [24,25]:

$$\frac{T_t - T_0}{T_m - T_0} = \exp(-(t - t_0)/\tau_d) \tag{5}$$

where cooling time constant is $\tau_d = 1/k_c$.

The resulting values for all the activated carbon fabrics are listed in Table 2. The values of τ_g for N10 and N11 are greater than those of A10, A11, C10, and C11 because of their higher resistivity.

Table 2. Characteristic parameters (τ_g, h_{r+c} , and τ_d) for Joule heating performance of all activated carbon fabric samples under applied voltages.

Carbonization Method	Carbonization Temperature	τ_g (S)	h_{r+c} (W/°C)	τ_d (S)
1	800	19.60	0.09	89.83
	900	24.11	0.08	107.52
	1000	19.84	0.07	57.82
	1100	19.63	0.07	60.66
2	800	30.36	0.04	100.77
	900	41.01	0.04	126.59
	1000	25.99	0.10	92.24
	1100	28.92	0.10	89.12
3	800	44.82	0.03	126.82
	900	38.86	0.03	105.76
	1000	42.17	0.09	88.94
	1100	41.68	0.10	70.21

The τ_d values obtained from nonlinear regression of experimental time-dependent temperature decay data, using Model (5), are summarized in Table 2. The τ_g and τ_d values of C10 and C11 were noticeably lower than those of A10, A11, N10, and N11. This means that C10 and C11 exhibited comparatively more rapid temperature responses to applied voltages and were easier to control.

In the maximum temperature zone (region of equilibrium), where the temperature as a function of time becomes constant, the heat gain by electric power is counteracted by the heat emitted to the surroundings through radiation and/or convection, due to conservation of energy. As such, the heat transferred through radiation and convection, h_{r+c} , can be expressed as [24,25]:

$$h_{r+c} = \frac{I_c V_0}{T_m - T_0} \tag{6}$$

where I_c is the steady-state current and V_0 is the applied voltage. It can be seen in Table 2 that the h_{r+c} increases with A10, A11, N10, and N11 as compared to C10 and C11, indicating that comparatively more electrical energy is required to maintain the maximum temperatures for these materials. In the third segment, the material at maximum temperature is left to cool down to the ambient temperature according to Equation (5).

4. Conclusions

In this work, simple and straightforward methods to utilize textile wastes in a sustainable manner with high carbon yield, electrical conductivity and joule heating behavior has been achieved. Carbonization of industrial para-aramid fabric wastes was carried out using three unadorned and straightforward methods to produce activated carbon fabric, which was then investigated for the realization of electrical resistivity and Joule heating. Inexpensive and commonly available compounds such as charcoal and ammonium bicarbonate salt (methods 1 and 2) were utilized to potentially create an oxygen-free atmosphere inside a furnace to assist in activation during the carbonization process, in comparison to N₂ gas, which was used in method 3. All three methods were shown to be effective at producing activated carbon fabrics from para-aramid. The electrical resistivity of the activated carbon fabrics processed by all three methods was shown to decrease significantly with increasing carbonization temperature. Methods 1 and 2 showed lower electrical resistivity in comparison to method 3. Both electrical resistivity and Joule heating characteristics were greatly influenced by the final carbonization temperatures for all three methods. For fabrics obtained by all three methods, it can be seen that in the T-V curves the surface temperature remained low with no significant changes when a low voltage ($V < 3$ V) was supplied. However, the surface temperature of the fabrics increased with higher voltage ($V > 3$ V). At maximum voltage (10 V), C10 and A10 showed the highest surface temperatures of 244 °C and 264 °C due to lower electrical resistivity, or greater conductivity. To further investigate the thermal properties of the carbonized materials, we expressed three heating/cooling kinetic parameters. The increase in temperature by Joule heating for fabrics obtained by all three methods greatly depended on the final carbonization temperature. The leveling-off temperature was higher for fabrics carbonized at 1000 °C and 1100 °C, for all three methods at the same applied voltage (5 V). The maximum temperature of C10 was slightly higher than that of A10 and N10. Moreover, the initial increase in surface temperature with respect to time was significantly higher for C10 than for A10 and N10. Cumulatively, we can say that methods 1 and 2, which utilized charcoal and ammonium bicarbonate salt, were comparatively more desirable in terms of both electrical and Joule heating characteristics, while also being cost-effective and sustainable. We concluded that this material retains structural integrity after carbonization at specified temperatures (800 to 1100°C), excellent electrical conductivity and Joule heating ability, and can thus be proposed as a material for protective panels, enabling EMI shielding and heat generation via external powering towards thermally and/or electrically regulated sensors.

Author Contributions: Conceptualization, D.K. and J.M.; data curation, Y.W.; formal analysis, D.K. and Y.W.; funding acquisition, M.V.; investigation, D.K.; methodology, D.K.; project administration, J.M. and M.V.; resources, Y.W. and M.V.; supervision, J.M.; visualization, D.K.; writing—original draft, D.K.; writing—review and editing, J.M. All authors have read and agreed to the published version of the manuscript.

Funding: This work was supported by the Czech Science Foundation (GACR)-project “Advanced structures for thermal insulation under extreme conditions” (Reg. No. 21-32510M).

Institutional Review Board Statement: Not applicable.

Informed Consent Statement: Not applicable.

Data Availability Statement: Additional details of the experiments and data may be asked via email to the corresponding author.

Conflicts of Interest: The authors declare no conflict of interest.

References

1. Kim, M.; Sung, D.H.; Kong, K.; Kim, N.; Kim, B.-J.; Park, H.W.; Park, Y.-B.; Jung, M.; Lee, S.H.; Kim, S.G. Characterization of resistive heating and thermoelectric behavior of discontinuous carbon fiber-epoxy composites. *Compos. Part B Eng.* **2016**, *90*, 37–44. [CrossRef]
2. Zhang, Q.; Yu, Y.; Yang, K.; Zhang, B.; Zhao, K.; Xiong, G.; Zhang, X. Mechanically robust and electrically conductive graphene-paper/glass-fibers/epoxy composites for stimuli-responsive sensors and Joule heating deicers. *Carbon* **2017**, *124*, 296–307. [CrossRef]
3. Isaji, S.; Bin, Y.; Matsuo, M. Electrical conductivity and self-temperature-control heating properties of carbon nanotubes filled polyethylene films. *Polymer* **2009**, *50*, 1046–1053. [CrossRef]
4. Lopes, H.; Ribeiro, J.E. Structural Health Monitoring in Composite Automotive Elements. In *New Advances in Vehicular Technology and Automotive Engineering*; Carmo, J., Ed.; InTech: London, UK, 2012. [CrossRef]
5. Zanjani, J.S.M.; Okan, B.S.; Pappas, P.-N.; Galiotis, C.; Menceloglu, Y.Z.; Yildiz, M. Tailoring viscoelastic response, self-heating and deicing properties of carbon-fiber reinforced epoxy composites by graphene modification. *Compos. Part A Appl. Sci. Manuf.* **2018**, *106*, 1–10. [CrossRef]
6. Athanasopoulos, N.; Kostopoulos, V. Resistive heating of multidirectional and unidirectional dry carbon fibre preforms. *Compos. Sci. Technol.* **2012**, *72*, 1273–1282. [CrossRef]
7. Redondo, O.; Prolongo, S.; Campo, M.; Sbarufatti, C.; Giglio, M. Anti-icing and de-icing coatings based Joule's heating of graphene nanoplatelets. *Compos. Sci. Technol.* **2018**, *164*, 65–73. [CrossRef]
8. Jiménez, V.; Sánchez, P.; Romero, A. Materials for activated carbon fiber synthesis. In *Activated Carbon Fiber and Textiles*; Woodhead Publishing: Sawston, UK, 2017; pp. 21–38. [CrossRef]
9. Ko, K.S.; Park, C.W.; Yoon, S.-H.; Oh, S.M. Preparation of Kevlar-derived carbon fibers and their anodic performances in Li secondary batteries. *Carbon* **2001**, *39*, 1619–1625. [CrossRef]
10. Mosquera, M.E.; Jamond, M.; Martinez-Alonso, A.; Tascon, J.M. Thermal Transformations of Kevlar Aramid Fibers During Pyrolysis: Infrared and Thermal Analysis Studies. *Chem. Mater.* **2002**, *6*, 1918–1924. Available online: <https://pubs.acs.org/doi/pdf/10.1021/cm00047a006> (accessed on 5 October 2021). [CrossRef]
11. Yang, M.; Zhu, X.L.; Liang, G. Pyrolysis Process of Kevlar Fibers with Thermogravimetric Analysis coupled and Fourier Transform Infrared Spectroscopy. *Guang Pu* **2016**, *36*, 1374–1377. [PubMed]
12. Ramgobin, A.; Fontaine, G.; Bourbigot, S. Thermal Degradation and Fire Behavior of High Performance Polymers. *Polym. Rev.* **2019**, *59*, 55–123. [CrossRef]
13. Chen, J.; Harrison, I. Modification of polyacrylonitrile (PAN) carbon fiber precursor via post-spinning plasticization and stretching in dimethyl formamide (DMF). *Carbon* **2002**, *40*, 25–45. [CrossRef]
14. EFitzer, E.; Frohs, W.; Heine, M. Optimization of stabilization and carbonization treatment of PAN fibres and structural characterization of the resulting carbon fibres. *Carbon* **1986**, *24*, 387–395. [CrossRef]
15. Edie, D.D. The effect of processing on the structure and properties of carbon fibers. *Carbon* **1998**, *36*, 345–362. [CrossRef]
16. Huang, X. Fabrication and Properties of Carbon Fibers. *Materials* **2009**, *2*, 2369–2403. [CrossRef]
17. Chen, J.Y. *Activated Carbon Fiber and Textiles*; Woodhead Publishing: Sawston, UK, 2016; p. 342.
18. Choma, J.; Osuchowski, L.; Marszewski, M.; Dziura, A.; Jaroniec, M. Developing microporosity in Kevlar[®]-derived carbon fibers by CO₂ activation for CO₂ adsorption. *J. CO₂ Util.* **2016**, *16*, 17–22. [CrossRef]
19. Brown, J.R.; Power, A.J. Thermal degradation of aramids: Part I—Pyrolysis/gas chromatography/mass spectrometry of poly(1,3-phenylene isophthalamide) and poly(1,4-phenylene terephthalamide). *Polym. Degrad. Stab.* **1982**, *4*, 379–392. [CrossRef]
20. Karthik, D.; Baheti, V.; Militky, J.; Naeem, M.S.; Tunakova, V.; Ali, A. Activated Carbon Derived from Carbonization of Kevlar Waste Materials: A Novel Single Stage Method. *Materials* **2021**, *14*, 6433. [CrossRef] [PubMed]
21. Suárez-García, F.; Martínez-Alonso, A.; Tascón, J.M. Activated carbon fibers from Nomex by chemical activation with phosphoric acid. *Carbon* **2004**, *42*, 1419–1426. [CrossRef]
22. Conte, G.; Stelitano, S.; Policicchio, A.; Minuto, F.D.; Lazzaroli, V.; Galiano, F.; Agostino, R.G. Assessment of activated carbon fibers from commercial Kevlar[®] as nanostructured material for gas storage: Effect of activation procedure and adsorption of CO₂ and CH₄. *J. Anal. Appl. Pyrolysis* **2020**, *152*, 104974. [CrossRef]
23. Naeem, S.; Baheti, V.; Tunakova, V.; Militky, J.; Karthik, D.; Tomkova, B. Development of porous and electrically conductive activated carbon web for effective EMI shielding applications. *Carbon* **2017**, *111*, 439–447. [CrossRef]
24. El-Tantawy, F.; Kamada, K.; Ohnabe, H. In situ network structure, electrical and thermal properties of conductive epoxy resin-carbon black composites for electrical heater applications. *Mater. Lett.* **2002**, *56*, 112–126. [CrossRef]
25. Kong, K.; Deka, B.K.; Kim, M.; Oh, A.; Kim, H.; Park, Y.-B.; Park, H.W. Interlaminar resistive heating behavior of woven carbon fiber composite laminates modified with ZnO nanorods. *Compos. Sci. Technol.* **2014**, *100*, 83–91. [CrossRef]

Disclaimer/Publisher's Note: The statements, opinions and data contained in all publications are solely those of the individual author(s) and contributor(s) and not of MDPI and/or the editor(s). MDPI and/or the editor(s) disclaim responsibility for any injury to people or property resulting from any ideas, methods, instructions or products referred to in the content.

Future prospects

- To prepare a wide range of particles from the Kevlar-derived activated carbon fibers by ball-milling method.
- To explore the possibilities of modification of particles for selected applications
- To select proper attachments of carbon particles onto textile structures
- To investigate ohmic heating processes and their connections with carbon materials prepared from various polymeric wastes under different conditions.
- Preparation of textile waste-derived porous carbon materials by molten salt-assisted carbonization (Sodium and Ammonium salts) using pyrolysis methods.

References

- [1] Z. Huang, E. Yilmaz, and S. Cao, “Analysis of Strength and Microstructural Characteristics of Mine Backfills Containing Fly Ash and Desulfurized Gypsum,” *Minerals*, vol. 11, no. 4, p. 409, Apr. 2021, doi: 10.3390/min11040409.
- [2] N. Pensupa *et al.*, “Recent Trends in Sustainable Textile Waste Recycling Methods: Current Situation and Future Prospects,” *Top. Curr. Chem.*, vol. 375, no. 5, p. 76, Oct. 2017, doi: 10.1007/s41061-017-0165-0.
- [3] M. Overcash, “A Comparison of Reusable and Disposable Perioperative Textiles: Sustainability State-of-the-Art 2012,” *Anesth. Analg.*, vol. 114, no. 5, pp. 1055–1066, May 2012, doi: 10.1213/ANE.0b013e31824d9cc3.
- [4] “A European policy framework for a climate-neutral textile industry: The Policy Hub - Circularity for Apparel and Footwear supports the EU Strategy for Sustainable and Circular Textiles.” <https://www.policyhub.org/articles/a-european-policy-framework-for-a-climate-neutral-textile-industry-the-policy-hub-circularity-for-apparel-and-footwear-supports-the-eu-strategy-for-sustainable-and-circular-textiles>.
- [5] “The Most Surprising Clothing Waste Statistics and Trends in 2023 • GITNUX,” Mar. 24, 2023. <https://blog.gitnux.com/clothing-waste-statistics/> (accessed Mar. 24, 2023).
- [6] ELENA PAPPAS, “Latest trend keeps clothes out of landfill | Research and Innovation.” <https://ec.europa.eu/research-and-innovation/en/horizon-magazine/latest-trend-keeps-clothes-out-landfill>.
- [7] “Circular fashion in Europe: Turning waste into value | McKinsey.” <https://www.mckinsey.com/industries/retail/our-insights/scaling-textile-recycling-in-europe-turning-waste-into-value>.
- [8] “Chemical_Upcycling_Polymers.pdf.” Accessed: May 11, 2023. https://science.osti.gov//media/bes/pdf/reports/2020/Chemical_Upcycling_Polymers.pdf
- [9] J. Choi, I. Yang, S.-S. Kim, S. Y. Cho, and S. Lee, “Upcycling Plastic Waste into High Value-Added Carbonaceous Materials,” *Macromol. Rapid Commun.*, vol. 43, no. 1, p. 2100467, 2022, doi: 10.1002/marc.202100467.
- [10] A. Castro-Muñiz, F. Suárez-García, A. Martínez-Alonso, and J. M. D. Tascón, “Activated carbon fibers with a high content of surface functional groups by phosphoric acid activation of PPTA,” *J. Colloid Interface Sci.*, vol. 361, no. 1, pp. 307–315, Sep. 2011, doi: 10.1016/j.jcis.2011.05.064.
- [11] S. Villar-Rodil, A. Martínez-Alonso, and J. M. D. Tascón, “Studies on pyrolysis of Nomex polyaramid fibers,” *J. Anal. Appl. Pyrolysis*, vol. 58–59, pp. 105–115, Apr. 2001, doi: 10.1016/S0165-2370(00)00124-8.
- [12] K. Cao *et al.*, “Reactive Aramid Nanostructures as High-Performance Polymeric Building Blocks for Advanced Composites,” *Adv. Funct. Mater.*, vol. 23, no. 16, pp. 2072–2080, 2013, doi: 10.1002/adfm.201202466.
- [13] Bhat G. S., Cook F. L., Abhiraman A.S., and Peebles L.H., “New aspects in the stabilization of acrylic fibers for carbon fibers, Carbon,” *Carbon*, vol. 28, p. 377, 1990.

- [14] E. Fitzer, W. Frohs, and M. Heine, "Optimization of stabilization and carbonization treatment of PAN fibres and structural characterization of the resulting carbon fibres," *Carbon*, vol. 24, no. 4, pp. 387–395, 1986, doi: 10.1016/0008-6223(86)90257-5.
- [15] D. Karthik, V. Baheti, J. Militky, M. Naeem, V. Tunakova, and A. Ali, "Activated Carbon Derived from Carbonization of Kevlar Waste Materials: A Novel Single Stage Method," *Materials*, vol. 14, p. 6433, Oct. 2021, doi: 10.3390/ma14216433.
- [16] Alberto Castro-Muniz, Amelia Martínez-Alonso, Juan M.D. Tascon, "Modification of the pyrolysis/carbonization of PPTA polymer by intermediate isothermal treatments," *Carbon*, vol. 46, 2008.
- [17] S. J. Pickering, "Recycling technologies for thermoset composite materials—current status," *Compos. Part Appl. Sci. Manuf.*, vol. 37, no. 8, pp. 1206–1215, Aug. 2006, doi: 10.1016/j.compositesa.2005.05.030.
- [18] S. Villar-Rodil, F. Suárez-García, J. I. Paredes, A. Martínez-Alonso, and J. M. D. Tascón, "Activated Carbon Materials of Uniform Porosity from Polyaramid Fibers," *Chem. Mater.*, vol. 17, no. 24, pp. 5893–5908, Nov. 2005, doi: 10.1021/cm051339t.
- [19] R. C. Bansal and M. Goyal, *Activated carbon adsorption*. Boca Raton: Taylor & Francis, 2005.
- [20] M. Afshari, Ed., *Electrospun nanofibers*. in Woodhead publishing series in textiles, no. volume number 186. Amsterdam: The Textile Institute; Elsevier, 2017.
- [21] R. Miandad *et al.*, "Catalytic Pyrolysis of Plastic Waste: Moving Toward Pyrolysis Based Biorefineries," *Front. Energy Res.*, vol. 7, 2019, Accessed: May 12, 2023. [Online]. Available: <https://www.frontiersin.org/articles/10.3389/fenrg.2019.00027>
- [22] X. J. Wang *et al.*, "Microwave-assisted preparation of bamboo charcoal-based iron-containing adsorbents for Cr (VI) removal," *Chem. Eng. J.*, vol. 174, no. 1, pp. 326–332, Oct. 2011, doi: 10.1016/j.cej.2011.09.044.
- [23] Z. Wang, K. G. Burra, T. Lei, and A. K. Gupta, "Co-pyrolysis of waste plastic and solid biomass for synergistic production of biofuels and chemicals-A review," *Prog. Energy Combust. Sci.*, vol. 84, p. 100899, May 2021, doi: 10.1016/j.peccs.2020.100899.
- [24] S. D. Anuar Sharuddin, F. Abnisa, W. M. A. Wan Daud, and M. K. Aroua, "A review on pyrolysis of plastic wastes," *Energy Convers. Manag.*, vol. 115, pp. 308–326, May 2016, doi: 10.1016/j.enconman.2016.02.037.
- [25] S. Das, C. Liang, and J. B. Dunn, "Plastics to fuel or plastics: Life cycle assessment-based evaluation of different options for pyrolysis at end-of-life," *Waste Manag.*, vol. 153, pp. 81–88, Nov. 2022, doi: 10.1016/j.wasman.2022.08.015.
- [26] M. C. dos Santos, M. C. Maynard, L. R. Aveiro, E. C. da Paz, and V. dos Santos Pinheiro, "Carbon-Based Materials: Recent Advances, Challenges, and Perspectives," in *Reference Module in Materials Science and Materials Engineering*, Elsevier, 2017. doi: 10.1016/B978-0-12-803581-8.09262-6.
- [27] E. A. Chiticaru, S. Muraru, and M. Ioniță, "From Unidimensional Carbonaceous Materials to Multidimensional Structures Through Molecular Modeling," in *Carbon Related Materials: Commemoration for Nobel Laureate Professor Suzuki Special Symposium at IUMRS-ICAM2017*, S. Kaneko, M. Aono, A. Pruna, M. Can, P. Mele, M. Ertugrul, and T. Endo, Eds., Singapore: Springer, 2021, pp. 1–21. doi: 10.1007/978-981-15-7610-2_1.
- [28] G. Speranza, "The Role of Functionalization in the Applications of Carbon Materials: An Overview," *C*, vol. 5, no. 4, Art. no. 4, Dec. 2019, doi: 10.3390/c5040084.
- [29] A. F. Abou-Hadid *et al.*, "Production of efficient carbon fiber from different solid waste residuals for adsorption of hazardous metals from wastewater samples," *Biomass Convers. Biorefinery*, Aug. 2022, doi: 10.1007/s13399-022-03097-6.
- [30] Y. Cheng *et al.*, "Synthesis of N-Doped Porous Carbon Materials Derived from Waste Cellulose Acetate Fiber via Urea Activation and Its Potential Application in Supercapacitors," *J. Electrochem. Soc.*, vol. 166, no. 6, p. A1231, Apr. 2019, doi: 10.1149/2.1081906jes.
- [31] L. Yaqoob, T. Noor, and N. Iqbal, "Conversion of Plastic Waste to Carbon-Based Compounds and Application in Energy Storage Devices," *ACS Omega*, vol. 7, no. 16, pp. 13403–13435, Apr. 2022, doi: 10.1021/acsomega.1c07291.
- [32] T. Lee, C.-H. Ooi, R. Othman, and F.-Y. Yeoh, "Activated Carbon Fiber - The Hybrid of Carbon Fiber and Activated Carbon", *Rev. Adv. Mater. Sci.* 36 (2014) 118-136
- [33] N. Kawasaki, H. Tominaga, F. Ogata, K. Inoue, and M. Kankawa, "Development of Novel Carbon Fiber produced from Waste Fiber by Carbonization," *J. Oleo Sci.*, vol. 61, no. 10, pp. 593–600, 2012, doi: 10.5650/jos.61.593.
- [34] M. Suzuki, "Activated carbon fiber: Fundamentals and applications," *Carbon*, vol. 32, no. 4, pp. 577–586, Jan. 1994, doi: 10.1016/0008-6223(94)90075-2.
- [35] M.F. Hassan, *et al.*, "Recent trends in activated carbon fibers production from various precursors and applications—A comparative review, Elsevier, <https://doi.org/10.1016/j.jaap.2019.104715>.

- [36] I. Mochida *et al.*, “Removal of SO_x and NO_x over activated carbon fibers,” *Carbon*, vol. 38, no. 2, pp. 227–239, Jan. 2000, doi: 10.1016/S0008-6223(99)00179-7.
- [37] Theydan S. K., and Ahmed M. J., “Optimization of preparation conditions for activated carbons from date stones using response surface methodology,” *Powder Technol.*, vol. 224, p. 101, 2012.
- [38] T. Deng, G. Zhang, F. Dai, and F. Zhang, “Mild surface modification of *para*-aramid fiber by dilute sulfuric acid under microwave irradiation,” *Text. Res. J.*, vol. 87, no. 7, pp. 799–806, May 2017, doi: 10.1177/0040517516639831.
- [39] M. Zięzio, B. Charnas, K. Jedynak, M. Hawryluk, and K. Kucio, “Preparation and characterization of activated carbons obtained from the waste materials impregnated with phosphoric acid (V),” *Appl. Nanosci.*, vol. 10, no. 12, pp. 4703–4716, Dec. 2020, doi: 10.1007/s13204-020-01419-6.
- [40] V. Sridhar, J.-H. Jeon, and I.-K. Oh, “Microwave extraction of graphene from carbon fibers,” *Carbon*, vol. 49, no. 1, pp. 222–226, Jan. 2011, doi: 10.1016/j.carbon.2010.09.007.
- [41] M. S. Abd Rahaman, A. Ismail, and A. B. Mustafa, “A Review of Heat Treatment on Polyacrylonitrile Fiber,” *Polym. Degrad. Stab.*, vol. 92, p. 1421, Apr. 2007, doi: 10.1016/j.polymdegradstab.2007.03.023.
- [42] E. Hammel *et al.*, “Carbon nanofibers for composite applications,” *Carbon*, vol. 42, no. 5, pp. 1153–1158, Jan. 2004, doi: 10.1016/j.carbon.2003.12.043.
- [43] S. Gu, J. F. Ren, and Q. Wu, “Preparation and structures of electrospun PAN nanofibers as a precursor of carbon nanofibers,” *Synth. Met. - Synth. Met.*, vol. 155, pp. 157–161, Oct. 2005, doi: 10.1016/j.synthmet.2005.07.340.
- [44] K. Kong, L. Deng, I. Kinloch, R. Young, and S. Eichhorn, “Production of carbon fibres from a pyrolysed and graphitised liquid crystalline cellulose fibre precursor,” *J. Mater. Sci.*, vol. 47, pp. 5402–5410, Jul. 2012, doi: 10.1007/s10853-012-6426-y.
- [45] “Free Analysis: Carbon Fiber Market.” <https://www.zionmarketresearch.com/market-analysis/carbon-fiber-market> (accessed Jun. 22, 2020).
- [46] M. R. Buchmeiser *et al.*, “A new carbon precursor: synthesis and carbonization of triethylammonium-based poly(*p*-phenylenevinylene) (PPV) progenitors,” *J. Mater. Chem. A*, vol. 1, no. 42, pp. 13154–13163, Oct. 2013, doi: 10.1039/C3TA12908J.
- [47] “5911.pdf.”: <https://www.nipponsteel.com/en/tech/report/nsc/pdf/5911.pdf>
- [48] “Kevlar,” *The 60's*. <http://the60s.weebly.com/kevlar.html>.
- [49] J. J. Freeman, J. B. Tomlinson, K. S. W. Sing, and C. R. Theocharis, “Adsorption of nitrogen and water vapour by activated Kevlar® chars,” *Carbon*, vol. 31, no. 6, pp. 865–869, 1993, doi: 10.1016/0008-6223(93)90186-E.
- [50] J. Choma, L. Osuchowski, M. Marszewski, A. Dziura, and M. Jaroniec, “Developing microporosity in Kevlar®-derived carbon fibers by CO₂ activation for CO₂ adsorption,” *J. CO₂ Util.*, vol. 16, pp. 17–22, Dec. 2016, doi: 10.1016/j.jcou.2016.05.004.
- [51] F. Suárez-García, A. Martínez-Alonso, and J. M. D. Tascón, “Activated carbon fibers from Nomex by chemical activation with phosphoric acid,” *Carbon*, vol. 42, no. 8–9, pp. 1419–1426, 2004, doi: 10.1016/j.carbon.2003.11.011.
- [52] A. Sanchez-Sanchez, F. Suárez-García, A. Martínez-Alonso, and J. Tascón, “Aromatic polyamides as new precursors of nitrogen and oxygen-doped ordered mesoporous carbons,” *Carbon*, vol. 70, pp. 119–129, Apr. 2014, doi: 10.1016/j.carbon.2013.12.080.
- [53] Y. Kawahara, S. Otoyama, and K. Yamamoto, “Direct Carbonization of High-performance Aromatic Polymers and the Production of Activated Carbon Fibers,” *J. Text. Sci. Eng.*, vol. 05, no. 06, 2015, doi: 10.4172/2165-8064.1000219.
- [54] K. S. Ko, C. W. Park, S.-H. Yoon, and S. M. Oh, “Preparation of Kevlar-derived carbon fibers and their anodic performances in Li secondary batteries,” *Carbon*, vol. 39, no. 11, pp. 1619–1625, Sep. 2001, doi: 10.1016/S0008-6223(00)00298-0.
- [55] Q. Wu and D. Pan, “A New Cellulose Based Carbon Fiber from a Lyocell Precursor,” *Text. Res. J. - TEXT RES J*, vol. 72, pp. 405–410, May 2002, doi: 10.1177/004051750207200506.
- [56] G. Duman, “Preparation of novel porous carbon from hydrothermal pretreated textile wastes: Effects of textile type and activation agent on structural and adsorptive properties,” *J. Water Process Eng.*, vol. 43, p. 102286, Oct. 2021, doi: 10.1016/j.jwpe.2021.102286.
- [57] M. Kaneko, S. Kumagai, T. Nakamura, and H. Sato, “Study of sulfonation mechanism of low-density polyethylene films with fuming sulfuric acid,” *J. Appl. Polym. Sci.*, vol. 91, no. 4, pp. 2435–2442, 2004, doi: 10.1002/app.13404.
- [58] J. W. Kim and J. S. Lee, “Preparation of carbon fibers from linear low-density polyethylene,” *Carbon*, vol. 94, pp. 524–530, Nov. 2015, doi: 10.1016/j.carbon.2015.06.074.
- [59] B. Xie, L. Hong, P. Chen, and B. Zhu, “Effect of sulfonation with concentrated sulfuric acid on the composition and carbonizability of LLDPE fibers,” *Polym. Bull.*, vol. 73, no. 3, pp. 891–908, Mar. 2016, doi: 10.1007/s00289-015-1525-y.

- [60] I. Karacan and H. Benli, "Use of sulfonation procedure for the development of thermally stabilized isotactic polypropylene fibers prior to carbonization," *J. Appl. Polym. Sci.*, vol. 123, no. 1, pp. 234–245, 2012, doi: 10.1002/app.34454.
- [61] L. Zhang *et al.*, "Converting PBO fibers into carbon fibers by ultrafast carbonization," *Carbon*, vol. 159, pp. 432–442, Apr. 2020, doi: 10.1016/j.carbon.2019.12.067.
- [62] Y. Yang, A. Centrone, L. Chen, F. Simeon, T. Hatton, and G. Rutledge, "Highly porous electrospun polyvinylidene fluoride (PVDF)-based carbon fiber," *Carbon*, vol. 49, pp. 3395–3403, Sep. 2011, doi: 10.1016/j.carbon.2011.04.015.
- [63] A. Mavinkurve, S. Visser, and A. J. Pennings, "AN INITIAL EVALUATION OF POLY(VINYLAACETYLENE) AS A CARBON FIBER PRECURSOR".
- [64] O. Krivoruchko, N. Maksimova, V. Zaikovskii, and A. Salanov, "Study of multiwalled graphite nanotubes and filaments formation from carbonized products of polyvinyl alcohol via catalytic graphitization at 600–800°C in nitrogen atmosphere," *Carbon*, vol. 38, pp. 1075–1082, Dec. 2000, doi: 10.1016/S0008-6223(99)00225-0.
- [65] T. A. Centeno and A. B. Fuertes, "Supported carbon molecular sieve membranes based on a phenolic resin," *J. Membr. Sci.*, vol. 160, no. 2, pp. 201–211, Jul. 1999, doi: 10.1016/S0376-7388(99)00083-6.
- [66] C. Guéret, M. Daroux, and F. Billaud, "Methane pyrolysis: thermodynamics," *Chem. Eng. Sci.*, vol. 52, no. 5, pp. 815–827, Mar. 1997, doi: 10.1016/S0009-2509(96)00444-7.
- [67] M. Devi, S. Rawat, and S. Sharma, "A comprehensive review of the pyrolysis process: from carbon nanomaterial synthesis to waste treatment," *Oxf. Open Mater. Sci.*, vol. 1, no. 1, p. itab014, Jan. 2021, doi: 10.1093/oxfmat/itab014.
- [68] Ming Yang, Xiao-ling Zhu, Guo zheng Liang, "Pyrolysis Process of Kevlar Fibers with Thermogravimetric Analysis coupled and Fourier Transform Infrared Spectroscopy," vol. 36(5), pp. 1374–1377, May 2016.
- [69] A. Ramgobin, G. Fontaine, and S. Bourbigot, "Thermal Degradation and Fire Behavior of High-Performance Polymers," *Polym. Rev.*, vol. 59, no. 1, pp. 55–123, Jan. 2019, doi: 10.1080/15583724.2018.1546736.
- [70] H. Guedidi *et al.*, "Ultrasonic pre-treatment of an activated carbon powder in different solutions and influence on the ibuprofen adsorption," *Comptes Rendus Chim.*, vol. 23, no. 1, pp. 17–31, 2020, doi: 10.5802/crchim.3.
- [71] D. W. Krevelen, *Properties of Polymers: Their Correlation with Chemical Structure, Their Numerical Estimation and Prediction from Additive Group Contributions*. Elsevier, 1990.
- [72] A. F. Grand and C. A. Wilkie, *Fire Retardancy of Polymeric Materials*. CRC Press, 2000.
- [73] A. V. Gribanov and Yu. N. Sazanov, "Polyacrylonitrile: Carbonization problems," *Russ. J. Appl. Chem.*, vol. 81, no. 6, pp. 919–932, Jun. 2008, doi: 10.1134/S1070427208060013.
- [74] S. Thomas, Y. Grohens, and P. T. Yasir Beeran, Eds., *Industrial Applications of Nanomaterials*. Micro & Nano Technologies Series. Amsterdam: Elsevier Inc., 2019.
- [75] C. Hu, L. Chen, R. Gu, J. Yu, J. Zhu, and Z. Hu, "Thermal Decomposition Behavior of a Heterocyclic Aramid Fiber," *J. Macromol. Sci. Part B*, vol. 52, no. 5, pp. 726–737, Apr. 2013, doi: 10.1080/00222348.2012.725641.
- [76] M. Blazsó, "Pyrolysis for recycling waste composites," in *Management, Recycling and Reuse of Waste Composites*, Elsevier, 2010, pp. 102–121. doi: 10.1533/9781845697662.2.102.
- [77] M. Faraday, "Chemistry and Physics of Fire and Liquid Fuels," p. 47.
- [78] S. Isaji, Y. Bin, and M. Matsuo, "Electrical conductivity and self-temperature-control heating properties of carbon nanotubes filled polyethylene films," *Polymer*, vol. 50, no. 4, pp. 1046–1053, Feb. 2009, doi: 10.1016/j.polymer.2008.12.033.
- [79] H. Lopes and J. Ribeiro, "Structural Health Monitoring in Composite Automotive Elements," in *New Advances in Vehicular Technology and Automotive Engineering*, J. Carmo, Ed., InTech, 2012. doi: 10.5772/46109.
- [80] J. Seyyed Monfared Zanjani, B. Saner Okan, P.-N. Pappas, C. Galiotis, Y. Z. Menciloglu, and M. Yildiz, "Tailoring viscoelastic response, self-heating and deicing properties of carbon-fiber reinforced epoxy composites by graphene modification," *Compos. Part Appl. Sci. Manuf.*, vol. 106, pp. 1–10, Mar. 2018, doi: 10.1016/j.compositesa.2017.12.008.
- [81] J. R. Brown and B. C. Ennis, "Thermal Analysis of Nomex[®] and Kevlar[®] Fibers," *Text. Res. J.*, vol. 47, no. 1, pp. 62–66, Jan. 1977, doi: 10.1177/004051757704700113.
- [82] M. Kopeć *et al.*, "Polyacrylonitrile-derived nanostructured carbon materials," *Prog. Polym. Sci.*, vol. 92, pp. 89–134, May 2019, doi: 10.1016/j.progpolymsci.2019.02.003.
- [83] M. E. G. Mosquera, M. Jamond, A. Martinez-Alonso, and J. M. D. Tascon, "Thermal Transformations of Kevlar Aramid Fibers During Pyrolysis: Infrared and Thermal Analysis Studies," *ACS Publications*, May 01, 2002. <https://pubs.acs.org/doi/pdf/10.1021/cm00047a006>.

- [84] T. Shin, O. Hajima, and W. Chuichi, "Pyrograms and Thermograms of 163 High Polymers, and MS Data of the Major Pyrolyzates," in *Pyrolysis, 2012; GC&MS Data Book of Synthetic Polymers*, Elsevier, 2011, pp. 7–335. doi: 10.1016/B978-0-444-53892-5.10002-1.
- [85] J. R. Brown and A. J. Power, "Thermal degradation of aramids: Part I—Pyrolysis/gas chromatography/mass spectrometry of poly(1,3-phenylene isophthalamide) and poly(1,4-phenylene terephthalamide)," *Polym. Degrad. Stab.*, vol. 4, no. 5, pp. 379–392, Sep. 1982, doi: 10.1016/0141-3910(82)90044-1.
- [86] A. T. Kalashik and N. P. Paiikarova, "Comparative Analysis of The Thermal Degradation of Poly-P-Benzamide and Poly-P-Phenylene Terephthalamide," p. 9.
- [87] H. L. Friedman, "Thermal degradation of plastics. I. The kinetics of polymer chain degradation," *J. Polym. Sci.*, vol. 45, no. 145, pp. 119–125, Jul. 1960, doi: 10.1002/pol.1960.1204514511.
- [88] H.-R. Schulten, B. Plage, H. Ohtani, and S. Tsuge, "[No title found]," *Angew. Makromol. Chem.*, vol. 155, no. 1, pp. 1–20, Nov. 1987, doi: 10.1002/apmc.1987.051550101.
- [89] X.-W. Wang, Z.-M. Hu, and Z.-F. Liu, "Thermal Degradation of Meta- and Para-Aramid Fibers in Different Atmospheres," *Int. Polym. Process.*, vol. 23, no. 1, pp. 81–87, Mar. 2008, doi: 10.3139/217.2046.
- [90] L. Giraldo, Y. Ladino, J. C. M. Piraján, and M. P. Rodríguez, "Synthesis and characterization of activated carbon fibers from Kevlar," *Eclética Quím.*, vol. 32, no. 4, pp. 55–62, 2007, doi: 10.1590/S0100-46702007000400008.
- [91] L. Wang, "Comparison and Analysis of Thermal Degradation Process of Aramid Fibers (Kevlar 49 and Nomex)," *J. Fiber Bioeng. Inform.*, vol. 3, no. 3, pp. 163–167, Jun. 2010, doi: 10.3993/jfbi12201008.
- [92] C. G. Slough, T. Instruments, L. Drive, and N. Castle, "Simultaneous Mass Spectrometry and Fourier Transform Infrared Spectrometry of Off-Gases from a Thermogravimetric Analyzer".
- [93] "The Difference Between Coal and Charcoal," *Pearson Fuels*, Feb. 13, 2020. <https://pearsonfuels.co.uk/the-difference-between-coal-and-charcoal>.
- [94] E. E. Kwon, S.-H. Cho, and S. Kim, "Synergetic Sustainability Enhancement via Utilization of Carbon Dioxide as Carbon Neutral Chemical Feedstock in the Thermo-Chemical Processing of Biomass," *Environ. Sci. Technol.*, vol. 49, no. 8, pp. 5028–5034, Apr. 2015, doi: 10.1021/es505744n.
- [95] E. E. Kwon, S. Kim, and J. Lee, "Pyrolysis of waste feedstocks in CO₂ for effective energy recovery and waste treatment," *J. CO₂ Util.*, vol. 31, pp. 173–180, May 2019, doi: 10.1016/j.jcou.2019.03.015.
- [96] Y. Shen, D. Ma, and X. Ge, "CO₂ -looping in biomass pyrolysis or gasification," *Sustain. Energy Fuels*, vol. 1, no. 8, pp. 1700–1729, 2017, doi: 10.1039/C7SE00279C.
- [97] J. Y. Chen, *Activated Carbon Fiber and Textiles*. 2016, p. 342.
- [98] G. Pilon and J.-M. Lavoie, "Pyrolysis of Switchgrass (*Panicum virgatum* L.) at Low Temperatures within N₂ and CO₂ Environments: Product Yield Study," *ACS Sustain. Chem. Eng.*, vol. 1, no. 1, pp. 198–204, Jan. 2013, doi: 10.1021/sc300098e.
- [99] H.-Y. Lin, M. Nurunnabi, W.-H. Chen, and C.-H. Huang, "Chapter 16 - Graphene in Neuroscience," in *Biomedical Applications of Graphene and 2D Nanomaterials*, Micro and Nano Technologies. Elsevier, 2019, pp. 337–351. doi: 10.1016/B978-0-12-815889-0.00016-7.
- [100] M. Yang *et al.*, "The influence of CO₂ on biomass fast pyrolysis at medium temperatures," *J. Renew. Sustain. Energy*, vol. 10, no. 1, p. 013108, Feb. 2018, doi: 10.1063/1.5005013.
- [101] E. E. Kwon, H. Yi, and M. J. Castaldi, "Utilizing Carbon Dioxide as a Reaction Medium to Mitigate Production of Polycyclic Aromatic Hydrocarbons from the Thermal Decomposition of Styrene Butadiene Rubber," *Environ. Sci. Technol.*, vol. 46, no. 19, pp. 10752–10757, Oct. 2012, doi: 10.1021/es301933p.
- [102] J. Kim, K.-H. Kim, and E. E. Kwon, "Enhanced thermal cracking of VOCs evolved from the thermal degradation of lignin using CO₂," *Energy*, vol. 100, pp. 51–57, Apr. 2016, doi: 10.1016/j.energy.2016.01.075.
- [103] D. Karthik, K. Kupka, J. Militky, and M. Venkataraman, "Study on thermal degradation of poly (1,4 phenylene terephthalamide) and its volatile products by unadorned setup of Pyrolysis and subsequent UV–VIS spectroscopy," *J. Anal. Appl. Pyrolysis*, vol. 172, p. 105985, Jun. 2023, doi: 10.1016/j.jaap.2023.105985.
- [104] Nederlandse Vereniging van Veiligheidstechnici and N. Veiligheidsinstituut Amsterdam Vereniging van de Nederlandse Chemische Industrie, *Handling chemicals safely 1980*. The Hague: Dutch Association of Safety Experts : Dutch Chemical Industry Association : Dutch Safety Institute, 1980.
- [105] J. L. Vetter, "Leavening Agents," in *Encyclopedia of Food Sciences and Nutrition (Second Edition)*, B. Caballero, Ed., Oxford: Academic Press, 2003, pp. 3485–3490. doi: 10.1016/B0-12-227055-X/00683-0.
- [106] G. Conte *et al.*, "Assessment of activated carbon fibers from commercial Kevlar[®] as nanostructured material for gas storage: Effect of activation procedure and adsorption of CO₂ and CH₄," *J. Anal. Appl. Pyrolysis*, vol. 152, p. 104974, Nov. 2020, doi: 10.1016/j.jaap.2020.104974.

- [107] D. Karthik, J. Militky, Y. Wang, and M. Venkataraman, "Joule Heating of Carbon-Based Materials Obtained by Carbonization of Para-Aramid Fabrics," *C*, vol. 9, no. 1, Art. no. 1, Mar. 2023, doi: 10.3390/c9010023.
- [108] R. J. Morgan and C. O. Pruneda, "The characterization of the chemical impurities in Kevlar 49 fibres," *Polymer*, vol. 28, no. 2, pp. 340–346, Feb. 1987, doi: 10.1016/0032-3861(87)90428-9.
- [109] L. Penn and F. Larsen, "Physicochemical properties of kevlar 49 fiber," *J. Appl. Polym. Sci.*, vol. 23, no. 1, pp. 59–73, Jan. 1979, doi: 10.1002/app.1979.070230106.
- [110] Q. Zhang, Y. Liang, and S. B. Warner, "Partial carbonization of aramid fibers," *J. Polym. Sci. Part B Polym. Phys.*, vol. 32, no. 13, pp. 2207–2220, Oct. 1994, doi: 10.1002/polb.1994.090321308.
- [111] P. Alafogianni, K. Dassios, S. Farmaki, S. K. Antiohos, T. E. Matikas, and N.-M. Barkoula, "On the efficiency of UV–vis spectroscopy in assessing the dispersion quality in sonicated aqueous suspensions of carbon nanotubes," *Colloids Surf. Physicochem. Eng. Asp.*, vol. 495, pp. 118–124, Apr. 2016, doi: 10.1016/j.colsurfa.2016.01.053.
- [112] G. Wypych, Ed., "2 - PHOTOPHYSICS," in *Handbook of UV Degradation and Stabilization (Second Edition)*, ChemTec Publishing, 2015, pp. 9–35. doi: 10.1016/B978-1-895198-86-7.50004-8.
- [113] R. M. Wallace, "Analysis of Absorption Spectra of Multicomponent Systems," *ACS Publications*, May 01, 2002. <https://pubs.acs.org/doi/pdf/10.1021/j100836a019>.
- [114] L. Guo, F. Kooli, and M. Garland, "A general method for the recovery of pure powder XRD patterns from complex mixtures using no a priori information," *Anal. Chim. Acta*, vol. 517, no. 1–2, pp. 229–236, Jul. 2004, doi: 10.1016/j.aca.2004.05.006.
- [115] A. Huck, M. Guillaume, and J. Blanc-Talon, "Minimum Dispersion Constrained Nonnegative Matrix Factorization to Unmix Hyperspectral Data," *IEEE Trans. Geosci. Remote Sens.*, vol. 48, no. 6, pp. 2590–2602, Jun. 2010, doi: 10.1109/TGRS.2009.2038483.
- [116] G. M. Cai and W. D. Yu, "Study on the thermal degradation of high-performance fibers by TG/FTIR and Py-GC/MS," *J. Therm. Anal. Calorim.*, vol. 104, no. 2, pp. 757–763, May 2011, doi: 10.1007/s10973-010-1211-0.
- [117] Z. Czégény and M. Blazsó, "Thermal decomposition of polyamides in the presence of poly(vinyl chloride)," *J. Anal. Appl. Pyrolysis*, vol. 58–59, pp. 95–104, Apr. 2001, doi: 10.1016/S0165-2370(00)00152-2.
- [118] X. Xie, B. Goodell, G. Daniel, Y. Qian, J. Jellison, and M. Peterson, "Carbonization of wood and nanostructures formed from the cell wall," *Int. Biodeterior. Biodegrad.*, vol. 63, no. 7, pp. 933–935, Oct. 2009, doi: 10.1016/j.ibiod.2009.06.011.
- [119] G. Pari, S. Darmawan, and B. Prihandoko, "Porous Carbon Spheres from Hydrothermal Carbonization and KOH Activation on Cassava and Tapioca Flour Raw Material," *Procedia Environ. Sci.*, vol. 20, pp. 342–351, Jan. 2014, doi: 10.1016/j.proenv.2014.03.043.
- [120] Y. P. Khanna *et al.*, "Aromatic polyamides. II. Thermal degradation of some aromatic polyamides and their model diamides," *J. Polym. Sci. Polym. Chem. Ed.*, vol. 19, no. 11, pp. 2817–2834, Nov. 1981, doi: 10.1002/pol.1981.170191115.
- [121] T. Kunugi, H. Watanabe, and M. Hashimoto, "Dynamic mechanical properties of poly(p-phenyleneterephthalamide) fiber," *J. Appl. Polym. Sci.*, vol. 24, no. 4, pp. 1039–1051, Aug. 1979, doi: 10.1002/app.1979.070240417.
- [122] I. Tomizuka, Y. Isoda, and Y. Amamiya, "Carbon Fibre from a High-Modulus Polyamide Fibre (Kevlar)," *TANSO*, vol. 1981, no. 106, pp. 93–101, 1981, doi: 10.7209/tanso.1981.93.
- [123] S. Naeem, V. Baheti, V. Tunakova, J. Militky, D. Karthik, and B. Tomkova, "Development of porous and electrically conductive activated carbon web for effective EMI shielding applications," *Carbon*, vol. 111, pp. 439–447, Jan. 2017, doi: 10.1016/j.carbon.2016.10.026.
- [124] F. Jiang, L. Chen, N. Song, L. Shi, and P. Ding, "Influence of activated carbon fibres with different specific surface areas on the thermal conductive and electrical insulating properties of polyamide-imide composites," *High Volt.*, vol. 2, no. 3, pp. 161–166, 2017, doi: 10.1049/hve.2017.0042.
- [125] A. Jain, R. Balasubramanian, and M. P. Srinivasan, "Hydrothermal conversion of biomass waste to activated carbon with high porosity: A review," *Chem. Eng. J.*, vol. 283, p. 789, 2016.
- [126] M. Z. Hossain *et al.*, "High-Surface-Area Mesoporous Activated Carbon from Hemp Bast Fiber Using Hydrothermal Processing," *C*, vol. 4, no. 3, Art. no. 3, Sep. 2018, doi: 10.3390/c4030038.
- [127] M. Endo, T. Takeda, Y. Kim, K. Koshiba, and K. Ishii, "High Power Electric Double Layer Capacitor (EDLC's); from Operating Principle to Pore Size Control in Advanced Activated Carbons," *Carbon Lett.*, vol. 1, Jan. 2001.
- [128] P. J. M. Carrott and J. J. Freeman, "Evolution of micropore structure of activated charcoal cloth," *Carbon*, vol. 29, no. 4, pp. 499–506, Jan. 1991, doi: 10.1016/0008-6223(91)90113-W.
- [129] J. Rouquerol, F. Rouquerol, P. Llewellyn, G. Maurin, and K. Sing, *Adsorption by Powders and Porous Solids: Principles, Methodology and Applications*. Academic Press, 2013.

- [130] S. J. Gregg, K. S. W. Sing, and H. W. Salzberg, "Adsorption Surface Area and Porosity," *J. Electrochem. Soc.*, vol. 114, no. 11, p. 279Ca, Nov. 1967, doi: 10.1149/1.2426447.
- [131] R. H. Hurt, A. F. Sarofim, and J. P. Longwell, "Gasification-induced densification of carbons: From soot to form coke," *Combust. Flame*, vol. 95, no. 4, pp. 430–432, Dec. 1993, doi: 10.1016/0010-2180(93)90009-R.
- [132] Z. Hashisho, M. Rood, S. Barot, and J. T. Bernhard, "Role of functional groups on the microwave attenuation and electric resistivity of activated carbon fiber cloth," *Carbon*, vol. 47, pp. 1814–1823, Jun. 2009, doi: 10.1016/j.carbon.2009.03.006.
- [133] S. L. Vittorio, M. S. Dresselhaus, M. Endo, J.-P. Issi, L. Piraux, and V. Bayot, "Transport properties of activated carbon fibers," *J. Mater. Res.*, vol. 6, pp. 778–783, Apr. 1991, doi: 10.1557/JMR.1991.0778.
- [134] S. Mrozowski, "Semiconductivity and Diamagnetism of Polycrystalline Graphite and Condensed Ring Systems," *Phys. Rev.*, vol. 85, no. 4, pp. 609–620, Feb. 1952, doi: 10.1103/PhysRev.85.609.
- [135] R. Song *et al.*, "The Combined Catalytic Action of Solid Acids with Nickel for the Transformation of Polypropylene into Carbon Nanotubes by Pyrolysis," *Chem. – Eur. J.*, vol. 13, no. 11, pp. 3234–3240, 2007, doi: 10.1002/chem.200601018.
- [136] Y. Wen, X. Wen, K. Wenelska, X. Chen, and E. Mijowska, "Novel strategy for preparation of highly porous carbon sheets derived from polystyrene for supercapacitors," *Diam. Relat. Mater.*, vol. 95, pp. 5–13, May 2019, doi: 10.1016/j.diamond.2019.03.015.
- [137] J. Sánchez-González, A. Macías-García, M. F. Alexandre-Franco, and V. Gómez-Serrano, "Electrical conductivity of carbon blacks under compression," *Carbon*, vol. 43, no. 4, pp. 741–747, 2005, doi: 10.1016/j.carbon.2004.10.045.
- [138] W. Djeridi, A. Ouederni, N. B. Mansour, P. L. Llewellyn, A. Alyamani, and L. El Mir, "Effect of the both texture and electrical properties of activated carbon on the CO₂ adsorption capacity," *Mater. Res. Bull.*, vol. 73, pp. 130–139, Jan. 2016, doi: 10.1016/j.materresbull.2015.08.032.
- [139] N. Angelidis, C. Y. Wei, and P. E. Irving, "The electrical resistance response of continuous carbon fibre composite laminates to mechanical strain," *Compos. Part Appl. Sci. Manuf.*, vol. 35, no. 10, pp. 1135–1147, Oct. 2004, doi: 10.1016/j.compositesa.2004.03.020.
- [140] C. N. Owston, "Electrical properties of single carbon fibres," *J. Phys. Appl. Phys.*, vol. 3, no. 11, p. 1615, Nov. 1970, doi: 10.1088/0022-3727/3/11/309.
- [141] Q. Zhao *et al.*, "Review on the Electrical Resistance/Conductivity of Carbon Fiber Reinforced Polymer," *Appl. Sci.*, vol. 9, no. 11, Art. no. 11, Jan. 2019, doi: 10.3390/app9112390.
- [142] J.-B. Donnet, R. C. Bansal, and M.-J. Wang, Eds., *Carbon black: science and technology*, 2nd ed., rev. Expanded. New York: Dekker, 1993.
- [143] T. Adinaveen, J. J. Vijaya, and L. J. Kennedy, "Comparative Study of Electrical Conductivity on Activated Carbons Prepared from Various Cellulose Materials," *Arab. J. Sci. Eng.*, vol. 41, no. 1, pp. 55–65, Jan. 2016, doi: 10.1007/s13369-014-1516-6.
- [144] A. Barroso-Bogeat, M. Alexandre-Franco, C. Fernández-González, A. Macías-García, and V. Gómez-Serrano, "Electrical conductivity of activated carbon–metal oxide nanocomposites under compression: a comparison study," *Phys. Chem. Chem. Phys.*, vol. 16, no. 45, pp. 25161–25175, Oct. 2014, doi: 10.1039/C4CP03952A.
- [145] A. Barroso Bogeat, "Understanding and Tuning the Electrical Conductivity of Activated Carbon: A State-of-the-Art Review," *Crit. Rev. Solid State Mater. Sci.*, vol. 46, no. 1, pp. 1–37, Jan. 2021, doi: 10.1080/10408436.2019.1671800.
- [146] W. W. Smeltzer and R. McIntosh, "The effect of physical adsorption on the electrical resistance of active carbon," *Can. J. Chem.*, vol. 31, no. 12, pp. 1239–1251, Dec. 1953, doi: 10.1139/v53-159.
- [147] V. Šafářová and J. Militký, "Electromagnetic shielding properties of woven fabrics made from high-performance fibers," *Text. Res. J.*, vol. 84, no. 12, pp. 1255–1267, Jul. 2014, doi: 10.1177/0040517514521118.
- [148] V. Šafářová, M. Tunák, and J. Militký, "Prediction of hybrid woven fabric electromagnetic shielding effectiveness," *Text. Res. J.*, vol. 85, no. 7, pp. 673–686, May 2015, doi: 10.1177/0040517514555802.
- [149] K.-W. Kim, W. Han, B.-S. Kim, B.-J. Kim, and K.-H. An, "A study on EMI shielding enhancement behaviors of Ni-plated CFs-reinforced polymer matrix composites by post heat treatment," *Appl. Surf. Sci.*, vol. 415, pp. 55–60, Sep. 2017, doi: 10.1016/j.apsusc.2017.01.108.
- [150] S. Kim *et al.*, "Electromagnetic Interference (EMI) Transparent Shielding of Reduced Graphene Oxide (RGO) Interleaved Structure Fabricated by Electrophoretic Deposition," *ACS Appl. Mater. Interfaces*, vol. 6, no. 20, pp. 17647–17653, Oct. 2014, doi: 10.1021/am503893v.
- [151] D. D. L. Chung, "Electromagnetic interference shielding effectiveness of carbon materials," *Carbon*, vol. 39, no. 2, pp. 279–285, Feb. 2001, doi: 10.1016/S0008-6223(00)00184-6.
- [152] M. Jaroszewski, S. Thomas, and A. V. Rane, *Advanced Materials for Electromagnetic Shielding: Fundamentals, Properties, and Applications*. John Wiley & Sons, 2018.

- [153] Y. Tao, P. Li, and S. Q. Shi, "Effects of Carbonization Temperature and Component Ratio on Electromagnetic Interference Shielding Effectiveness of Woodceramics," *Materials*, vol. 9, no. 7, Art. no. 7, Jul. 2016, doi: 10.3390/ma9070540.
- [154] M. A. Gervasoni Nasar Ali, William I. Milne, Cengiz S. Ozkan, Stanislaw Mitura, Juana L., Ed., *Graphene Science Handbook: Electrical and Optical Properties*. Boca Raton: CRC Press, 2016. doi: 10.1201/b19642.
- [155] J. Kruželák, A. Kvasničáková, K. Hložeková, and I. Hudec, "Progress in polymers and polymer composites used as efficient materials for EMI shielding," *Nanoscale Adv.*, vol. 3, no. 1, pp. 123–172, 2021, doi: 10.1039/D0NA00760A.
- [156] J. Cheng *et al.*, "Recent Advances in Design Strategies and Multifunctionality of Flexible Electromagnetic Interference Shielding Materials," *Nano-Micro Lett.*, vol. 14, no. 1, p. 80, Mar. 2022, doi: 10.1007/s40820-022-00823-7.
- [157] Y. Wang *et al.*, "Easily fabricated and lightweight PPy/PDA/AgNW composites for excellent electromagnetic interference shielding," *Nanoscale*, vol. 9, no. 46, pp. 18318–18325, Nov. 2017, doi: 10.1039/C7NR05951E.
- [158] K. Armstrong and C. C. C. Ltd, "Guide to Testing Conducted Emissions (Based on the Methods in EN 55022 and EN 55011)," *In Compliance Magazine*, Jul. 01, 2011. <https://incompliancemag.com/article/guide-to-testing-conducted-emissions-based-on-the-methods-in-en-55022-and-en-55011/> (accessed May 16, 2023).
- [159] S. Geetha, K. K. Satheesh Kumar, C. R. K. Rao, M. Vijayan, and D. C. Trivedi, "EMI shielding: Methods and materials—A review," *J. Appl. Polym. Sci.*, vol. 112, no. 4, pp. 2073–2086, 2009, doi: 10.1002/app.29812.
- [160] "waveguides-for-emi-rf-shielding-3.pdf." Accessed: May 17, 2023. [Online]. Available: <https://www.euro-emc.co.uk/admin/resources/datasheets/waveguides-for-emi-rf-shielding-3.pdf>
- [161] M. Yuksek, "Electromagnetic wave shielding and mechanical properties of vapor-grown carbon nanofiber/polyvinylidene fluoride composite fibers," *J. Eng. Fibers Fabr.*, vol. 15, p. 155892502098595, Jan. 2020, doi: 10.1177/1558925020985959.
- [162] O. Redondo, S. G. Prolongo, M. Campo, C. Sbarufatti, and M. Giglio, "Anti-icing and de-icing coatings-based Joule's heating of graphene nanoplatelets," *Compos. Sci. Technol.*, vol. 164, pp. 65–73, Aug. 2018, doi: 10.1016/j.compscitech.2018.05.031.
- [163] A.-T. Chien, S. Cho, Y. Joshi, and S. Kumar, "Electrical conductivity and Joule heating of polyacrylonitrile/carbon nanotube composite fibers," *Polymer*, vol. 55, no. 26, pp. 6896–6905, Dec. 2014, doi: 10.1016/j.polymer.2014.10.064.
- [164] J. C. Chen and I. R. Harrison, "Modification of polyacrylonitrile (PAN) carbon fiber precursor via post-spinning plasticization and stretching in dimethyl formamide (DMF)," *Carbon*, vol. 40, no. 1, pp. 25–45, Jan. 2002, doi: 10.1016/S0008-6223(01)00050-1.
- [165] D. D. Edie, "The effect of processing on the structure and properties of carbon fibers," *Carbon*, vol. 36, no. 4, pp. 345–362, 1998, doi: 10.1016/S0008-6223(97)00185-1.
- [166] S. Yang, L. Chen, L. Mu, B. Hao, and P.-C. Ma, "Low-cost carbon fiber aerogel derived from bamboo for the adsorption of oils and organic solvents with excellent performances," *RSC Adv.*, vol. 5, no. 48, pp. 38470–38478, Apr. 2015, doi: 10.1039/C5RA03701H.
- [167] L. R. Pahalagedara, I. W. Siriwardane, N. D. Tissera, R. N. Wijesena, and K. M. N. de Silva, "Carbon black functionalized stretchable conductive fabrics for wearable heating applications," *RSC Adv.*, vol. 7, no. 31, pp. 19174–19180, 2017, doi: 10.1039/C7RA02184D.
- [168] F. El-Tantawy, K. Kamada, and H. Ohnabe, "In situ network structure, electrical and thermal properties of conductive epoxy resin–carbon black composites for electrical heater applications," *Mater. Lett.*, vol. 56, no. 1–2, pp. 112–126, Sep. 2002, doi: 10.1016/S0167-577X(02)00401-9.

List of Publications

Journal publications

- [1] **Daniel Karthik**, Karel Kupka, Jiri Militky, Mohanapriya Venkataraman, Study on Thermal Degradation of poly (1,4 phenylene terephthalamide) and its volatile products by unadorned setup of Pyrolysis and subsequent UV-VIS spectroscopy, *Journal of Analytical and Applied Pyrolysis*, 2023, ISSN 0165-2370, <https://doi.org/10.1016/j.jaap.2023.105985> (IF: 6.437, Quartile: Q1).

- [2] **Daniel Karthik**, Vijay Baheti, Jiri Militky, Muhammad Salman Naeem, Veronika Tunakova, and Azam Ali. 2021. "Activated Carbon Derived from Carbonization of Kevlar Waste Materials: A Novel Single Stage Method" *Materials* 14, no. 21: 6433. <https://doi.org/10.3390/ma14216433> (**IF: 3.748, Quartile: Q2**).
- [3] Salman Naeem, Vijay Baheti, Veronika Tunakova, Jiri Militky, **Daniel Karthik**, Blanka Tomkova, Development of porous and electrically conductive activated carbon web for effective EMI shielding applications, *Carbon*, Volume 111, 2017, Pages 439-447, ISSN 0008-6223, <https://doi.org/10.1016/j.carbon.2016.10.026> (**IF: 11.307, Quartile: Q1**).
- [4] Mohanapriya Venkataraman, Jiří Militký, Alžbeta Samková, **Daniel Karthik**, Dana Křemenáková, and Michal Petru. 2022. "Hybrid Prepreg Tapes for Composite Manufacturing: A Case Study", *Materials* 15, no. 2: 619, <https://doi.org/10.3390/ma15020619> (**IF: 3.748, Quartile: Q2**).
- [5] **Daniel Karthik**, Jiri Militky, Yuanfeng Wang, and Mohanapriya Venkataraman. 2023. "Joule Heating of Carbon-Based Materials Obtained by Carbonization of *Para*-Aramid Fabrics" *C* 9, no. 1: 23. ISSN 2311-5629, <https://doi.org/10.3390/c9010023> (**Web of Science (ESCI), tracked for impact factor, projected quartile is Q2**).
- [6] Palanisamy, S., Tunakova, V., Wang, Y.F., **Karthik, D.**, Militký, J., 2022. EMI Shielding of the Copper/Nickel-Coated Polyester Nonwoven. *Solid State Phenomena*. <https://doi.org/10.4028/p-om1446>.
- [7] **Karthik D.**, Baheti V, Tunakova V. and Militky J. ^[1]_[SEP]Carbonization Of Kevlar Fabrics For Effective Emi Shielding Applications, *Fibres and Textiles* (4), *Vlákna a textil*, 2018; 41-44. ISSN 2585-8890.

Conference publications

- [1] **Karthik, D.**, Militky, J., Venkataraman, M. Eradicating spread of virus by using activated carbon (2020) *Textile Bioengineering and Informatics Symposium Proceedings 2020 - 13th Textile Bioengineering and Informatics Symposium*, TBIS 2020, pp. 56-63.
- [2] **Daniel Karthik**, Vijaykumar Baheti, Jiri Militky, Carbon and Silicon Based Electrically Conductive Elastomeric Textile Sensors, 46th Textile Research Symposium, The Textile Machinery Society of Japan, 2018.
- [3] **Daniel Karthik**, Vijay Baheti, Veronika Tunakova, Jiri Militky, Sundaramurthy Palanisamy, Development of Electrically Conductive Activated Carbon Fabric from Kevlar Fabric for Effective Emi Shielding Applications, *Textile Bioengineering and Informatics Symposium*, Wuhan, China 2017; 1044; ISSN:19423438. DOI: 10.3993/tbis2017.
- [4] **Daniel Karthik**, Vijay Baheti, Jiri Militky, Sundaramurthy Palanisamy, Studies on Organic and Inorganic Micro/Nano Particle Reinforced Epoxy Composites, *Textile Bioengineering and Informatics Symposium Proceedings*, Manchester, UK, 2018, pp.149, ISSN: 1942-3438, DOI: 10.3993/tbis2018.

- [5] **Karthik, D.**, Baheti, V., Novotna, J., Samkova, A., Pulicek, R., Venkataraman, M., Srb, P., Voleska, K., Wang, Y., Militky, J. Effect of particulate fillers on creep behaviour of epoxy composites. *Materials today: Proceedings*. 1. ed. Oxford: Elsevier, 2020 Pp. 1–4. ISSN 2214-7853.
- [6] Sundaramoorthy Palanisamy, Veronika Tunakova, Benny Malengier, **Daniel Karthik**, Lieva Van Langenhova, Jiri Militky, Development Of The Force Sensitive Resistors Using Polypyrrole Coated Cotton Woven Fabric For Pressure Sensing Application, 22nd International Conference, STRUTEX, 2018.
- [7] **Daniel Karthik**, Vijaykumar Baheti, Jiri Militky CEC 2017, TUL, Liberec, Czech Republic – “Carbonization of Kevlar Fabric for Effective EMI Shielding Applications”
- [8] **Daniel Karthik**, A.I. Wasif, Vijaykumar Baheti, Jiri Militky Presented a poster entitled “Study on Gauze Bandages” at STRUTEX conference, December 2016, Czech Republic.
- [9] S. Palanisamy, V. Tunakova, Y. Wang, **D. Karthik**, J. Militky, EMI Shielding Of The Copper/ Nickel Coated Nonwoven. Autex Conference 2021.
- [10] Palanisamy, S., Tunakova, V., Venkataraman, M., **Karthik, D.**, Wiener, J., Militky, J. Modeling of an electrically conductive nonwoven strip for electromagnetic shielding, *Textile Bioengineering and Informatics Symposium Proceedings 2021 - 14th Textile Bioengineering and Informatics Symposium, TBIS 2021*, 2021, pp. 37–43
- [11] Baheti, V., **Karthik, D.**, Novotna, J., Samkova, A., Pulicek, R., Venkataraman, M., Srb, P., Voleska, K., Militky, J. Creep Behavior Of Particle Filled Epoxy Composites. *The Twenty-Sixth Annual International Conference on Composites/Nano Engineering*, 2018. Not numbered (2 pages).
- [12] Jiří Militký; Vijay Baheti, Wang Yuanfeng & **Daniel Karthik**, Utilization of Fibrous Waste For The Preparation Of Advanced Carbon Materials, *Book of Proceedings (International textile, clothing & design conference)*, ISSN 1847-7275, p.41.

Book Chapters

- [1] **Daniel Karthik**, Jiri Militky, Mohanapriya Venkataraman (2021). Eradicating spread of Virus by using Activated Carbon. *Textiles and Their Use in Microbial Protection: Focus on COVID-19 and Other Viruses*. Technical Fibres. 2. ed. United Kingdom: Woodhead publishing (Elsevier), 2018. Pp. 367–419. ISBN 978-0-08-101272-7.
- [2] Daniel Karthik, Jiri Militky, Mohanapriya Venkataraman (In process-proposed to be published in 2023). *Carbon-based Functional Materials derived from Fibrous Wastes. Advanced Multifunctional Materials from Fibrous Structures*. Springer Publication.